

# Electrophoresis-Driven Lateral Flow Immunoassay and Aptamer Selection

**EDEN T. TECLEMICHAEL**

A THESIS SUBMITTED TO  
THE FACULTY OF GRADUATE STUDIES  
IN PARTIAL FULFILMENT OF THE REQUIREMENTS  
FOR THE DEGREE OF MASTER OF SCIENCE

GRADUATE PROGRAM IN BIOLOGY

YORK UNIVERSITY

TORONTO, ONTARIO

November 2023

©Eden Teclemichael, 2023

## **ABSTRACT**

Electrophoresis has become an indispensable tool in Biochemistry and Molecular Biology, essential for analyzing proteins and nucleic acids. My work focuses on new bioanalytical applications of electrophoresis: lateral flow immunoassay (LFIA) and the selection of oligonucleotide aptamers. Electrophoretically-driven LFIA (eLFIA) is a new technique aiming to enhance diagnostic sensitivity of LFIA in both antigen and serological tests. While previously applied to Hepatitis B and C, I aimed to extend eLFIA's scope to analyze the SARS-CoV-2 spike protein, demonstrating a 77% reduction in the limit of detection compared to conventional LFIA. Shifting focus to aptamers, I utilized capillary electrophoresis (CE), with the highest partitioning efficiency, to address challenges in aptamer selection. I determined the optimum target concentration and developed bulk affinity assays workflow that quantitatively assesses the progress of selection. Understanding these parameters can significantly influence aptamer selection efficiency and can guide researchers in designing assays and developing novel diagnostic tools.

## **DEDICATION**

To my beloved family for being my motivation and supporting me all the way and to the  
almighty God

## ACKNOWLEDGMENTS

First and foremost, I would like to express my heartfelt gratitude to my research supervisor, Dr. Sergey N. Krylov, for giving me a chance to join his lab and his invaluable guidance, unwavering support, and constructive feedback throughout the course of this research. I would also like to extend my gratitude to Dr. Svetlana Krylova for closely managing my project, her expertise and encouragement that has been instrumental in shaping the direction of my graduate study and help me strive to become the best researcher I can be. Their combined support is truly invaluable and I am truly thankful for their mentorship and dedication to my academic and personal growth.

I would also like to extend my heartfelt gratitude to Dr. Katalin Hudak, a valued member of my committee, for her consistent support and for offering invaluable insights that encouraged me to view the broader scope of my research throughout my Masters.

Special thanks also go to Dr. Vasily Panferov who has helped me in a tremendous amount in the last year of my study. I could not thank him enough for introducing me to the beauty of nanoparticles and guiding me on every step of my project.

I would also like to thank my colleagues turned friends An Le Thi Hoai and Shakiba Ghaffari for not only in sharing their expertise of aptamer selection with me but for being my friends whom I share my accomplishments and struggles in research and personal lives. I would have not completed my Masters without them.

I would also like to thank the rest of the Krylov lab: Dr. Liang Hu, Dr. Nikita Ivanov, Jean Luc Rukundo, Tong Ye Wang, and Giammarco Nebbioso for never hesitating to help me with any issues I encountered and lending me their technical support.

Finally, I cannot thank my beloved family enough for their lifelong support, unconditional love, and for making me who I am. This work would have not been possible without them.

# TABLE OF CONTENTS

<b>ABSTRACT.....</b>	<b>ii</b>
<b>DEDICATION .....</b>	<b>iii</b>
<b>ACKNOWLEDGMENTS.....</b>	<b>iv</b>
<b>TABLE OF CONTENTS .....</b>	<b>vi</b>
<b>LIST OF TABLES .....</b>	<b>ix</b>
<b>LIST OF FIGURES .....</b>	<b>x</b>
<b>LIST OF ABBREVIATIONS .....</b>	<b>xii</b>

## **CHAPTER 1. INTRODUCTION OF ANTIBODIES AND APTAMERS AND METHODOLOGY OVERVIEW.....1**

1.1 Intermolecular Interactions.....	1
1.1.1 Reversible Binding Kinetics .....	2
1.2 Antibodies as Ligands .....	3
1.2.1 Antibodies as Diagnostics.....	4
1.2.2 Lateral Flow Immunoassay Basics .....	5
1.2.3 Challenges and Recent Advances, Including Our Research Endeavors.....	9
1.3 Aptamers as Ligands .....	11
1.3.1 Systemic Evolution of Ligands by Exponential Enrichment .....	12
1.3.2 Introduction to Capillary Electrophoresis.....	13
1.3.3 Capillary Electrophoresis-based Selection .....	15

## **CHAPTER 2. VALIDATING AND OPTIMIZING CURRENT ELECTROPHORESIS-ASSISTED MULTILAYER ASSEMBLY OF NANOPARTICLES FOR SENSITIVE LATERAL FLOW IMMUNOASSAY AS DIAGNOSTICS TOOL .....19**

2.1 Introduction.....	19
2.1.1 Working principle of enhanced LFIA .....	21
2.2 Materials and Methods .....	23
2.2.1 Chemicals and Materials.....	23
2.2.2 Synthesis GNP.....	23
2.2.3 Biotinylating antibodies.....	23
2.2.4 GNP-Ab Conjugation .....	24
2.2.5 Assembly of test strips.....	24

2.2.6 Conventional and Enhanced LFIA .....	25
2.3 Results and Discussion .....	26
2.3.1 Synthesis of GNPs, Antibody Conjugation, and its Characterization .....	26
2.3.2 Optimization of Different Parameters of the Immunoassay .....	30
2.4 Conclusion .....	37

**CHAPTER 3. INFLUENCE OF BULK AFFINITY AND TARGET CONCENTRATION IN APTAMER SELECTION .....38**

**3.1 BULK AFFINITY ASSAYS IN APTAMER SELECTION: CHALLENGES, THEORY, AND WORKFLOW .....38**

3.1.1 Introduction.....	38
3.1.2 Materials and Methods .....	40
3.1.2.1 Chemicals and Materials.....	40
3.1.2.2 DNA Sequences.....	41
3.1.2.3 CE Instrumentation.....	41
3.1.2.4 Fraction Collection .....	42
3.1.2.5 PCR Procedures and Generation of Binder-Enriched DNA Library .....	42
3.1.2.6 Bulk Affinity Assays .....	43
3.1.3 Results and Discussions.....	44
3.1.3.1 Definitions of $R$ and $K_d^-$ .....	44
3.1.3.2 Requirement for Complete Separation of L from TL in Bulk Affinity Assays .....	44
3.1.3.3 Suitability Criterion for Quantitative Measures of Bulk Affinity .....	46
3.1.3.4 Advantages and Limitations of $R$ and $K_d^-$ in Bulk Assays.....	47
3.1.3.5 Algorithm of Choosing $[T]_0$ in $R$ -Based Bulk Affinity Assay .....	48
3.1.3.6 Experimental Demonstration of Proposed Bulk-Affinity Assay Algorithm.....	51
3.1.4 Concluding Remarks .....	52

**3.2 INFLUENCE OF TARGET CONCENTRATION ON APTAMER SELECTION: EXPERIMENTAL STUDY .....54**

3.2.1 Introduction.....	54
3.2.2 Materials and Methods .....	56
3.2.2.1 Materials and solutions .....	56
3.2.2.2 DNA sequences .....	56
3.2.2.3 CE Instrumentations .....	57

3.2.2.4 Specifics of CE-based fraction collection.....	57
3.2.2.5 PCR procedures and generation of binder-enriched library .....	58
3.2.2.6 Specifics of bulk affinity test .....	59
3.2.3 Results and Discussion .....	60
3.2.4 Conclusion .....	67
<b>LIMITATIONS .....</b>	<b>68</b>
<b>CONCLUSION AND FUTURE WORKS.....</b>	<b>70</b>
<b>LIST OF PUBLICATION .....</b>	<b>71</b>
<b>REFERENCES.....</b>	<b>72</b>
<b>APPENDICES .....</b>	<b>78</b>

## LIST OF TABLES

<b>Table 1.</b> The Influence of Nitrocellulose Blocking with PVA and BSA Reagents .....	32
<b>Table 2.</b> The impact of various buffer compositions in a blocked NC and a non-blocked NC ..	34
<b>Table B1.</b> Determined $R$ values at different selection round with adding different concentrations of target. ....	83
<b>Table C1.</b> Relative standard deviation of $q$ .....	85
<b>Table C2.</b> Summary of $k_N$ and $q$ values obtained in MutS selections .....	86
<b>Table C3.</b> Summary of $k_N$ and $q$ values obtained in thrombin selections.....	87
<b>Table C4.</b> Summary of $R$ values for MutS selections.....	89
<b>Table C5.</b> Summary of $R$ values for thrombin selections .....	91

## LIST OF FIGURES

<b>Figure 1.</b> Schematic depiction of conventional LFIA. ....	7
<b>Figure 2.</b> Schematic representation of SELEX. ....	13
<b>Figure 3.</b> Schematic representation of the basic capillary electrophoresis instrumental set-up..	15
<b>Figure 4.</b> Schematic of Non-Equilibrium Capillary Electrophoresis of Equilibrium Mixtures..	17
<b>Figure 5.</b> Schematic depiction of both conventional and enhanced LFIA.....	22
<b>Figure 6.</b> Characterization of GNP.....	27
<b>Figure 7.</b> Optimum conjugation conditions of antibodies. ....	29
<b>Figure 8.</b> Optical spectra of nanoparticles .....	30
<b>Figure 9.</b> LFIA of varying concentrations of RBD antigen using PBS assay buffer supplemented with 0.05% tween 20 and 1% casein.....	35
<b>Figure 10.</b> LFIA of varying concentrations of RBD antigen using borate assay buffer supplemented with 1% BSA and 0.1% triton x-100.....	36
<b>Figure 11.</b> LFIA of varying concentrations of RBD antigen using borate assay buffer supplemented with 0.05% tween 20 and 0.1% casein.....	37
<b>Figure 12.</b> Modeled distributions of $K_d$ values for progressive rounds of aptamer selection. ....	49
<b>Figure 13.</b> Proposed bulk affinity workflow.....	51
<b>Figure 14.</b> Experimental His-tagged MutS protein bulk affinity assay based on the proposed bulk affinity assay workflow.....	52
<b>Figure 15.</b> Schematic representation of SELEX. ....	55
<b>Figure 16.</b> Schematic representation of efficient partitioning of binders ( $B$ ) from nonbinders ( $N$ ) in a mixture of oligonucleotide library and protein target. ....	62
<b>Figure 17.</b> Comparison of $q$ values (a) and bulk affinities represented by $R$ values (b) to evaluate the selection outcomes for MutS and thrombin under four different schemes of constant target concentrations throughout the selection. ....	65
<b>Figure A1.</b> Determination of optimum pH for antibody conjugation .....	78
<b>Figure A2.</b> Western blot analysis for RBD antigen-antibody binding .....	78
<b>Figure B1.</b> Experimental electropherograms of His-tagged MutS protein bulk affinity assay based on the proposed.....	82

**Figure C1.** Determination of binder-elution window for NECEEM-based selection for MutS (a) and thrombin (b) ..... 84

**Figure C2.** Bulk affinity tests of the starting library and the binder-enriched libraries obtained in MutS selections at four different target concentrations using the published bulk affinity workflow ..... 88

**Figure C3.** Bulk affinity tests of the starting library and binder-enriched libraries obtained from thrombin selections at four different target concentrations using the published bulk affinity workflow ..... 90

## LIST OF ABBREVIATIONS

Ab	antibody
Ab-GNP	antibody-gold nanoparticle
ACE2	angiotensin-converting enzyme 2
<i>Bin</i>	output quantity of binders
<i>Bout</i>	output quantity of non-binders
BSA	bovine serum albumin
CE	capillary Electrophoresis
cLFIA	conventional lateral flow immunoassay
CZ	control zone
dd	deionized water
DNA	deoxyribonucleic acid
E	applied electrical field
eLFIA	electrophoresis-driven lateral flow immunoassay
ELISA	enzyme-linked immunosorbent assays
EOF	electroosmotic flow
GNP	gold nanoparticles
GNP-Str	streptavidin conjugated gold nanoparticles

GNP-Ab <sub>B</sub>	biotinylated antibodies conjugated gold nanoparticles
HEPES	4-(2-hydroxyethyl)-1-piperazineethanesulfonic acid
KCE	kinetic capillary electrophoresis
$K_d$	equilibrium dissociation constant
$\bar{K}_d$	equilibrium pseudo constant
$k_N$	transmittance of partitioning for nonbinders
$k_{on}$	rate constant of complex association
$k_{off}$	rate constant of complex dissociation
L	ligand
[L] <sub>0</sub>	total concentrations of the ligand
LFIA	lateral flow immunoassay
LIF	laser induced fluorescence
LOD	limit of detection
$L_T$	the output quantity of library in the presence of target
MW	molecular weight
$\mu$	electrophoretic mobility
$N$	unique ligands
NC	nitrocellulose membrane

NECEEM	non-equilibrium capillary electrophoresis of equilibrium mixtures
$N_{in}$	quantities of nonbinders at the input
$N_{out}$	quantities of nonbinders at the output
nt	nucleotide
OD	optical density
PBS	phosphate-buffered saline
PCR	polymerase chain reaction
POCT	point-of-care testing
$q$	relative yield of DNA
qPCR	quantitative polymerase chain reaction
pH	potential of hydrogen
pI	isoelectric point
PVA	poly (vinyl alcohol)
$R$	fraction of the unbound (or bound)
RBD	receptor-binding-domain
RT	room temperature
S	cumulative signal
SD	standard deviation

SDS	sodium dodecyl sulphate
SELEX	systematic evolution of ligands by exponential enrichment
SL	signal from all unbound ligands
STL	signal from all the bound ligands
T	target
TZ	test zone
$[T]_0$	total concentration of the target
$T \cdot L$	complex
TEM	transmission electron microscope
Tris	tris(hydroxymethyl)aminomethane
UV	ultraviolet
$v$	velocity of the molecule
X	quantitative measure of affinity
$\sigma$	standard deviation
$\varphi$	coefficient of sign

# CHAPTER 1. INTRODUCTION OF ANTIBODIES AND APTAMERS AND METHODOLOGY OVERVIEW

## 1.1 Intermolecular Interactions

Molecular interactions constitute an essential aspect of various biological processes, thereby playing a pivotal role in cellular functions, disease profiling, and drug mechanisms. Critical biological activities, such as cell division, metabolic pathways, immune responses, and gene transcription, rely on precise intermolecular interactions that ensure structural adaptability and selective molecular recognition.<sup>1</sup> The structural flexibility, selectivity and specificity are explicitly required in all macromolecules for biomolecular complex formation.<sup>2</sup> Deciphering interaction mechanisms are crucial undertaking in comprehending molecular biology, contemporary drug development, and drug delivery.<sup>3</sup> Biosensors and affinity probes provide accurate quantitative analysis of targets by binding the target with high affinity and specificity to form a highly stable molecular complexes thus serving as detectors or biomarkers for diagnostics. Besides diagnostics, intermolecular interactions can also be used for biomolecular separations and purifications.<sup>4,5</sup> Hence, understanding and quantitative analysis of biomolecular interactions is of paramount importance in various fields, including medicine, biochemistry, cell biology, molecular biology, pharmacology, and biotechnology. Studying the mechanisms and consequences of these interactions can lead to the development of novel therapeutic interventions, drug design, and the exploration of disease mechanisms.<sup>6</sup>

### 1.1.1 Reversible Binding Kinetics

Reversible binding kinetics refers to the process of molecular interactions between two or more molecules, where the binding and unbinding of the molecules can occur in both directions. In other words, the association and dissociation of the molecules are reversible and can reach an equilibrium state. In affinity based biomolecular interaction, a discrete time dependent reversible binding exists between the molecular complex and the unbound molecules of a pair of biomolecules combined and equilibrated together. The reversible binding, designated as the binding ligand (L) and the target (T), with the formation of their intermolecular complex ( $T \cdot L$ ), can be illustrated by the following general reaction equation 1:



Where the forward rate of reaction is known as  $k_{on}$  which is the rate constant of complex association and the reverse rate of reaction which is rate constant of complex dissociation is known as  $k_{off}$ . Both rate constants and binding affinity of the two molecules can be characterized by the measurement of its equilibrium dissociation constant ( $K_d$ ) which is a ratio of  $k_{off}/k_{on}$  or calculated based on the concentrations of the pair of biomolecules at equilibrium as shown in equation 2.<sup>7</sup>

$$K_d = \frac{k_{off}}{k_{on}} = \frac{[T]_{eq}[L]_{eq}}{[T \cdot L]_{eq}} \quad 2$$

$K_d$  is the most used quantitative characteristics of intermolecular interaction and by convention lower  $K_d$  means stronger binders which can provide vital information in ranking drug candidates and ligand screening. Different methodologies exist in the separating target-ligand complexes from non-binders and further elucidate kinetics of the target-ligand binding, such as nuclear magnetic resonance, affinity chromatography, isothermal titration calorimetry, bio-layer interferometry and capillary electrophoresis to name a few.<sup>8</sup> Hence, information of biomolecular

interactions help researchers to make more biological relevant and scientific sound predications and analysis.

## **1.2 Antibodies as Ligands**

In the fields of molecular biology and biochemistry, antibodies serve as vital ligands, selectively binding to specific antigens through their antigen-binding regions situated at the ends of the Fab "arms." This intricate binding process relies on precise mechanisms, making antibodies sensitive, and thus integral in areas like molecular biology, diagnostics, and therapy.<sup>9</sup>

Recently there have been significant advancements in the field of antibodies, particularly in their applications as ligands, which have paved the way for innovative research and practical applications in various fields. Some recent advances include the development of bispecific and multi-specific antibodies that has gained considerable momentum, allowing for the simultaneous targeting of multiple antigens or cells. These engineered antibodies have shown promising results in targeted drug delivery, cancer therapy, and immunotherapy.<sup>10</sup> Antibody-Drug Conjugates have also emerged as highly targeted therapies, effectively minimizing harming healthy cells while destroying tumor cells.<sup>11</sup> Moreover, antibody-based immunotherapies, including immune checkpoint inhibitors and chimeric antigen receptor -T cell therapies, have significantly transformed cancer treatment, enhancing patient outcomes.<sup>12</sup>

Furthermore, recent breakthroughs in the field of antibody engineering include employing methodologies like phage display and yeast surface display, have led to the production of antibodies demonstrating improved specificity, enhanced stability, and diminished immunogenicity. This has led to improved properties and increased effectiveness in various applications. Furthermore, the development of humanized antibodies has been instrumental in

augmenting their therapeutic capabilities. These modified antibodies, designed to be less immunogenic, maintain their antigen-binding functions while minimizing the risk of adverse immune responses. Humanized antibodies have significantly propelled targeted therapies, especially in addressing complex illnesses like cancer, expanding the realm of immunotherapy and offering more personalized treatment alternatives for patients.<sup>13</sup> Overall, antibodies can be precisely tailored to bind to diverse targets, offering a specialized means to manipulate specific molecules and cells across a broad range of scientific, medical, and biotechnological applications.

### **1.2.1 Antibodies as Diagnostics**

Antibodies are pivotal components in immunoassays, robust analytical techniques employed to detect and quantify specific molecules, frequently antigens, across diverse biological samples. Their inherent attribute is their high specificity, rendering each antibody exquisitely designed to bind with remarkable precision to a particular antigen or epitope. This specificity forms the cornerstone of immunoassay accuracy.

In the realm of immunoassays, antibodies often serve as primary reagents. For instance, in enzyme-linked immunosorbent assays (ELISA), immobilized antibodies capture target antigens, enabling subsequent detection steps. These antibodies can be further labeled with various tags for detection purposes, including enzymes, fluorophores, radioactive isotopes, or gold nanoparticles (GNP). Upon the formation of the antibody-antigen complex, these labels generate measurable signals.<sup>14</sup>

The practicality of immunoassay is evident in their extensive use in point-of-care testing (POCT), characterized by its speed and simplicity. Devices like lateral flow assays, which

harness antibodies, facilitate rapid diagnostic tests for conditions such as infectious diseases and pregnancy. In clinical diagnostics, immunoassays play an indispensable role, encompassing the measurement of hormones, enzymes, and viral antigens.<sup>14</sup> Their significance extends to research, where they facilitate biomarker discovery, drug development, and the monitoring of disease progression. Beyond healthcare, immunoassays find application in industries such as pharmaceuticals and food testing, where they are instrumental in ensuring quality control, from detecting contaminants to guaranteeing product consistency.<sup>15</sup>

In summary, antibodies stand as irreplaceable constituents of immunoassays, giving them the precision and specificity needed to detect a wide spectrum of molecules accurately. This versatility establishes immunoassays as indispensable tools in the domains of medical diagnostics, research, and various industries.

### **1.2.2 Lateral Flow Immunoassay Basics**

Traditional laboratory-based analytical techniques, including high-performance liquid chromatography, mass spectrometry, gas chromatography, real-time polymerase chain reaction (qPCR), and ELISA, typically involve intricate and time-consuming procedures for acquiring results. However, numerous scenarios demand rapid and on-site detection of analytes. Consequently, recent scientific endeavors have increasingly concentrated on the enhancement and advancement of portable, cost-effective, and user-friendly rapid analysis methods suitable for POCT.<sup>16</sup>

Lateral flow immunoassay (LFIA) is a foundational technology within various detection systems, offering rapid, economical, and straightforward identification of a particular analyte within intricate sample mixtures. This methodology involves the application of a sample to a

testing device, providing quick results, often within minutes. Initially recognized as the "sol particle immunoassay," as pioneered by Leuvering et al. in 1980, it is now commonly known as LFIA. Recent years have witnessed a growing interest in LFIA-based diagnostic tools due to their cost-effective development and their utility in numerous fields requiring rapid detection capabilities.<sup>17</sup>

The core concept of LFIA centers on the migration of the sample, containing the target analyte, across a strip. This strip, typically composed of polymeric materials, incorporates distinct zones where molecules are linked with a label. As the analyte-containing sample moves across these zones, it engages with molecules precisely engineered to exclusively bind with the analyte within the sample. Facilitating this process is a sample pad, located at one end of the strip, aiding in the facilitation and uniform dispersion of the sample to the subsequent element, the conjugate pad. The material composition of the sample pad, typically comprising cellulose, cross-linked silica, or glass fibers, is selected based on its capacity to retain specific buffer solutions, proteins, surfactants, etc., during the application process, thereby ensuring a seamless flow following buffer addition.<sup>17</sup>

The conjugate pad, typically composed of cross-linked silica or glass fiber, fulfills the crucial function of housing and preserving the operational integrity of the probe particles. Moreover, it is essential for the bond between nanoparticles and the sample pad to be not strong, facilitating the release of conjugated particles when they encounter a moving fluid. This is achieved using a buffer or a mixture of buffers typically containing carbohydrate molecules, such as sucrose, which envelop the probe particles, safeguarding them from degradation.<sup>18</sup>

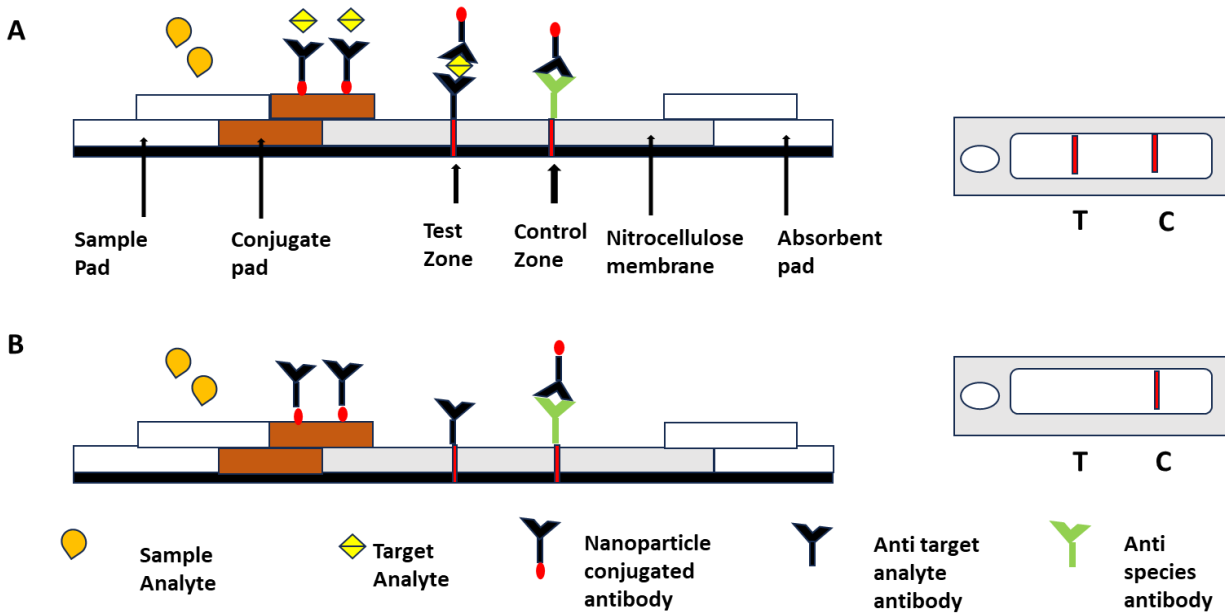


**Figure 1.** Schematic depiction of conventional LFIA. (A) A positive outcome demonstrating the presence of the target analyte in the sample, and (B) a negative outcome indicating the absence of the target analyte in the sample.

The probe particles are typically conjugated to an antibody or a molecule with a specific affinity for the target analyte. Nanoparticles are predominantly employed as probe molecules and serve as the detection components within LFIA devices. Their selection is rooted in several advantageous attributes: robustness, tunable opto-electronic properties contingent on size and shape, rapid synthesis and functionalization capabilities, biocompatibility, inherent stability, capacity for visual signal interpretation marked by a high signal-to-noise ratio, and cost-effectiveness. In most cases, colloidal GNP is employed as the probe. Nevertheless, recent reports have also explored the utilization of alternative nanoparticles, including colored latex particles, selenium, carbon, platinum, or silver, as probes for LFIA devices.<sup>18</sup>

Following their passage through the conjugate pad, the fluid, now potentially carrying potentially carrying unbound or bound probe particles, proceeds to the nitrocellulose membrane

(NC) with two distinct zones: the test and control zones, each immobilizing with biological components, usually antigens (antigen assay) or antibodies (serological assay). For this thesis, all assays discussed refer to the antigen assay.

The subsequent step involves the interaction between the target analyte and specific antibodies coated within the test and control zones. As illustrated in **Figure 1**, the design of the assay ensures that if the analyte of interest is present in the sample, it will be captured by the antibody at the test zone. This antigen-antibody interaction results in a positive test with the development of color or the formation of a band at the test zone, depending on the label type of nanoparticles used. To verify the proper flow of fluid through the membrane, a response in the control zone need to be observed.<sup>17</sup> This response is independent of the target analyte, consistently forming a band, even in the absence of analyte molecules in the given sample as in the case of a negative test. A response only in the test zone without a corresponding control zone response, or no response in any of the zones, indicates an invalid result.

There are two formats of LFIA namely sandwich assay and competitive assay. The sandwich format caters to analytes with multiple epitopes. Initially, the target analyte binds to the antibody-GNP label. Upon membrane traversal, it encounters another specific antibody in the test zone. This results in a visual or detector-based pattern through the capture of the antibody-GNP-antigen conjugate and the antibody in the test zone. Conversely, the competitive format addresses low molecular weight analytes or haptens with a solitary binding site. The bound analyte-GNP antibody is applied to the test line, producing a strong signal. As the analyte traverses, it competes with the antibody, releasing the antibody-gold nanoparticle conjugate and reducing the signal with increasing analyte concentration. The competitive format particularly

focuses on the competitive binding of labeled primary antibodies, shedding light on the presence or absence of the analyte in the sample.<sup>19</sup>

In summary, the LFIA architecture represents a sophisticated and well-engineered system for rapid analyte detection. Hence, LFIA finds diverse applications, including pregnancy tests, infectious disease diagnostics, food and beverage testing, drug testing, and environmental monitoring, owing to its simplicity, speed, and adaptability in clinical and non-clinical settings.

### **1.2.3 Challenges and Recent Advances, Including Our Research Endeavors**

Although LFIA devices enjoy great application already, there are still some limitations associated with LFIA-based devices. Most LFIAs are still based on subjective interpretation by the user, which is a major limitation for those assays. It limits the technology to qualitative applications; also, data loss and user error in interpretation are major challenges, especially in a POCT or home-testing environment.<sup>20</sup> Thus, developing LFIAs with an integrated reader system is often a required product design specification for next-generation assays. In modern LFIA setups, smartphones have been incorporated to yield precise and quantifiable outcomes, mitigating user discrepancies.<sup>21</sup> However, further advancements are warranted, particularly in light of the ongoing AI revolution, to fully harness the potential of this technology.

Another limitation could be multiplexing where detecting multiple analytes simultaneously on a single LFIA strip can be complicated due to potential cross-reactivity between antibodies. Progress is being made in developing multiplexed LFIA for various diagnostic applications. For example, a multiplexed disease diagnostic strip using silver-nanoparticles labels with three different sizes and having different colors, was designed to detect three different types of viruses causing Dengue, Yellow fever and Ebola but reduction in

sensitivity was observed due to competition for binding sites.<sup>22</sup> Thus, ensuring the specificity of multiple detection lines concurrently is also a complex task, often requiring careful optimization of reagents and components. Overcoming these challenges necessitates sophisticated engineering of assay components, innovative signal amplification strategies, and stringent validation procedures to ensure the accuracy and reliability of multiplexed LFIA.

However, the most significant challenge of LFIA remains sensitivity. Different strategies have been proposed for enhancing the sensitivity LFIA by designing and engineering nanoparticles with unique properties or amplifying the signal from immunocomplexes through increased labeling of nanoparticles per complex. One approach involves crosslinking functionalized nanoparticles, where a primary conjugate binds to the antigen and a secondary conjugate attach to the primary one, resulting in higher label accumulation per immunocomplex. This strategy, common in bioanalytical methods like ELISA and biosensing, is challenging to implement in LFIA due to its capillary-action-based design. Capillary-driven mass transfer becomes ineffective once the membrane is wetted during sample loading.<sup>23</sup>

To address this limitation, the Krylov lab proposes using electrophoresis to control the migration of conjugates. Electrophoresis-assisted migration permits controlled delivery of multiple conjugates to the test zone on a wet strip, overcoming the challenges of uncontrollable crosslinking and micrometer-sized aggregate formation associated with capillary action. This innovation enables the application of the signal amplification strategy within the LFIA framework, enhancing sensitivity and accuracy in detecting target analytes.<sup>23</sup>

The ensuing chapter, namely the second chapter, will offer proof of concept to ensure the developed technique of electrophoresis-assisted signal amplification works in principle by developing an assay for the Receptor-Binding Domain (RBD) antigen.

Furthermore, another concern of LFIA devices is the importance of maintaining the stability of nanoparticles and antibodies on the LFIA strips for long-term storage and transport. Ensuring that the components remain stable under various environmental conditions is challenging. In the trajectory of LFIA development, a pivotal objective involves the substitution of antibodies with aptamers which have higher stability and long shelf lives due to their unique features. Thus, the forthcoming third chapter will delve into the multifaceted challenges encountered in the process of aptamer selection.

### **1.3 Aptamers as Ligands**

Aptamers are single stranded oligonucleotides ligands which are a class of protein binders capable of target binding with high affinity and specificity. Aptamers are also capable of forming secondary structures like hairpin-like scaffold structures due to their distinctive intramolecular hydrogen bonding between their nucleobase complementarities.<sup>24</sup> Aptamers are considered as a substitute for antibodies and widely known as “chemical antibodies”. Aptamers have unique features compared to antibodies. Aptamers can retain their structures over repeated cycles of renaturation/denaturation maintaining higher thermal stability. Moreover, aptamers can easily be labeled, adjusted, and generated by chemical synthesis. Unlike antibodies, aptamers can discriminate between different conformations of the same target protein.<sup>25</sup> Since aptamers are nucleic acids not typically recognized by the human immune system as foreign agents, aptamers are neither immunogenic nor toxic molecules. Thus, aptamers are used as affinity probes in diagnostics and as drug candidates in therapeutic applications.<sup>26</sup>

### 1.3.1 Systemic Evolution of Ligands by Exponential Enrichment

Aptamers are typically obtained from highly random-sequence combinatorial oligonucleotide libraries using the general Systematic Evolution of Ligands by **EX**ponential Enrichment termed as SELEX which was developed by Larry Gold and Jack Szostak independently developed in 1990.<sup>27</sup> In vitro selection involves multiple rounds of partitioning in order to isolate aptamers from large libraries consisting of  $10^{12}$ - $10^{15}$  unique sequences. First the target and a library are mixed and incubated until equilibrium has reached. The next step would be partitioning the target bound ligands from non-binders followed by polymerase chain reaction (PCR) amplification of target-binders. The amplified target-bound sequences then serve as aptamer enriched feed for the subsequent round of selection until no further enrichment is observed (**Figure 2**).

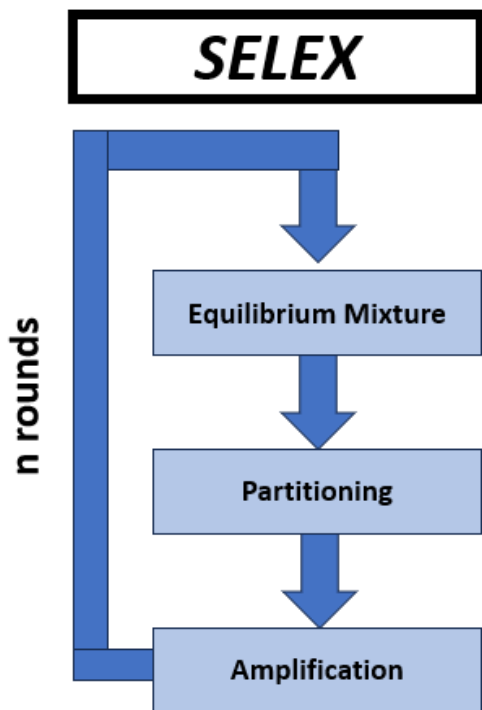


*Figure 2. Schematic representation of SELEX. The first step is preparing equilibrium mixture of ligand and target. The second step is partitioning ligand-target complexes followed by the third step of amplification of complex binders. The amplified target-bound sequences then serve as aptamer enriched feed for the subsequent round of selection.*

The most crucial yet difficult step of SELEX is the partitioning of potential aptamers from non-binders. Most common methods exist in aptamer selection are heterogenous methods such as affinity chromatography and filtrations where separation occur on a resin or filter, suffer from high background of non-binders due to non-specific binding and simultaneously losing high affinity aptamers. On the contrary, homogenous methods where the separation occurs in solution are more efficient separation methods. Hence, the efficiency of partitioning is crucial in successfully selecting high binding aptamers and minimizing the number of rounds required to isolate high affinity aptamers.<sup>28</sup>

### 1.3.2 Introduction to Capillary Electrophoresis

One of the common methods used as homogenous partitioning technique is capillary electrophoresis (CE). CE is a versatile and powerful analytical technique that offers high

resolution, sensitivity, and speed for the separation and analysis by taking advantage of variations in charge and size.<sup>29</sup> Its broad applicability and ability to handle a wide range of analytes make it an indispensable tool in modern analytical chemistry and bioanalytical research. The central principle of CE is that analytes are separated based on their ability to move with different velocities in the presence of electric field which can be illustrated by the following equation 3.

$$v = \mu E \quad 3$$

Where  $v$  is velocity,  $\mu$  is an electrophoretic mobility of a given macromolecules and  $E$  is the function of an applied electric field.

The typical CE setup consists of a capillary placed in a cartridge, two platinum electrodes submerged with one end in an inlet and the other end in an outlet containing running buffer reservoirs. The high voltage supply (1-30 kV) is connected to each electrode supplying electric field which makes the analytes migrate from the anode to the cathode end of the electrodes subsequently resulting in the creation of electroosmotic flow (EOF). EOF carries molecules across the capillary in different velocities to detection window equipped with UV or laser-induced fluorescence (LIF) system that is located near the outlet. Depending on the charge of the molecules, molecules can move faster, slower, or along with EOF. The outcome of the detection window can be read in an electropherograms which is two-dimensional spectrum computer interface which plots the signal versus the migration time of the analytes as shown in **Figure 3**. Overall, the CE set-up is a well-coordinated arrangement of components, each serving a specific purpose to achieve accurate, efficient, and high-resolution separation of analytes.

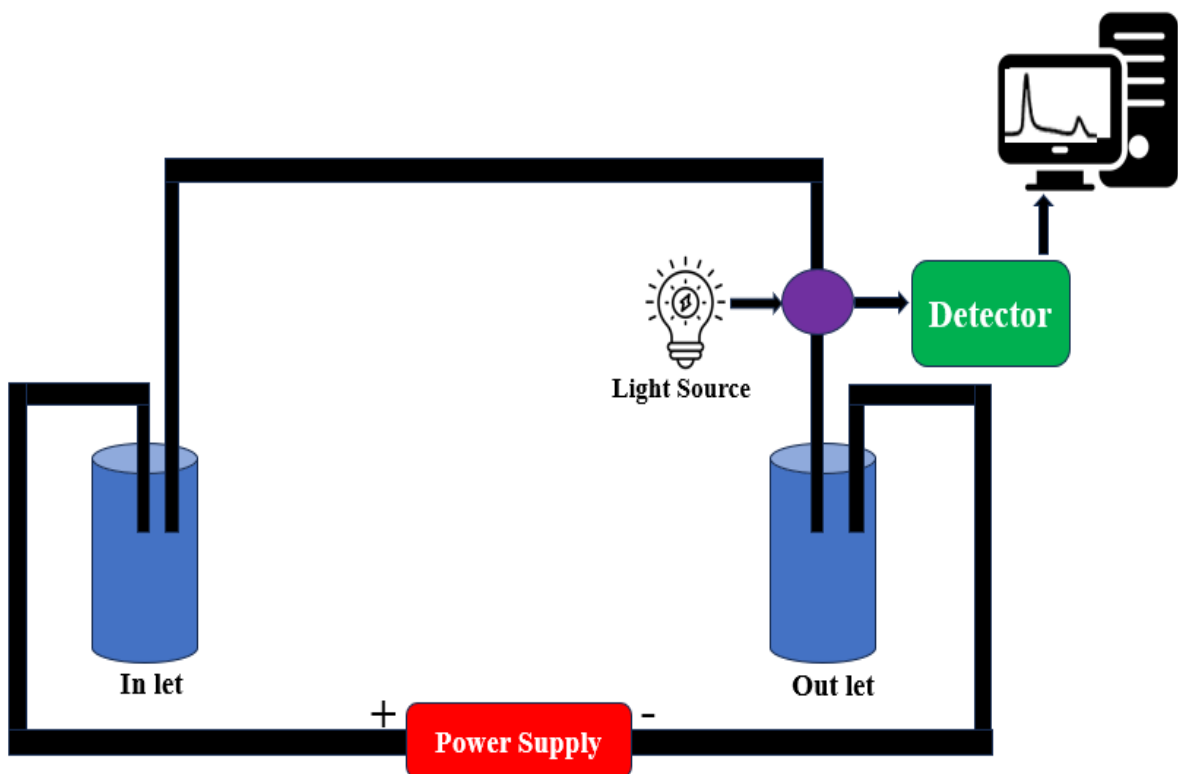


**Figure 3.** Schematic representation of the basic capillary electrophoresis instrumental set-up. The typical CE setup consist of a capillary placed in a cartridge, two platinum electrodes submerged with one end in an inlet and the other end in an outlet containing running buffer reservoirs.

### 1.3.3 Capillary Electrophoresis-based Selection

The success of aptamer selection highly depends on the efficiency of partitioning tool used. CE is powerful separation tool in selecting aptamers from a homogenous equilibrium mixture facilitating SELEX process. Due to unique electrophoretic velocities of molecules in CE, target-bound deoxyribonucleic acid (DNA) libraries can be efficiently partitioning from unbound DNA molecules. Moreover, DNA libraries are highly negatively charged molecules compared to the less negatively charged target bound DNA molecules which provides adequate resolution and separation window. In early 2000's, the Krylov lab developed CE-based selection that elucidate kinetic and equilibrium constants via a method known as kinetic capillary electrophoresis

(KCE).<sup>30</sup> KCE-based partitioning enabled characterization of binding affinities and minimized the number of rounds required from more than 10 rounds to 3-4 rounds. Moreover, aptamer selection involving modified library which typically does not require PCR amplification can also be executed via KCE-based methods in a technique known as “Non-SELEX” approach.<sup>31</sup>

A highly efficient KCE-based technique was also developed by the Krylov Lab in 2002 which is known as non-equilibrium capillary electrophoresis of equilibrium mixtures (NECEEM). In NECEEM, sample is prepared by mixing and incubation of target and ligand in equilibrium mixture. The sample is then injected and migrate across the capillary which results in the formation of three distinct zones; non-binding ligand, target-ligand complex and target zone (**Figure 4**).<sup>32</sup> For better resolution, the ligand is usually fluorescently labelled and two of the mentioned zones linked by a dissociation region of ligand, can be detected via LIF detection system.

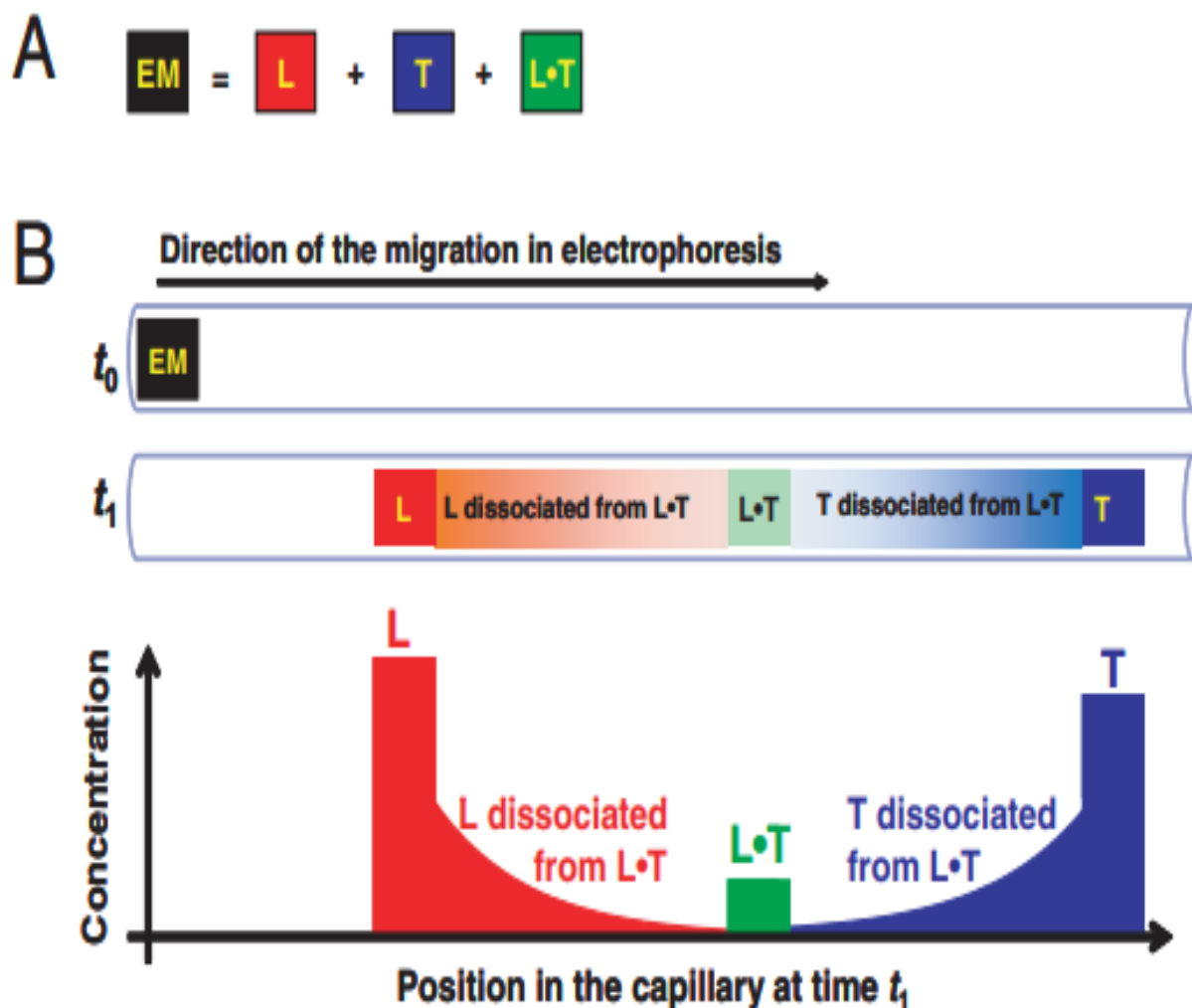


**Figure 4.** Schematic of Non-Equilibrium Capillary Electrophoresis of Equilibrium Mixtures. Where EM stands for equilibrium mixture, L stands for ligand, T stands for target, and L·T stands for target-ligand complex. A) Ligand and target combined to form the equilibrium mixture. B) Capillary electrophoresis experiment separating the plug of EM within a capillary filled with background electrolyte that is not in equilibrium with EM. This setup causes dissociation of L·T during the separation of the three components of the EM. Adapted from Krylov, S.N. Non-equilibrium capillary electrophoresis of equilibrium mixtures (NECEEM): a novel method for biomolecular screening. *Journal of Biomolecular Screening* 2006, 11, 115–122. doi.org/10.1177/1087057105284339.

The resulting electropherogram also will be used to determine the optimum collection window of the target-ligand bound complexes. The collected fraction is then subjected to PCR amplifications and purifications. The enriched sequence pools are then later used as a feed in the subsequent rounds. NECEEM-based SELEX can be performed until the 3rd or 4<sup>th</sup> rounds until

the pool with desired binding affinity is obtained. The pool is finally sequenced and will be subjected to binding kinetic studies to elucidate its binding constants by calculating the peak areas in electropherograms in binding affinity assays.

In the upcoming third chapter, an in-depth examination will be undertaken to address the paramount challenges inherent in the selection of aptamers. This endeavor will be facilitated through the utilization of model proteins as discerning benchmarks. Specifically, the pivotal focus will be on delineating the critical considerations surrounding the determination of optimal target concentrations for aptamer selection. Furthermore, the chapter will propose a workflow on the strategic significance of effectively monitoring the trajectory of selection progress throughout this complex process.

# **CHAPTER 2. PROOF OF PRINCIPLE FOR ELECTROPHORESIS-ASSISTED MULTILAYER ASSEMBLY OF NANOPARTICLES FOR SENSITIVE LATERAL FLOW IMMUNOASSAY**

## **2.1 Introduction**

The RBD of SARS-CoV-2, the virus responsible for COVID-19, is a crucial component located on the spike protein's surface. This domain is primarily responsible for binding to the host cell's angiotensin-converting enzyme 2 (ACE2) receptor, enabling the virus to enter the host cell. The RBD's specific interaction with the ACE2 receptor is pivotal in facilitating viral entry and subsequent infection.<sup>33</sup> Given its significance in the infection process, the RBD has become a key target for diagnostics and therapeutic interventions. Moreover, detecting the RBD can help distinguish SARS-CoV-2 from other coronaviruses and respiratory viruses, ensuring accurate diagnosis.<sup>34</sup> Thus, early detection is crucial for timely isolation and appropriate medical care, which can help control the spread of the virus.

In the beginning of COVID-19 outbreak, the most used tests for COVID-19 were reverse transcription polymerase chain reaction (RT-PCR) and immunoassays. The choice of test depends on the specific clinical situation: RT-PCR is more accurate, reliable, and ideal for asymptomatic cases, but it is more expensive and time-consuming while immunoassays particularly LFIA are less sensitive but are faster, less expensive, and can be used for rapid screening in large populations.<sup>35</sup>

Recent years have witnessed significant progress in boosting signal amplification for developed LFIA. These advancements include the introduction of various labels such as silver enhancement technology, gold nanorods, and the incorporation of carbon and magnetic

nanomaterials combined with enzymes like horseradish peroxidase. While these approaches support the improvement of quantification systems, it's worth noting that their synthesis processes can be intricate and costly. Consequently, colloidal GNP has emerged as a prominent choice for LFIA. This is attributed to their distinctive optical properties, compatibility with various biomolecules, stability, cost-effectiveness, and straightforward synthesis.<sup>36</sup>

Additionally, optimizing the sensitivity of GNP for LFIA of viral infections is crucial to ensure accurate and reliable detection, especially in cases where viral loads are low. Our lab recently developed novel technique using electrophoresis driven multilayer assembly of nanoparticles which significantly increased the sensitivity of LFIA for Hepatitis B surface antigen without compromising specificity.<sup>23</sup> The improvement was attained through the implementation of signal amplification techniques, intended to enhance the distinct signal stemming from the interlinked immunocomplexes. This process entails the deliberate movement of biotin- and streptavidin-functionalized GNP along the test strip via electrophoresis. The nanoparticles connect to immunocomplexes and each other, forming multiple layers of aggregates on the test strip, thereby amplifying the signal. This, in turn, enhances the binding capability of antibodies and increases the efficiency of capturing the target analyte.<sup>23</sup>

Following the pandemic there is a growing need for more enhanced devices that can offer improved sensitivity, specificity, and reliability. In this chapter therefore, we develop an assay for the detection of SARS COV2 RBD protein using our recently developed technique of electrophoresis-driven LFIA and referred as enhanced LFIA in short.

### 2.1.1 Working principle of enhanced LFIA

LFIA is an affordable and portable diagnostic tool leveraging GNP as a colorimetric marker to detect target proteins in a sample. As described in the preceding section, a standard LFIA strip comprises four key components: a sample pad, a conjugate pad, an absorbent pad, and a NC (as depicted in **Figure 1**).

The process begins with the application of the sample onto the sample pad, facilitating interaction with the biotinylated secondary antibodies (GNP- Ab<sub>B</sub>) probe located on the conjugate pad. The sample pad effectively enables the binding of the target analyte which is SARS-CoV-2 RBD antigen from the sample analyte to the capture probe GNP- Ab<sub>B</sub> on the conjugate pad. When the RBD antigen is captured by the specific RBD GNP- Ab<sub>B</sub> probe, a complex form and migrates along the NC towards the detection zone.<sup>36</sup>

On the NC, two lines are present: the anti-RBD-Ab (primary Ab against RBD) as the test line and protein G as the control line. These lines facilitate colorimetric analysis and are observable to the naked eye. The control line's appearance confirms the proper functionality of the test strip. Additionally, the absorbent pad is situated at the strip's opposite end to maintain liquid flow via capillary action and prevent backflow.

The second step of the assay involves enhancement through electrophoresis. Following the initial LFIA, the strip terminals are immersed in two reservoirs containing an electrolyte solution and electrodes. Given that GNPs are negatively charged, the cathode is positioned at the loading terminus of the membrane. A voltage is applied, and a drop of GNP-streptavidin conjugate (GNP-Str) is loaded first, followed by GNPs conjugated with GNP- Ab<sub>B</sub>, and so forth.<sup>23</sup> It's important to note that GNP- Ab<sub>B</sub> is utilized in the standard LFIA (as depicted in

**Figure 5A)** to label the antigen in the test zone. Each of the two GNP conjugates undergoes electrophoretic movement towards the anode terminus of the membrane. Within the test zone, these conjugates interact with preassembled sandwich immunocomplexes (comprising anti-RBD-Ab: RBD antigen: GNP- Ab<sub>B</sub>), leading to the formation of multilayer aggregates. Any excess, unreacted GNP conjugates are electrophoretically moved beyond the test zone. The color intensity of the test line and control line, both before and after enhancement, is further assessed using the TotalLab TL120.<sup>23</sup>

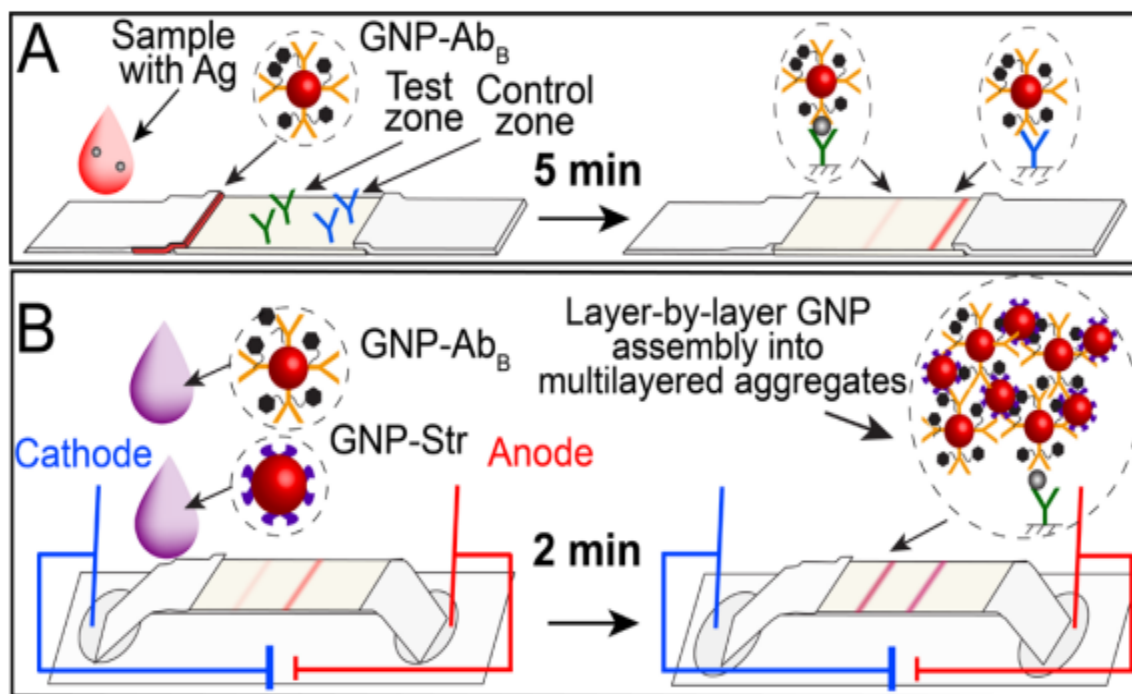


**Figure 5.** Schematic depiction of both conventional and enhanced LFIA. (A) conventional LFIA and (B) enhancement step performed after completion of LFIA by means of electrophoretically assisted layer-by-layer assembly of gold nanoparticles (GNPs). The antigen (Ag) is present in the sample. The biotinylated capture probe antibody against the antigen (GNP-Ab<sub>B</sub>) is represented by the color yellow. The primary antibody (anti-RBD-Ab), immobilized in the test zone, is depicted as the color green. The color blue represents protein G, which is immobilized in the control zone. Adopted from Panferov, V.G.; Ivanov, N.A.; Mazzulli, T.; Brinc, D.; Kulasingam, V.; Krylov, S.N. Electrophoresis-assisted multilayer assembly of nanoparticles for sensitive later-flow immunoassay. *Angewandte Chemie International Edition* 2023, 62(2), e202215548.

## 2.2 Materials and Methods

**2.2.1 Chemicals and Materials.** All chemicals and buffer components were purchased from Sigma-Aldrich (Oakville, ON, Canada). Goat-anti-mouse anti-species antibodies (Cat no. ABGAM-0500) and protein G (Cat no. AGPTG-0101) were purchased from Arista Biologicals (Allentown, PA, USA). SARS-COV-2 Spike RBD-His Recombinant protein (Cat no. 40592-V08B), SARS-COV-2 Spike RBD antibody, chimeric monoclonal (Cat no. 40150-D003) and SARS COV 2 Spike RBD antibody, rabbit polyclonal (Cat no. 40150-T30) were purchased from SinoBiological (Wayne, PA, USA). NC (Millipore 75), cellulose absorbent pads (Millipore C083), and glass-fiber membranes (Millipore G041) were purchased from Millipore (Billerica, MA, USA).

**2.2.2 Synthesis of GNP.** GNP were synthesized by the reduction of  $\text{HAuCl}_4$  with sodium citrate.<sup>37</sup> All glassware was washed with aqua regia. MilliQ water (50 mL) was mixed with 25 %  $\text{HAuCl}_4$  (20  $\mu\text{L}$ ) and heated to the boiling point during continuous mixing. After boiling started, 1% sodium citrate (1 mL) was injected, and the mixture was boiled for 30 min. An Allihn condenser was used to avoid water evaporation during synthesis. Synthesized nanoparticles were stored at  $+4^\circ\text{C}$ . The synthesized GNP was characterized using transmission electron microscope (Hitachi HT7700 TEM) at University of Toronto.

**2.2.3 Biotinylating antibodies.** For the biotinylation, monoclonal antibodies (6  $\mu\text{M}$ ) in 20 mM 4-(2-hydroxyethyl)-1-piperazineethanesulfonic acid (HEPES) buffer pH 7.5 were mixed with 15-molar excess of biotinamidohexanoyl-6-aminohexanoic acid N-hydroxysuccinimide ester and incubated for 2 hrs at room temperature. After the incubation, biotinylated antibodies were purified from the excess of activated biotin ester using Amicon centrifugal filters with cut-off 100 kDa provided by Sigma Aldrich (Oakville, ON, Canada). Biotinylated antibodies were

stored at 4°C in 10 mM tris(hydroxymethyl)aminomethane (Tris) buffer containing 0.02% sodium azide, pH 8.<sup>23</sup>

**2.2.4 GNP-Ab Conjugation.** Physical adsorption of proteins was used for the conjugation with GNP. For conjugation with streptavidin (GNP-Str), the pH of GNP was adjusted to 6.5 using 0.5 M K<sub>2</sub>CO<sub>3</sub>, and streptavidin was added to the final concentration of 10 µg/mL. The mixture was incubated for 2 hrs, for another 10 min after the addition of 2 mg/mL bovine serum albumin (BSA), and particles were concentrated by centrifugation 16,000×g for 15 min at 4°C. The conjugates were redispersed in MilliQ water containing 0.02% sodium azide and were stored at 4°C.<sup>23</sup> For conjugation with biotinylated antibodies (GNP-Ab<sub>B</sub>), the pH of GNP was adjusted to 9.5 using 0.5 M K<sub>2</sub>CO<sub>3</sub>, and antibodies were added to the final concentration of 12 µg/mL. Incubation and centrifugation of conjugates were like the above-described streptavidin conjugates.

**2.2.5 Assembly of test strips.** A custom reagent dispenser consisting of a syringe pump “Pump 11 Elite” from Harvard Instruments (Holliston, MA, USA) and a 3D moving platform from Sain Smart Genmitsu CNC router machine was used. For RBD assay, monoclonal antibodies were dispensed as the test line, protein G was dispensed as the control line. The antibodies and protein G were diluted by 20 mM sodium phosphate buffer, pH 7.5 to the final concentration of 0.5 mg/mL and dispensed at a rate of 1.5 µL/cm. For RBD assay, conjugate of GNP with biotinylated monoclonal antibodies was diluted with 20 mM Tris-acetate, pH 7.6, 1% BSA, 0.5% lactose, 0.05% NaN<sub>3</sub>, 0.03% SDS to OD<sub>520 nm</sub> = 0.6 measured in a cuvette with a 1-mm optical pathlength. The fiberglass membrane (width 4 mm) was soaked with the diluted conjugate (2.5 µL per mm of length) and dried at room temperature for 12 hrs. Cellulose and fiberglass membranes were glued to a NC. The membranes were cut manually to the test strips

with a width of 4 mm and stored at room temperature in zip pockets. Manufacturing of test strip holder Holders of test strips for electrophoresis were designed in Solid Edge (Siemens Digital Industries Software) and fabricated of poly(methyl methacrylate) plastic according to our previously developed fabrication procedure.<sup>38</sup> The holders were fabricated using MODELA MDX-540 Benchtop Milling Machine from Roland DGA (Irvine, CA, USA). Platinum wires electrodes (0.25 mm) were inserted into the buffer reservoirs on both sides. Solid Edge files of the holders' geometry are available as supporting materials.<sup>23</sup>

### **2.2.6 Conventional and enhanced LFIA.**

**Step 1. Conventional LFIA.** Conventional and enhanced LFIA was performed for RBD protein diluted by 50 mM sodium borate buffer, pH 8.1, containing 0.1% casein, 0.05% tween 20. For the conventional LFIA, test strips were vertically immersed in the sample (100  $\mu$ L) and incubated for 5 min. After 5 min incubation, the test strips were scanned using Epson V600 scanner, and digital images of the test strips were used for the quantification of test zone color intensity using TotalLab TL120 from Nonlinear Dynamics (Newcastle, UK). The acquired digital images underwent a transformation into grayscale mode and were subsequently subjected to analysis employing the 1D gel analysis mode within the software interface. Focused attention was directed towards the delineation of rectangular regions proximal to the test zone, while areas beyond the test zone were systematically replaced to establish a suitable background for each individual test strip. The quantification of the colorimetric signal was effectuated through the computation of the ratio between the volume and area values pertinent to the designated zone. The calibration plots were obtained as the function of the measured colorimetric signals (relative units, RU) versus RBD concentrations (ng/mL) using OriginPro 2021 from OriginLab corporation (Northampton, MA, USA). The limit of detection (LOD) of the assay was

determined as RBD concentrations corresponding to the value of the colorimetric signal of the test zone deducted from a value of blank samples.

**Step 2. Enhanced LFIA.** The test strips from the conventional assay for RBD protein were used in the enhanced LFIA. The ends of the test strips were immersed into two wells containing running buffer (the same as used for the conventional LFIA) and Pt-wire electrodes. The voltage was applied (current was limited to 1 mA) using electrophoresis power supply EPS 3501 from Amersham Pharmacia Biotech (Amersham, UK). Each of the GNP-Str and GNP-Ab<sub>B</sub> conjugates was diluted with the running buffer to OD<sub>520 nm</sub> = 0.4 measured in a cuvette with a 1-mm optical pathlength. First, GNP-Str was introduced (1.5 μL), followed by the same volume of GNP-Ab<sub>B</sub>. The colorimetric signals of test zones and LOD were evaluated as described above for the conventional LFIA.<sup>23</sup>

## 2.3 Results and Discussion

### 2.3.1 Synthesis of GNPs, Antibody Conjugation, and its Characterization

Our first task was to synthesis GNP and validate the desired size of GNP. The size of GNP can significantly affect the process of antibody conjugation and the resulting performance of the conjugated nanoparticles. Even though the use of larger GNP is desirable, the use of large GNP is hindered by poor migration through porous membranes.<sup>39</sup> Comparing to larger GNP, smaller nanoparticles can provide higher surface area and higher antibody density, resulting in improved sensitivity, but they may also be more prone to aggregation issues.<sup>40</sup> Thus, we characterized the GNP and conjugates. The synthesized GNP did not show any signs of aggregation using TEM and the average size of GNP were measured to be  $18.8 \pm 1.2$  nm, **Figure 6**.

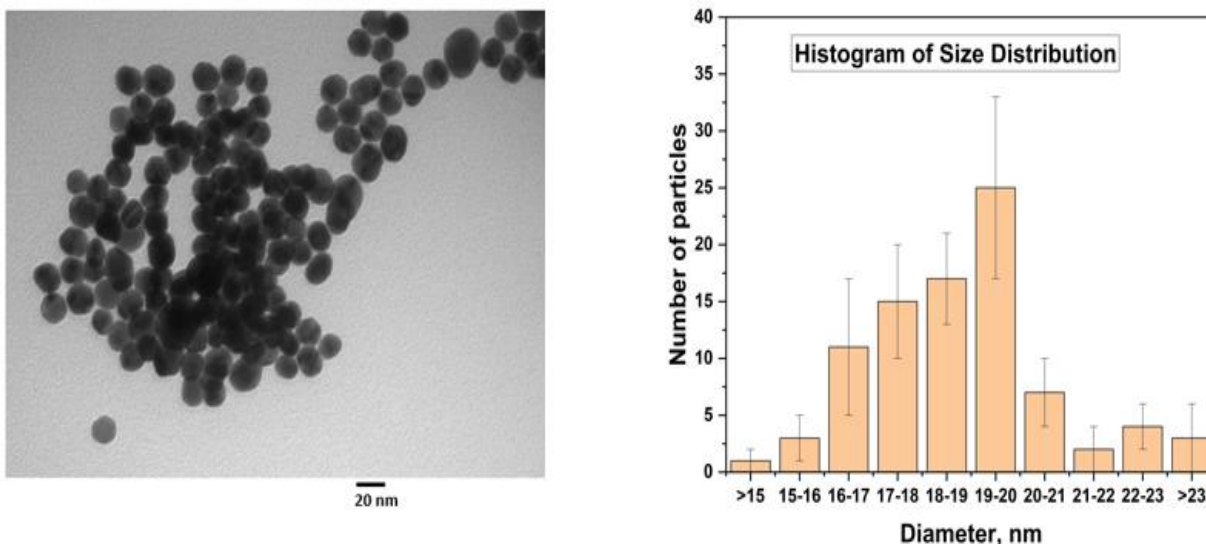


**Figure 6.** Characterization of GNP. Microphotograph of GNP taken by TEM and histogram of size distribution for GNP, mean diameter of  $18.8 \pm 1.2$  nm.

The next step after the synthesis of GNP is antibody conjugation. An effective conjugation method should preserve the colloidal stability of GNP while maintaining the antigen recognition capability of the Ab-GNP conjugates. Antibody conjugation can be achieved either through physical adsorption or chemisorption.<sup>41</sup> Physisorption primarily relies on attractive forces such as electrostatic interactions, hydrophobic interactions, hydrogen bonding, and van der Waals forces between GNPs and antibodies. It stands out as the simplest and most direct method for conjugation, requiring minimal expertise in surface chemistry. Its simplicity stems from the fact that there's no need for chemical modification of either the antibody or the GNPs.<sup>42</sup>

During the creation of Ab-GNP conjugates via physical adsorption, several key parameters come into play: (a) the antibody's isoelectric point (pI), (b) the pH of the reaction, and (c) the quantity of antibody added. Generally, it is widely acknowledged that proteins are most effectively adsorbed when the pH is in proximity to, or slightly higher than, their pI. Therefore, various pH levels are typically tested to identify the optimum pH for conjugation. However, it's worth noting that many antibodies tend to achieve maximum adsorption at a pH of 9.<sup>43</sup> For successful

development of stable and sensitive Ab-GNP conjugates for immunoassays, optimum conjugation conditions should be studied in advance by plotting a flocculation curve. A flocculation curve is used to evaluate the aggregation behavior of Ab-GNP under high ionic strength salts like NaCl. It helps determine the optimal conditions for stability and sensitivity in immunoassays.<sup>44</sup> In order to plot the curve, first a set of Ab-GNP, ranging from high to low concentration of antibodies were prepared and flocculation was observed which is visible aggregation or clumping of nanoparticles, which can be seen as changes in the color or turbidity of the solution after the addition of NaCl. Then, the absorbance or optical density (OD) of the nanoparticle suspension was measured at each dilution using a plate reader. Finally, the curve is plotted with the measured absorbance values against the antibody concentration to identify the optimal concentration range for stable and non-aggregated Ab-GNP. Hence, to determine the optimum concentration of antibody conjugation, goat anti mouse anti species antibody conjugate was studied. The pH of GNP was adjusted to pH 9 which is around the pI of the antibody and after serial dilution of the antibody was added, absorbance was measured as shown in **Figure 7A**. Two other GNP pH 4 and 6 were also explored, showing clear evidence of aggregation therefore discarded as shown in **Figure A1**. At the end the flocculation curve that corresponds to pH 9 was plotted and, the optimum concentration was identified as 12 µg/mL as shown in **Figure 7B**.

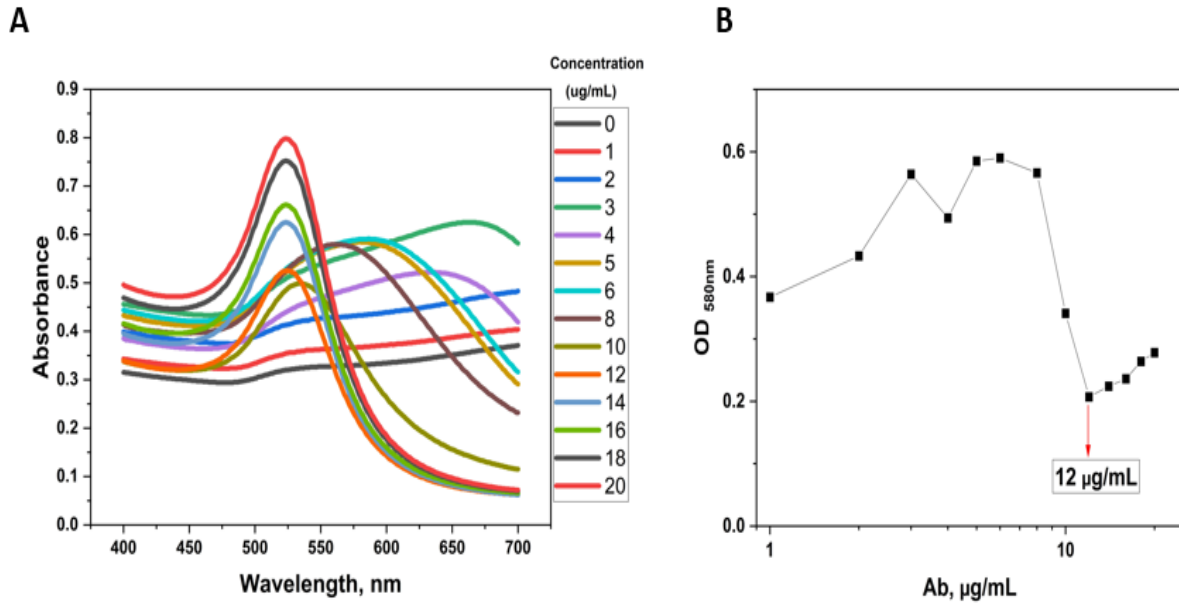


**Figure 7.** Optimum conjugation conditions of antibodies. A. OD of the nanoparticle suspension measured at each dilution for goat-anti-mouse anti-species antibody conjugates using UV-Vis spectroscopy B. The concentration of Ab was measured at the OD of 580 nm to plot flocculation curve.

Based on our results then, we preceded with the conjugation of RBD monoclonal antibody. Moreover, synthesized conjugates were found to be stable with no signs of aggregation detected during their preparation. Aggregated conjugates could also be identified by showing two light absorption maxima which also is associated with the color change of the solution.<sup>45</sup> The OD of the antibody and streptavidin conjugates was measured using spectrophotometer as shown in **Figure 8.**

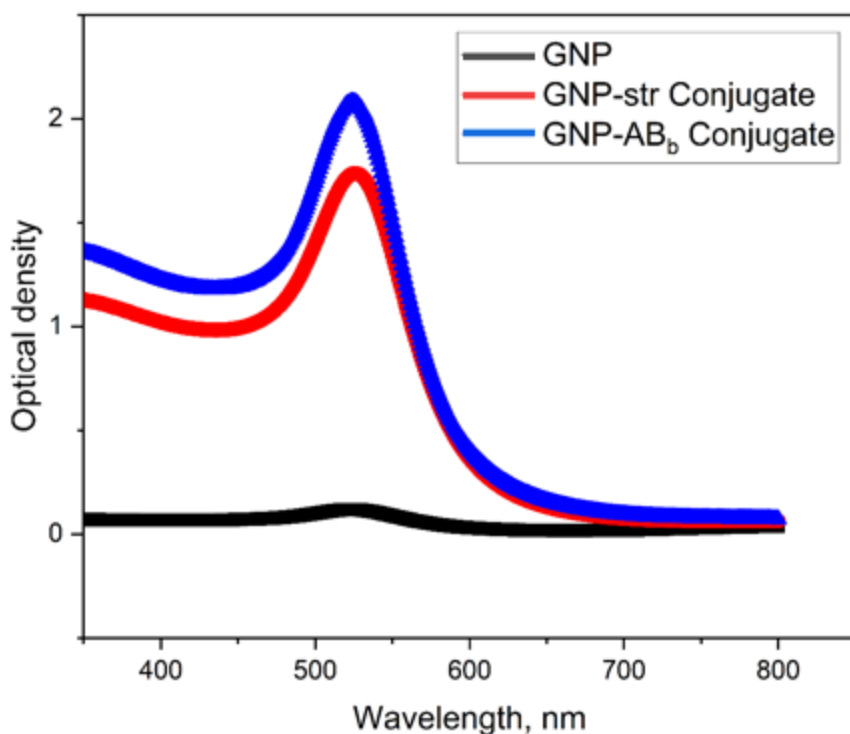


*Figure 8. Optical spectra of nanoparticles. The synthesized GNP and the corresponding antibody and streptavidin conjugates were analyzed for stability using spectrophotometer.*

### 2.3.2 Optimization of different parameters of the immunoassay

LFIA strips comprise a range of distinct components, each possessing characteristic properties that vary according to the specific detection method and underlying principles. In our optimization process, our endeavor aimed at augmenting the assay's specificity. The chosen approach for the assay design entails the immobilization of polyclonal antibodies on the membrane while employing monoclonal antibodies in the composition of the Ab-GNP conjugates. Monoclonal antibodies, being the product of a single type of immune cell, exhibit an exceptional level of specificity, primarily recognizing a sole epitope on an antigen. Conversely, polyclonal antibodies are generated from a blend of diverse immune cells, enabling them to recognize a spectrum of epitopes on an antigen.

This distinctive strategy was adopted due to its inherent advantages, notably in terms of

broader coverage and flexibility. Polyclonal antibodies on the membrane offer the capacity to capture a multitude of epitopes on the target antigen, thereby extending the scope of coverage and enabling the detection of diverse antigen variants. This attribute becomes particularly pertinent in scenarios involving the detection of SARS-CoV-2 antigens, as the pathogen has exhibited numerous outbreaks stemming from distinct viral variants. The specificity of the antibodies was verified with western blot experiments and interestingly we were also able to detect the binding of Ab-GNP conjugates in the western blot experiments as illustrated in **Figure A2**. However, it is imperative to acknowledge that the approach of using polyclonal antibodies on the membrane and monoclonal antibodies on the conjugates does present certain limitations. It can be susceptible to potential cross-reactivity and the generation of high background signals from non-specific binding events. Consequently, our strategy for enhancing specificity encompasses the identification of optimal blocking reagents and the fine-tuning of antibody-conjugate concentrations.

The identification of an effective blocking agent for the NC is critical for mitigating potential negative interactions. This process plays a pivotal role in standardizing the samples prior to their interaction with the test and control lines. Moreover, the application of a blocking agent serves to prevent non-specific binding and promote the reproducibility of the LFIA. Consequently, two distinct blocking reagents, namely 1% BSA and 1% Polyvinyl alcohol (PVA), were employed to determine the optimal blocking agent. While milk-based proteins, like skim milk, are commonly utilized to minimize non-specific binding, their potential interference with the biotin-streptavidin-based assay configuration led us to exclude them in favor of BSA, a more refined protein, and PVA, a synthetic polymer.

Treatment of the membrane with BSA resulted in the most pronounced intensity band within the control lines and minimal non-specific binding within the test line as shown in **Table**

1. Further increases in BSA concentration did not yield a subsequent reduction in non-specific binding and extending the duration of the blocking step to overnight led to a significant increase in non-specific binding.

**Table 1.** The Influence of Nitrocellulose Blocking with PVA and BSA Reagents. The NC was treated with immobilized antibodies in 10 mM PBS along with varying concentrations and durations of PVA (1% for 1 hr at RT) and BSA (1% for 2 hrs at RT, 1% overnight at 4°C, 5% for 2 hrs at RT, and 5% overnight at 4°C). Subsequently, the membrane was washed with ddH<sub>2</sub>O, dried, and inserted in 50 mM PBS, pH 7.4 buffer, followed by the assessment of the colorimetric signal at the test zone to gauge the extent of non-specific signal. All tests were performed in duplicates.

Blocking Reagent	1% PVA (Blocked for 1 hr )	1% BSA (Blocked 2 hrs )	5% BSA (Blocked 2 hrs)	1% BSA (Blocked for overnight at 4°C)	5% BSA (Blocked for overnight at 4°C)
CZ →  TZ →					
Colorimetric signal, RU (TZ)	4.9 ± 1.6	2.7 ± 1.0	2.5 ± 0.1	13.5 ± 6.7	18.6 ± 9.3

Furthermore, an additional critical factor influencing the sensitivity of LFIA is the quantity of labeled-reaction antibody conjugates administered on the conjugate pad. The observed color intensities at both the test and control lines are directly associated with the abundance of labeled-reaction antibodies. The quantity of captured labeled-antibody on these lines corresponds directly to the initial amount of labeled reaction antibody conjugates applied to the conjugate pad.<sup>46</sup> To quantify the concentration of the antibody or the quantity of conjugated GNP in the solution, the OD of the antibody conjugate is measured. Studies have demonstrated that an excessively high

OD may lead to signal saturation without enhancing sensitivity, while an excessively low OD might result in weak signals that are challenging to detect.<sup>47</sup> The optimal conjugate OD was determined to be  $OD_{520nm} = 0.6$ , as measured in a cuvette with a 1-mm optical path length, in accordance with Panferov et al. in 2023. Therefore, for the all experiments, we maintained the use of  $OD_{520nm} = 0.6$  and focused on optimizing the assay buffer to mitigate any instances of non-specific binding.

In the subsequent series of experiments, our objective was to explore the potential of reducing non-specific binding by incorporating BSA into the assay buffer. Despite introducing additional blocking detergents alongside BSA, we noted an extensive occurrence of non-specific binding. These findings suggested that the presence of BSA on both the NC and within the assay buffer resulted in undesirable crosslinking, subsequently influencing the precision and specificity of the assay. Comparable outcomes were observed when substituting BSA with casein for membrane blocking and assay buffer use (see **table 2**). Considering our goal to minimize the risk of non-specific interactions among sample components and other assay materials, including the sample pad, in addition to the NC, our approach was to solely employ BSA in the assay buffer.

**Table 2.** The impact of various buffer compositions in a blocked NC and a non-blocked NC. The assessment of the colorimetric signal at the test zone to determine the extent of non-specific signal. All tests were performed in duplicates.

NC Blocking Reagent	1% BSA (Blocked for 2 hrs)	1% BSA (Blocked for 2 hrs)	1% BSA (Blocked for 2 hrs)	1% BSA (Blocked for 2 hrs)	1% BSA (Blocked for 2 hrs)	N/A	N/A	N/A	N/A	N/A
CZ TZ										
Buffer Composition	50 mM sodium borate pH 8.1, 0.1 % triton X-100, 1% BSA	50 mM sodium borate pH 8.1, 0.1 % triton X-100, 1% BSA, 0.05% tween 20	50 mM sodium borate pH 8.1, 0.1 % triton X-100, 1% BSA, 0.05% tween 20, 0.1% casein	50 mM sodium borate pH 8.1, 0.05% tween 20, 0.1% casein	50 mM PBS pH 7.4, 0.05% tween 20, 1% Casein	50 mM sodium borate pH 8.1, 0.1 % triton X-100, 1% BSA	50 mM sodium borate pH 8.1, 0.1 % triton X-100, 1% BSA, 0.05% tween 20	50 mM sodium borate pH 8.1, 0.1 % triton X-100, 1% BSA, 0.05% tween 20, 0.1% casein	50 mM sodium borate pH 8.1, 0.05% tween 20, 0.1% casein	50 mM PBS pH 7.4, 0.05% tween 20, 1% Casein

As illustrated in **table 2**, while PBS represents the optimal buffer owing to its compatibility with biological samples, stable ionic strength, and suitable pH and buffering capacity, its high conductivity rendered it unsuitable for the enhanced LFIA. This implies that the addition of biotinylated antibodies and streptavidin during the enhancement step would result in accelerated movement without ample opportunity to bind to immunocomplexes (refer to calibration **Figure 9**).

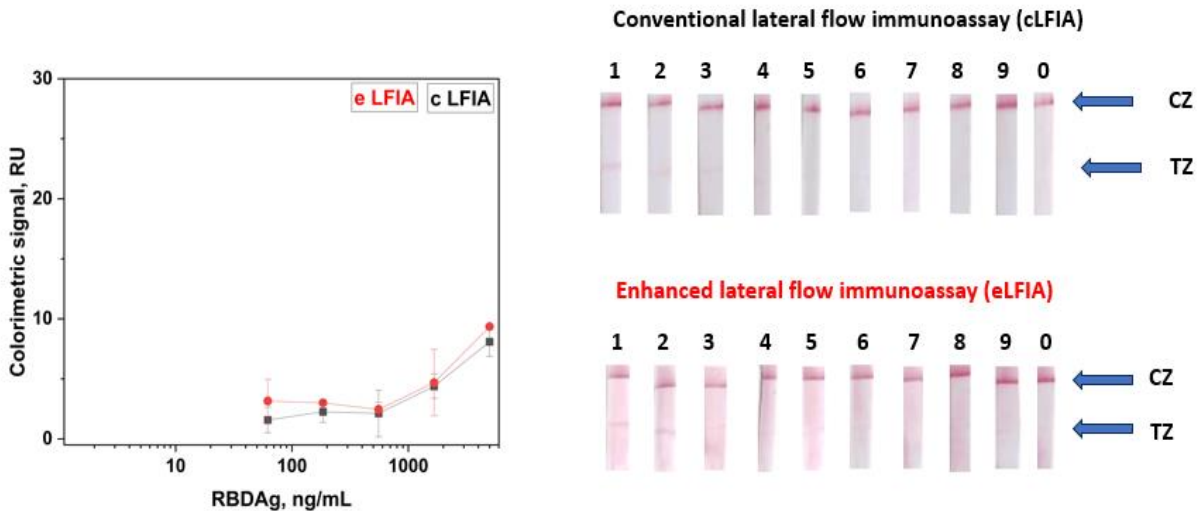


**Figure 9.** LFIA of varying concentrations of RBD antigen using PBS assay buffer supplemented with 0.05% tween 20 and 1% casein. Semilogarithmic calibration plot and images of test strips for conventional LFIA and enhanced LFIA. The numbers above the test-strip images correspond to concentrations of RBD in ng/mL: 1 – 5000, 2 – 1666.6, 3 – 555.5, 4 – 185.2, 5 – 61.7, 6 – 20.6, 7 – 6.9, 8 – 2.3, 9 – 0.8, and 0 – blank.

Given the lower conductivity associated with borate buffer, we undertook both conventional and enhanced assays, employing two distinct compositions of borate buffer supplemented with varying blocking reagents. Titration experiment using borate buffer produced promising outcomes, showcasing evident enhancement. However, the first titration, incorporating borate containing triton and BSA, yielded heightened sensitivity along with increased non-specific binding, ultimately reducing the LOD of the RBD antigen from 185 ng/mL in the conventional assay to approximately 8 ng/mL in the enhanced assay as shown in **Figure 10**.

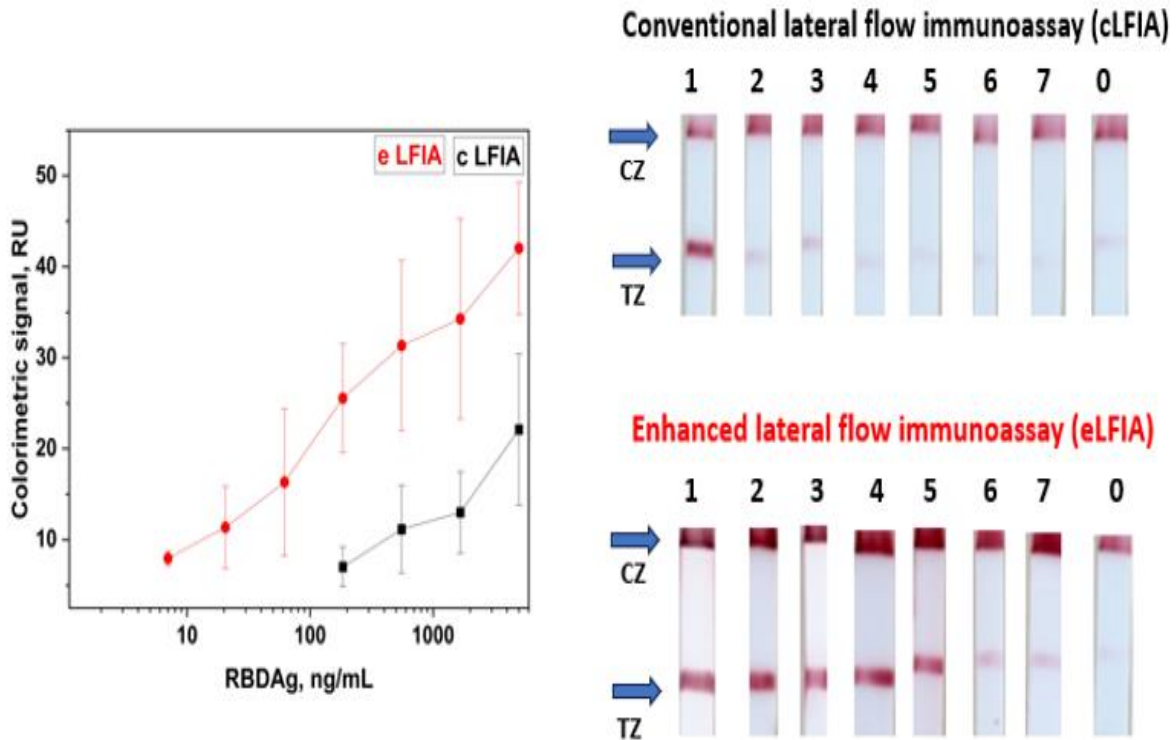


**Figure 10.** LFIA of varying concentrations of RBD antigen using borate assay buffer supplemented with 1% BSA and 0.1% triton x-100. Semilogarithmic calibration plot and images of test strips for conventional LFIA and enhanced LFIA. The numbers above the test-strip images correspond to concentrations of RBD in ng/mL: 1 – 5000, 2 – 1666.6, 3 – 555.5, 4 – 185.2, 5 – 61.7, 6 – 20.6, 7 – 6.9, and 0 – blank.

In contrast, the second titration experiment as illustrated in **Figure 11**, involving borate buffer containing tween 20 and casein, while existing non-specific binding induced by slow migration during the enhancement step, the enhancement step managed to reduce the LOD by 77%

which is an LOD of 62 ng/mL of the RBD antigen in the conventional assay, compared to around 0.8 ng/mL in the enhanced assay which is comparable to the recent reported LFIA LOD for RBD antigen.<sup>36</sup> Thus, the experiment effectively showcased the technique's functionality.

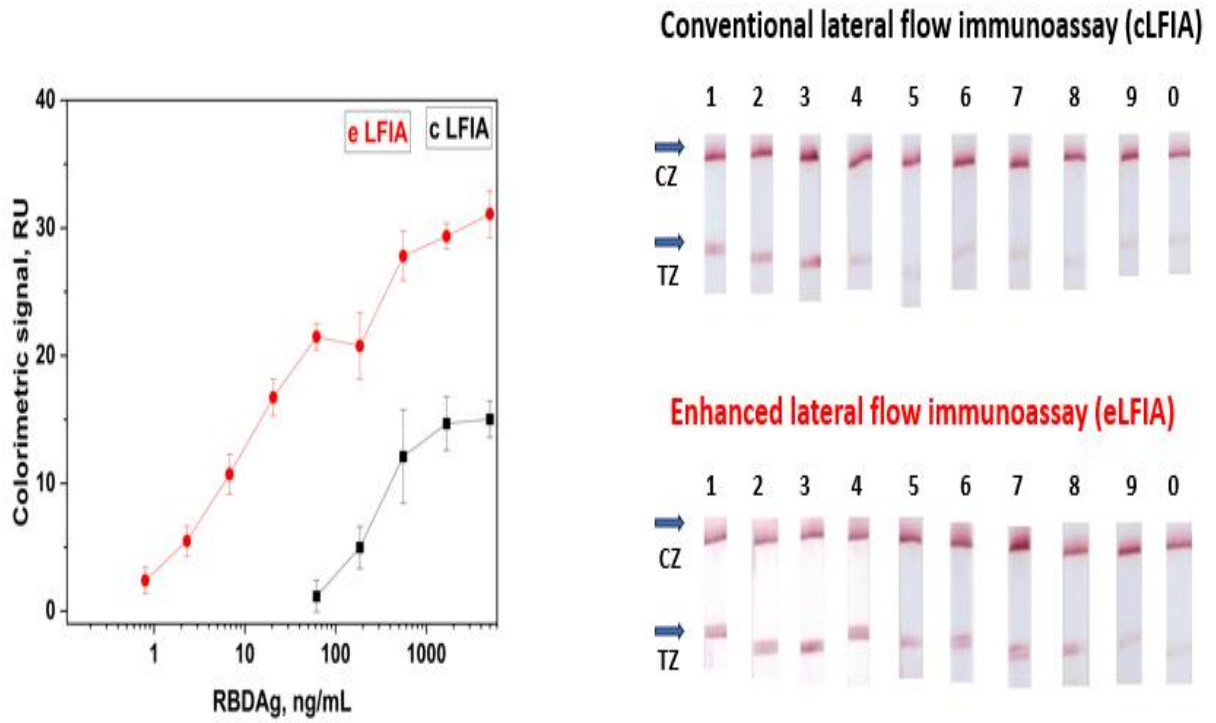


**Figure 11.** LFIA of varying concentrations of RBD antigen using borate assay buffer supplemented with 0.05% tween 20 and 0.1% casein. Semilogarithmic calibration plot and images of test strips for conventional LFIA and enhanced LFIA. The numbers above the test-strip images correspond to concentrations of RBD in ng/mL: 1 – 5000, 2 – 1666.6, 3 – 555.5, 4 – 185.2, 5 – 61.7, 6 – 20.6, 7 – 6.9, 8 – 2.3, 9 – 0.8, and 0 – blank.

## **2.4 Conclusion**

In this work we have validated the enhanced LFIA technique by developing an assay for RBD antigen for proof of concept. The technique allows for lower detection limits, improved signal intensity, and enhanced sensitivity, making it a promising approach for ultrasensitive LFIA applications in various infectious disease diagnostics and analytical settings. Further developments besides replacing of antibodies with aptamers, aim at the validation of conventional and enhanced LFIA in clinical samples (saliva, sputum) and comparison of the qualitative and quantitative results with clinically approved PCR methods/kits.

## CHAPTER 3. INFLUENCE OF BULK AFFINITY AND TARGET CONCENTRATION IN APTAMER SELECTION

### 3.1 BULK AFFINITY ASSAYS IN APTAMER SELECTION: CHALLENGES, THEORY, AND WORKFLOW

The presented material was published previously and reprinted with permission from “**Teclmichael, E.**; Le, A.T.H.; Krylova, S.M.; Wang, T.Y.; Krylov, S.N. Bulk Affinity Assays in Aptamer Selection: Challenges, Theory, and Workflow. *Analytical Chemistry* 2022, 94(44), 15183–15188.” Copyright 2022 American Chemical Society.

My contributions to the article were: (i) performing all presented experiments, (ii) preparing all figures, (iii) interpreting results, and (iv) writing and editing manuscript. The theoretical background and model proposed were done by Dr. Sergey N. Krylov.

#### 3.1.1 Introduction

Aptamers are single-strand oligonucleotides capable of tightly binding to targets for which they have been selected.<sup>48,49</sup> Aptamers selected for protein targets can serve as affinity probes and therapeutic agents.<sup>50,51,52,53,54,55,56,57</sup> Aptamers are selected from random-sequence oligonucleotide libraries using their ability to bind to the target as a driver of selection. A common aptamer-selection process involves repetitive rounds of four major steps. In step 1, a ssDNA library is reacted with the target to form target–DNA complexes (target–binder complexes).<sup>58,31</sup> In step 2, the complexes are partitioned from the unbound oligonucleotides and collected. In step 3, the collected oligonucleotides are amplified and purified to obtain a large amount of the binder-enriched ssDNA library. Finally, in step 4, the progress of selection is

assessed.<sup>59,60</sup> While being a “service” step, the assessment of selection progress is of critical importance as its results are used to decide on whether to proceed to the next round or to stop.

Methods used for assessment of the selection progress can be categorized into two types: nonaffinity assays and bulk affinity assays. Nonaffinity assays follow the change in melting temperature during the selection process to assess library diversity.<sup>61,62</sup> These assays assume that the decreasing diversity unconditionally correlates with increasing fitness of the library for binding to the target, which is not true. In contrast, bulk affinity assays assess library binding to the target and, thus, are a preferable analytical tool for assessing the progress of aptamer selection.<sup>63</sup> Despite their importance, bulk affinity assays lack any theoretical foundation, and this limitation imposes a problem: theoretical and experimental uncertainties that can lead to misinterpretation of the selection results. This work focuses on bulk affinity assays in aptamer selection. Bulk affinity assays are procedurally similar to the classic affinity assay used for the determination of the equilibrium dissociation constant  $K_d$  of a target–ligand complex (TL) formed in the binding reaction of a target (T) and a ligand (L):



4

Yet, there is a fundamental difference between these two classes of assays. Classic affinity assays analyze a single complex characterized by a single  $K_d$  value, which is a thermodynamic constant independent of ligand and target concentrations. In contrast, bulk affinity assays are to assess the affinity of a highly heterogeneous pool of oligonucleotide ligands characterized by a wide scope of  $K_d$  values. A single parameter determined for a heterogeneous pool using the formal rules of  $K_d$  determination is not a thermodynamic constant; for example, it depends on the ligand and target concentrations. Therefore, we call it here an equilibrium pseudo

constant  $\bar{K}_d$ . The dependence of  $\bar{K}_d$  on concentrations questions both the validity and the utility of  $\bar{K}_d$  as a measure of bulk affinity. This dependence makes less obvious the advantage of  $\bar{K}_d$  over the other parameter, which is intrinsically concentration dependent: fraction  $R$  of the unbound (or bound) library. Both  $\bar{K}_d$  and  $R$  are used as affinity measures in the bulk affinity assays without scientific justification. Accordingly, the goal of this work was to consider a theoretical foundation for the bulk affinity assays. Specifically, we intended to compare theoretical grounds for using  $R$  and  $\bar{K}_d$ . Our theoretical analysis suggests  $R$  as a preferable measure of bulk affinity. Because  $R$  is concentration dependent, we worked out an algorithm for choosing a suitable constant library concentration and for adjusting the target concentration with the progress of selection. The application of this bulk affinity-assay algorithm was demonstrated experimentally in a de novo selection of DNA aptamers for MutS protein using CE for partitioning of the target-bound oligonucleotides from free oligonucleotides.

### **3.1.2 MATERIALS AND METHODS**

**3.1.2.1 Chemicals and Materials.** All chemicals and buffer components were purchased from Sigma-Aldrich (Oakville, ON, Canada) unless otherwise stated. All solutions were prepared in deionized water filtered through a 0.22- $\mu\text{m}$  Milipore filter membrane (Nepean, ON, Canada). Fused-silica capillaries with inner and outer diameters of 75 and 360  $\mu\text{m}$ , respectively, were purchased from Molex Polymicro (Phoenix, AZ, USA). Recombinant His-tagged MutS protein (MW  $\approx$  93 kDa, pI 5.67) was purchased from Prospec Protein Specialist (Ness-Ziona, Israel). All DNA molecules were custom synthesized by Integrated DNA Technologies (Coralville, IA, USA). Polymerase chain reaction (PCR) reagents Q5<sup>®</sup> High-Fidelity 2 $\times$  Master Mix, Q5<sup>®</sup> Reaction Buffer, deoxynucleotide solution mix were purchased from New England BioLabs (Whitby, ON, Canada) and SYBR Green was purchased from Thermo Fisher Scientific

(Rockford, IL, USA). MinElute PCR purification kit was purchased from Qiagen (Toronto, ON, Canada). The CE running buffer was 50 mM Tris-HCl pH 8.0. The sample buffer was always the same as the running buffer to avoid the adverse effects of buffer mismatch. Accordingly, all dilutions of sample components in CE experiments were done by adding the same running buffer.

**3.1.2.2 DNA Sequences.** All DNA stock solutions were subjected to annealing by incubating at 90°C for 2 min before cooling it to 20°C at a rate of 0.5°C/s, prior to dilution and preparation of equilibrium mixtures. We used a synthetic FAM-labeled DNA library (N40) with a 40-nt random region: 5'-FAM-CTC CTC TGA CTG TAA CCA CG-N40-GCA TAG GTA GTC CAG AAG CC-3'. For qPCR, the sequence of forward and reverse primers are as follows: 5'-CTC CTC TGA CTG TAA CCA CG-3', and 5'-GGC TTC TGG ACT ACC TAG GC-3' respectively. For asymmetric PCR (aPCR), the fluorescently-labeled version of the forward primer was used instead, 5'-Alexa Fluor®488-CTC CTC TGA CTG TAA CCA CG-3'.

**3.1.2.3 CE Instrumentation.** All CE experiments were performed with a P/ACE MDQ apparatus from SCIEX (Concord, ON, Canada) equipped with a laser-induced fluorescence (LIF) detection system. Fluorescence was excited with a blue line (488 nm) of a solid-state laser and detected at 520 nm using a spectrally optimized emission filter system.<sup>64</sup> The poly (vinyl alcohol) (PVA)-coated capillaries were prepared as described elsewhere.<sup>65</sup> The total lengths of capillaries were 50 cm for bulk affinity assays and 80 cm for fraction collections; the distances to the detection window were 40 and 70 cm, respectively. Prior to every CE run, the PVA-coated capillaries were rinsed with the running buffer at 20 psi (138 kPa) for 3 min. The coolant temperature was set at 15°C.

**3.1.2.4 Fraction Collection.** In the first round of selection, the equilibrium mixture contains 10  $\mu\text{M}$  annealed DNA library and 100 nM His-tagged MutS. For later rounds, the equilibrium mixtures contain 330 nM binder-enriched library and 100 nM His-tagged MutS protein. The mixtures were all incubated for at least 30 min to reach equilibrium. The equilibrium mixture was injected into the capillary by a pressure pulse of 1 psi (6.9 kPa)  $\times$  28 s. The sample plug was propagated by a pressure pulse of 0.9 psi (6.2 kPa)  $\times$  45 s (yield a 5.4 cm-long buffer plug) to avoid the uncooled region of the capillary to the cooled region. Partitioning was carried out using reversed polarity (anode at the outlet) at 25 kV for 28 min followed by pressure propagation of buffer at 5 psi (34.5 kPa) for 1 min to elute the His-tagged MutS–DNA complex into a collection vial containing 20  $\mu\text{L}$  of the running buffer. A total of five rounds of selection were conducted.

**3.1.2.5 PCR Procedures and Generation of Binder-Enriched DNA Library.** The collected binder-enriched library was amplified and quantitated by two rounds of qPCR using CFX Connect<sup>TM</sup> instrument (Bio-Rad, ON, Canada). qPCR reagent mixture was prepared to obtain final concentrations of 1 $\times$  Q5<sup>®</sup> High-Fidelity 2 $\times$  Master Mix, 1 $\times$  SYBR Green, unlabeled 500 nM forward primer and unlabeled 500 nM reverse primer. Before thermocycling, qPCR reaction mixture was prepared by adding a 2  $\mu\text{L}$  aliquot of the collected fraction to 18  $\mu\text{L}$  of the qPCR reagent mixture. The PCR thermocycling protocol is as follows: 98  $^{\circ}\text{C}$  for 30 s (initialization, performed once), 98  $^{\circ}\text{C}$  for 10 s (denaturation), 65  $^{\circ}\text{C}$  for 20 s (annealing), and 72  $^{\circ}\text{C}$  for 20 s (extension), followed by a plate read at 72  $^{\circ}\text{C}$  and a return to the denaturation step for a total of 40 cycles. All qPCR reactions were performed in duplicate. In the first round of qPCR, the collected fraction was quantitated using an eight-point standard curve. An S-shaped amplification curve was plotted, and in the second round of the qPCR, the qPCR product was removed two cycles into the exponential phase of the amplification curve. After qPCR, 100  $\mu\text{L}$  of the qPCR product was later purified using the MinElute PCR purification kit as per manufacturer's recommendation (**Note B1**).

The purified double stranded DNA product was then subjected to aPCR strand separation using the following procedure. Initially, aPCR reagent mixture was prepared to obtain the final concentrations of 1× Q5® Reaction Buffer, 1 μM Alexa Fluor®488 labelled forward primer, 50 nM unlabelled reverse primer, 200 μM deoxynucleotide solution mix. Before thermocycling, aPCR reaction mixture was prepared by adding a 5 μL aliquot of the qPCR product to 45 μL of the aPCR reagent mixture. The aPCR thermocycling protocol is as follows: a single step of initiation at 98 °C for 30 s followed by 18 cycles of denaturation at 98 °C for 10 s, annealing at 65 °C for 20 s, extension at 72 °C for 20 s, and fluorescence plate reading at 72 °C. The fluorescently-labeled single stranded DNA product of aPCR was purified using the MinElute PCR purification kit as per vendor's instructions (**Note B1**).

The concentration of the purified DNA product was determined by measuring its fluorescence intensity with the NanoDrop™ 3300 Fluorospectrometer (Thermo Fisher Scientific, Wilmington, DE, USA) at 519 nm and converting fluorescence intensity into DNA concentration using a standard curve built using serial dilutions of fluorescently-labeled forward primer (2,000, 1,000, 500, 250, 125, 62.5, and 31.25 nM). The purified aPCR product was then used for the next round of partitioning.

**3.1.2.6 Bulk Affinity Assays.** Equilibrium mixtures of 1 nM of DNA library and varying target concentrations were prepared and incubated at room temperature for a minimum of 30 min prior to injection. The sample was injected to the capillary inlet by a pressure pulse of 0.5 psi (3.4 kPa) × 20 s. The sample plug was propagated by a pressure pulse of 0.9 psi (6.2 kPa) × 45 s (yield a 5.4 cm-long buffer plug) to avoid the uncooled region of the capillary.<sup>66</sup> Separation was carried out at 25 kV with reversed polarity (anode at the outlet) for 15 min.

### 3.1.3 Results and Discussions

#### 3.1.3.1 Definitions of $R$ and $\bar{K}_d$ .

Fraction  $R$  of unbound library is defined as:

$$R = [L] / [L]_0 \quad 5$$

where  $[L]$  is the concentration of unbound library at equilibrium and  $[L]_0$  is the total concentration of the library.

Equilibrium pseudo-constant  $\bar{K}_d$  is a parameter determined using the formal rules utilized for the determination of a true  $K_d$  value. Finding  $K_d$  and, thus,  $\bar{K}_d$  requires a set of  $R$  values obtained for single  $[L]_0$  but different  $[T]_0$  (total concentration of target). The unknown  $\bar{K}_d$  is found by varying it while fitting a theoretical expression for  $R$  into an experimental dependence of  $R$  on  $[T]_0$  (typically termed a binding isotherm):

$$R = -\frac{\bar{K}_d + [T]_0 - [L]_0}{2[L]_0} + \sqrt{\left(\frac{\bar{K}_d + [T]_0 - [L]_0}{2[L]_0}\right)^2 + \frac{\bar{K}_d}{[L]_0}} \quad 6$$

It is important to re-emphasize that  $\bar{K}_d$  is calculated based on values of  $R$ . Hence,  $R$  is a primary parameter determined experimentally, while  $\bar{K}_d$  is a secondary parameter.

#### 3.1.3.1 Requirement for Complete Separation of L from TL in Bulk Affinity Assays.

The general procedure of a bulk affinity assays starts with preparing the equilibrium mixture of the library and the target. Then, two signals are measured from this mixture: one is a cumulative signal from all unbound ligands ( $S_L$ ) and the other one is a cumulative signal from all the bound ligands ( $S_{TL}$ ). This measurement is done *via* physical or spectral separation of L from TL. The separation is complete if the peaks or spectra do not overlap, and the separation is

incomplete if they do overlap. The choice of a signal processing approach depends on whether or not L and TL are completely separated.

Complete separation of L from TL allows one to express  $R$  for given total concentrations of the target,  $[T]_0$ , and the library,  $[L]_0$ , through the two signals:<sup>67</sup>

$$R = \frac{[L]}{[L]_0} = \frac{S_L}{S_L + S_{TL} / \varphi}$$

7

there  $\varphi$  is a coefficient of signal changes when L bind T, *e.g.*, the quantum yield of TL relative to that of L.

If separation of L from TL is incomplete, then only a cumulative signal  $S$  from them can be measured. If the signals from L and TL do not interfere (which is true in most detection modes), then the cumulative signal follows the principle of superposition:<sup>68,69</sup>

$$S = S_L \frac{[L]}{[L]_0} + S_{TL} \frac{[TL]}{[L]_0}$$

8

In this case, the fraction of unbound ligand can still be determined, but with a formula which includes three signals:

$$R = \frac{S - S_{TL}}{S_L - S_{TL}}$$

9

Using this formula requires measuring signals from pure L ( $S_L$ ) and pure TL ( $S_{TL}$ ) along with the signal from their mixture ( $S$ ). Measuring  $S_L$  is trivial; it is the signal from the ligand in the absence of the target. Measuring  $S_{TL}$  requires that  $[TL] \gg [L]$  which is achieved (when a single ligand is studied instead of a heterogeneous library) *via* using a saturating total concentration of the target:

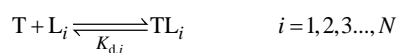
$$[T]_0 > K_d \gg [L]_0$$

where  $K_d$  characterizes this ligand. The problem is that in a bulk affinity assay the saturating concentration is theoretically unachievable as the library may contain individual ligands with  $K_d \rightarrow \infty$  (nonbinders). The above consideration leads to an important practical conclusion: bulk affinity assays require that L and TL be completely separated from each other either spectrally or physically.

### 3.1.3.2 Suitability Criterion for Quantitative Measures of Bulk Affinity.

It is useful to define a criterion which a quantitative measure of bulk affinity should satisfy to adequately characterize the affinity of the library to the target. We assume that the library is composed of  $N$  unique oligonucleotides, and that every oligonucleotide in the library is a ligand capable of binding the target and forming a complex.  $K_d$  values of such complexes theoretically range from 0 to  $\infty$  to cover the entire library. The library is thus composed of  $N$  unique ligands. In a bulk affinity assay, the library is mixed and incubated with the target to reach equilibrium in a complete set of  $N$  binding reactions for  $N$  unique ligands:

11



We postulate that to be suitable for a bulk affinity assay, a quantitative measure of affinity  $X$  must satisfy the principle of superposition:

12

$$X_{\text{sup}} = X_{L_1} \frac{[L_1]_0}{[L]_0} + X_{L_2} \frac{[L_2]_0}{[L]_0} + \dots + X_{L_N} \frac{[L_N]_0}{[L]_0}$$

In the other words,  $X$  for the library must be equal to a weighted sum of  $X$  values for each

individual ligand.

$R$  satisfies eq 12 by its very nature of being a fraction as illustrated in eq 5, in contrast,  $\bar{K}_d$  does not satisfy this criterion. Theoretical validation of superposition principle for  $R$  and  $\bar{K}_d$  is demonstrated in **Note B2**. Thus,  $R$  is a theoretically sound measure of bulk affinity while  $\bar{K}_d$  is not. The theoretical preference of  $R$  over  $\bar{K}_d$  does not mean that  $\bar{K}_d$  is invalidated as an acceptable parameter for bulk affinity assays, but it suggests strongly that  $R$  should be chosen over  $\bar{K}_d$  unless  $R$  has limitations weighing more than limitations of  $\bar{K}_d$ . Thus, while deciding on the practical preference, advantages and limitations of  $R$  and  $\bar{K}_d$  in bulk affinity assays should be considered.

### 3.1.3.3 Advantages and Limitations of $R$ and $\bar{K}_d$ in Bulk Assays.

$R$  is a primary parameter while  $\bar{K}_d$  is a secondary parameter depending not only on  $R$  but also on  $[L]_0$  and  $[T]_0$ . Hence,  $R$  can be determined, in general, more accurately than  $K_d$ . On the downside,  $R$  has two basic limitations as a measure of affinity: it intrinsically depends on both  $[L]_0$  and  $[T]_0$ , and it has a limited dynamic range (from 0 and 1).  $R$  can be made independent on  $[L]_0$  by choosing excess of the target:  $[T]_0 \gg [L]_0$ , but the dependence of  $R$  on  $[T]_0$  remains. Thus, using  $R$  as a measure of bulk affinity for monitoring round-to-round library enrichment only makes sense if there is a sound algorithm of choosing suitable  $[T]_0$ . Since it is impossible to choose *a priori*  $[T]_0$  which satisfies bulk affinity assays for all progressively enriched libraries, varying  $[T]_0$  will be required when using  $R$  as a measure of bulk affinity.

When eq 6 is used to determine a true thermodynamic constant,  $K_d$ , the resulting  $K_d$  convolutes values of  $R$  measured for different  $[T]_0$  which makes  $K_d$  a constant theoretically independent on  $[L]_0$  or  $[T]_0$ . This independence is a great advantage of  $K_d$  over  $R$ . However,  $\bar{K}_d$  is not a true thermodynamic constant and, thus, should depend on  $[T]_0$ , but, advantageously, this dependence must be much weaker than that of  $R$ . Another advantage of  $\bar{K}_d$  over  $R$  is its wide

dynamic range (from 0 to  $+\infty$ ). On the other hand, errors of true  $K_d$  can be very large when  $[L]_0/K_d > 1$ .<sup>70</sup> This disadvantage must translate into a similar disadvantage for  $\bar{K}_d$ .

Thus, using  $R$  and  $\bar{K}_d$  as measures of affinity in bulk assays have their advantages and limitations. A priori, we can summarize them as follows. Using  $\bar{K}_d$  is inferior from the theoretical rigorousness and accuracy standpoints, but provides a formalized way of convoluting data for  $R$  measured at different  $[T]_0$ . In contrast,  $R$  is a theoretically-sound bulk-affinity parameter that can be measured accurately, especially around  $R = 0.5$ . Using  $R$  potentially may require fewer experiments as no binding isotherms are needed (unlike calculation of  $\bar{K}_d$  with eq 6). Using  $R$  is, thus, should be preferred over  $\bar{K}_d$ , provided that a suitable algorithm of choosing  $[T]_0$  is found. Our next goal was, thus, to propose such an algorithm.

#### **3.1.3.4 Algorithm of Choosing $[T]_0$ in $R$ -Based Bulk Affinity Assay.**

We propose the following criteria while designing the algorithm. The accuracy for  $R$  measurements is the highest near the point  $R = 0.5$ ; therefore, it is ideal that  $[T]_0$  is adjusted to keep  $R$  values close to  $R = 0.5$ . On the other hand, a reasonably large range of acceptable  $R$  values is required to keep the number of  $[T]_0$ -adjustment experiments to the bare minimum.

The first bulk affinity assay is the one with the starting library (before enrichment). Typically, bulk affinity of such libraries is low and, therefore, it makes sense to start with the highest attainable value of target concentration denoted as  $[T]_{0,1}$  (1 stands for the first value of  $[T]_0$ ). It is expected that  $R > 0.5$  will be typically obtained for the starting library. Progressing enrichment will gradually lower the value of  $R$  measured at  $[T]_{0,1}$  to  $R < 0.2$ , where  $R$  measurements become unacceptably inaccurate. At this stage, target concentration should be decreased to  $[T]_{0,2}$  (e.g.,  $[T]_{0,2} = 0.1[T]_{0,1}$ ) in order to increase  $R$  to the optimum range of  $R$  values designated by us as  $0.3 < R < 0.7$ . Bulk affinity assays are carried out with  $[T]_{0,2}$  for the following

rounds of selection until  $R$  reaches the level of  $R < 0.2$  again, when target concentration should be further decreased to  $[T]_{0,3}$  (e.g.,  $[T]_{0,3} = 0.1[T]_{0,2}$ ). This process of gradual decrease of  $[T]_0$  should proceed with progress of selection until no change in  $R$  is detected in consecutive rounds of selection with the final  $R$  being in a range of  $0.3 < R < 0.7$ .

To visualize this algorithm, we simulated progressive library enrichment by constructing a virtual starting library of 24 oligonucleotides with the semi-log distribution of their  $K_d$  values.<sup>71</sup> The aptamer-enriched libraries would be progressively shifted to the left and become narrower while keeping the same semi-log nature of  $K_d$  distribution (**Figure 12**).

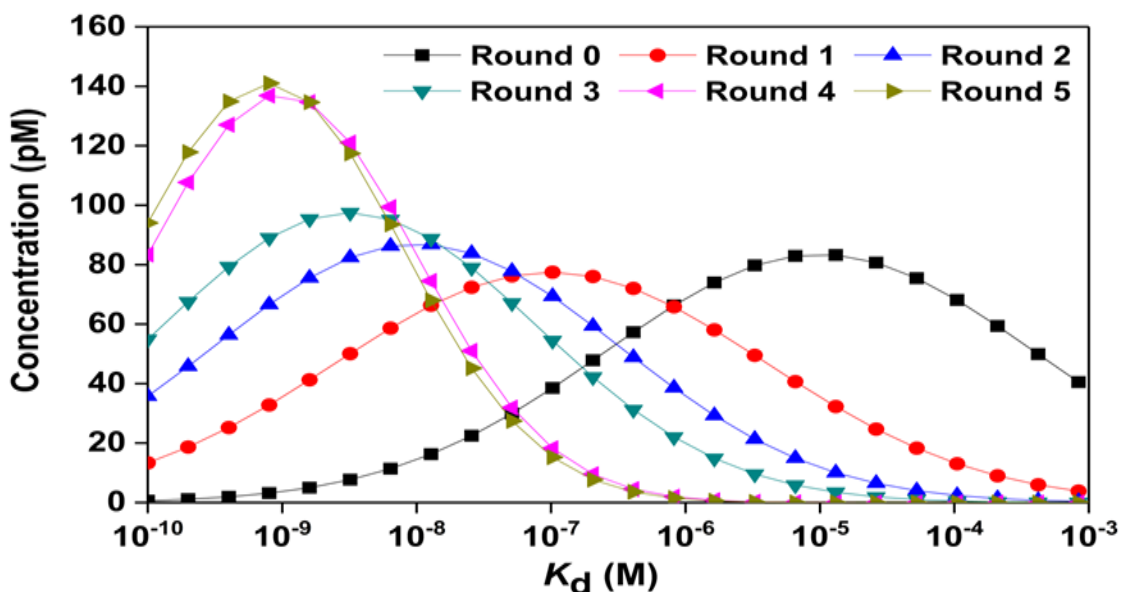


**Figure 12.** Modeled distributions of  $K_d$  values for progressive rounds of aptamer selection. The shape of all distributions was assumed to be Gaussian in semi-log coordinate.<sup>71</sup>

$R$  values for every ligand in the library was calculated with the following equation:

$$R = \frac{K_d}{[T]_0 + K_d}$$

which is obtained from a basic equation for  $K_d$ :<sup>72</sup>

$$K_d = \frac{[T]_0 - [L]_0(1-R)}{(1/R-1)}$$

under an assumption that  $[L]_0 \ll [T]_0$ . A bulk  $R$  value for the library was calculated using the superposition principle (eq 12). The details are shown in **Note B2**. Then, we used our algorithm of choosing/changing  $[T]_0$ . The details are shown in **Note B3**.

Using the theoretical model, we have simulated the dependency of  $R$  on multiple rounds of selection as shown in **Note B2**. A wide range of target concentrations (0, 0.1, 1, 10, 100, 1,000, and 10,000 nM) was considered to evaluate the optimum target concentration needed for bulk affinity assays. Usually, the bulk affinity of the starting library tends to be in micromolar range hence, a target concentration of  $[T]_{0,1} = 1,000$  nM was chosen as a starting concentration with  $R > 0.5$  as illustrated in **Figure 13**. After the second round, the  $R$  value for 1,000 nM falls below 0.2 and is deemed to be no longer accurate. Hence, the target concentration was reduced gradually by 10 folds to  $[T]_{0,2} = 100$  nM and later to  $[T]_{0,3} = 10$  nM until  $R$  value fell into the range of  $0.3 < R < 0.7$ . The enrichment of the libraries for the rest of the selection rounds after the second round was evaluated using  $[T]_{0,3} = 10$  nM until saturation was reached.

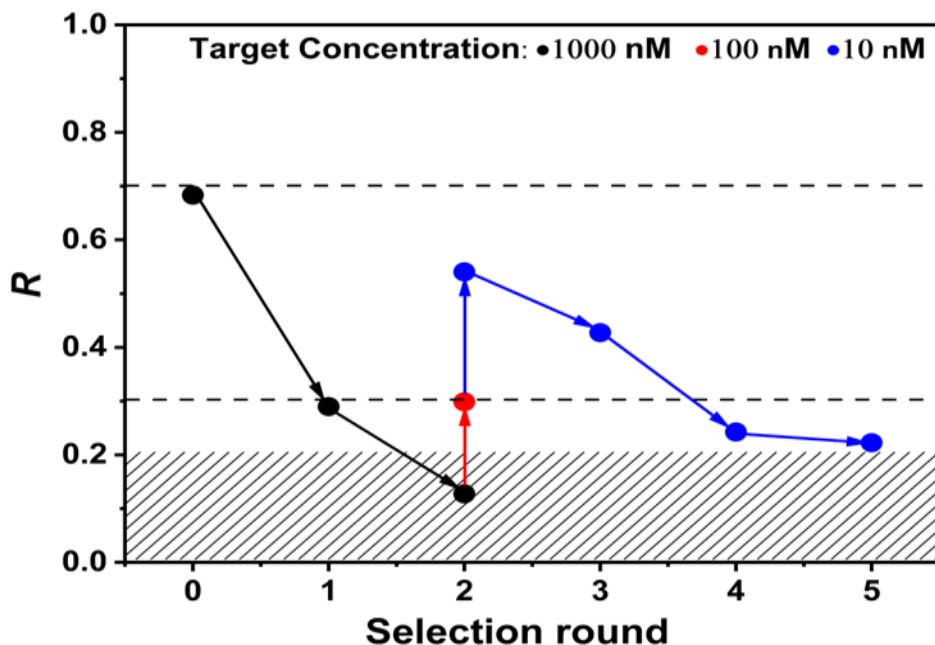


**Figure 13.** Proposed bulk affinity workflow.  $R$  value in the shaded region indicates the point where the target concentration needs to be decreased to the point where the  $R$  value falls between the dashed lines. From left to right, the points represent 1 nM DNA with: (i) 1,000 nM protein in rounds 0, 1, and 2 (black dots), (ii) 100 nM protein in round 2 (red dot), and (iii) 10 nM protein in rounds 2, 3, 4, and 5 (blue dots).

### 3.1.3.5 Experimental Demonstration of Proposed Bulk-Affinity Assay Algorithm.

We used the proposed algorithm of bulk affinity assay to guide selection of aptamers for MutS protein from a random-sequence DNA library by CE-based partitioning. The target was His-tagged MutS for which aptamers have not been previously selected. This His-tagged MutS was found to excessively adsorb to the fused-silica inner capillary wall (unlike the tagless MutS which is no longer commercially available). We found that using PVA-coated capillaries can largely reduce the protein adsorption to capillary walls.<sup>73</sup> Since PVA coating suppresses the electroosmotic flow, we applied the “complex-last” NECEEM mode for the aptamer selection.<sup>74</sup>

It is beneficial for affinity assays to use the lowest library concentration at which the signal to noise ratio (S/N) is still sufficiently high to ensure accurate  $R$  determination. To satisfy this condition, we chose  $[L]_0 = 1$  nM for all our bulk affinity assays. Five rounds (rounds 1–5) of aptamer selection were performed, and the random-sequence oligonucleotide library was

considered as the product from round 0. For the library obtained from each round of selection, bulk affinity assays were conducted in accordance with the theoretical proposed workflow. Specifically, for round 0, 1 and 2, the binding experiments were performed with using 1,000 nM protein. In round 2, the  $R$  value fell below 0.3, hence, the protein concentration was decreased in a stepwise fashion to 100 nM and 10 nM subsequently to reach the desired range of  $R$  values ( $0.3 < R < 0.7$ ). All experiments were performed in triplicate. The results of  $R$  values are summarized in **Figure 14** (see **Note B4** for detailed data analysis procedure). According to **Figure 14**, the saturation of selection was reached at round 4 and 5, since the  $R$  values obtained in these two rounds were greater than 0.2 and consistent within the uncertainties.

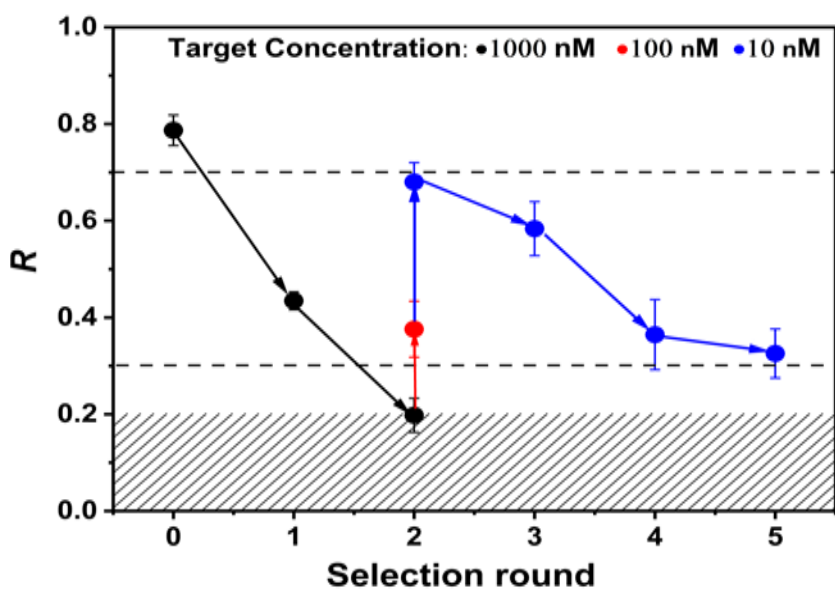


**Figure 14.** Experimental His-tagged MutS protein bulk affinity assay based on the proposed bulk affinity assay workflow.  $R$  value in the shaded region indicates the point where the target concentration needs to be decreased to the point where the  $R$  value falls between the dashed lines. From left to right, the points represent 1 nM DNA with: (i) 1,000 nM protein in rounds 0, 1, and 2 (black dots), (ii) 100 nM protein in round 2 (red dot), and (iii) 10 nM protein in rounds 2, 3, 4, and 5 (blue dots).

### 3.1.4 CONCLUDING REMARKS

To conclude, monitoring the progress of library enrichment is key to effective aptamer selection. Bulk affinity assays are the only analytical tool that can provide direct information about the fitness of the library for binding the target. Therefore, bulk affinity assays are preferred over

non-affinity assays. We demonstrated that a fraction  $R$  of unbound (bound) library is theoretically preferred over an equilibrium pseudo-constant  $\bar{K}_d$  as a measure of bulk affinity. Yet,  $R$  has three limitations: it depends on target concentration, its dynamic range is narrow (0 to 1), and its accuracy is poor when it is close to 0 or 1. To compensate these limitations, we propose an algorithm of target concentration change that keeps  $R$  within a range of 0.3 to 0.7. We demonstrated the use of this algorithm in a simulated aptamer selection as well as in experimental aptamer selection. Our approach allows one to avoid screening a wide range of target concentrations for every round and avoid very large errors associated with using a single target concentration for bulk affinity assays in all rounds of selection. We suggest this approach as conventional. Having a single approach used by different aptamer-selection teams would allow comparative analysis of selection progress.

## 3.2 INFLUENCE OF TARGET CONCENTRATION ON APTAMER SELECTION: EXPERIMENTAL STUDY

The presented material is a manuscript titled “Influence of Target Concentration on Aptamer Selection: Experimental Study” that is recently submitted to *Angewandte Chemie International* and currently under review.

“Le, A.T.H.; **Teclmichael, E.**; Krylova, S.M.; Krylov, S.N. Influence of target concentration on aptamer selection: experimental study. Under Review.”

My contribution to the manuscript was: i) performing experiments regarding the protein target MutS ii) interpreting results iii) preparing figures, and iv) editing the manuscript. The experiments regarding the protein target thrombin were performed by Dr. An Le who was also responsible for writing major part of the manuscript.

### 3.2.1 Introduction

Aptamers are oligonucleotides that can bind target tightly and selectivity via multiple non-covalent bonds.<sup>48,75</sup> Major applications of aptamers are diagnostic and therapeutic.<sup>50,51</sup> Aptamers are typically obtained from random-sequence oligonucleotide libraries in an iterative selection process termed SELEX.<sup>76</sup> SELEX comprises repeating rounds of three major steps (**Figure 15**). Step 1 is reacting to the starting library with the target to allow target-binding oligonucleotide (binders, denoted as *B*) to form complexes with the target while leaving target-nonbinding oligonucleotides (nonbinders, denoted as *N*) unbound. Step 2 is partitioning target–binder complexes from nonbinders. The partitioning is imperfect, i.e., the binders are always contaminated by nonbinders. Step 3 is amplifying, e.g., by the polymerase-chain-reaction (PCR),

all oligonucleotides collected in Step 2 to generate a binder-enriched library. This binder-enriched library is used in Step 1 of the next round of SELEX. The fitness of binder-enriched library for binding the target is tested in a bulk-affinity assay, and selection ends when the bulk binding stops improving significantly.

Target concentration is a key variable in SELEX for any given target and library, and it is broadly accepted that SELEX performance (e.g., round-to-round progress in binder enrichment) depends on target concentration.<sup>71</sup> However, the effect of target concentration on quantitative parameters of selection has never been studied experimentally owing to the complexity of such a study. While being conceptually simple, SELEX is very cumbersome and fails to select binders from non-modified oligonucleotide libraries in approximately 70% of attempts.<sup>49</sup> Completing one successful selection, i.e., obtaining aptamers, is an achievement on its own. Completing multiple successful selections for systematically varied target concentrations is objectively very difficult. Doing this for multiple targets would further multiply the difficulty. Performing such a study quantitatively, so that conclusive results could be obtained for the influence of target concentration on the quantitative characteristics of SELEX, is the ultimate leap.

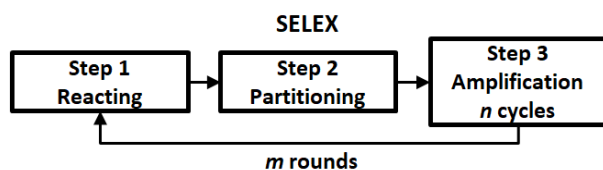


**Figure 15.** Schematic representation of SELEX. See text for details.

Whereas there are no experimental studies, there are multiple theoretical works on the effect of target concentration on aptamer selection.<sup>71</sup> However, all theoretical works unavoidably utilize hard-to-prove assumptions and fundamentally-unknown parameters thus leading to non-instructive and impossible-to-test conclusions. Our analysis of the literature on experimental

SELEX suggests that experimenters always choose target concentration arbitrarily — in this respect, SELEX is still more an art than a science. Accordingly, the goal of our work was to study the effect of target concentration on aptamer selection experimentally and draw conclusions which could help experimenters to rationalize their choice of target concentration in SELEX.

### **3.2.2 Materials and Methods**

**3.2.2.1 Materials and solutions.** All chemicals were purchased from Sigma-Aldrich (Oakville, ON, Canada) unless otherwise stated. Fused-silica capillaries with inner and outer diameters of 75 and 360  $\mu\text{m}$ , respectively, were purchased from Molex Polymicro (Phoenix, AZ, USA). Recombinant His-tagged MutS protein (MW  $\approx$  90 kDa, pI 6.0) was purchased from Prospec Protein Specialist (Ness Ziona, Israel). Recombinant human alpha-thrombin protein (MW  $\approx$  36.7 kDa, pI 6.4–7.6) was purchased from Fisher Scientific (Mississauga, ON, Canada). All DNA molecules were custom synthesized by Integrated DNA Technologies (Coralville, IA, USA). CE running buffers were 50 mM Tris-HCl pH 8.0 and 50 mM Tris-acetate pH 8.2 for MutS and thrombin selections, respectively. The sample buffer was always identical to the running buffer to avoid the adverse effects of buffer mismatches. Accordingly, all dilutions of sample components in CE experiments were done by adding the corresponding running buffer.

**3.2.2.2 DNA sequences.** All DNA stock solutions were subjected to annealing by incubation at 90 °C for 2 min before being cooled to 20 °C at a rate of 0.5 °C/s, prior to the dilution and preparation of the equilibrium mixtures. To avoid cross-contamination between the selections for two different protein targets, distinct synthetic fluorescein amidite (FAM)-labeled, 40-nt random DNA libraries (referred to as N40) with unique primer regions were used as follows: (i) for MutS: 5'-FAM-CTC CTC TGA CTG TAA CCA CG-N40-GC ATA GGT AGT CCA GAA GCC-3', and (ii) for thrombin: 5'-FAM-CTA CGG TAA ATC GGC AGT CA-(N40)-AT CTG AAG CAT AGT CCA GGC-3'.

Two sets of primers were used to amplify binders selected from the starting library. The primers in the first set were unlabeled and employed for qPCR. These primers had the following sequences: (i) for MutS: 5'-CTC CTC TGA CTG TAA CCA CG-3'(forward) and 5'-GGC TTC TGG ACT ACC TAT GC (reverse), and (ii) for thrombin: 5'-CTA CGG TAA ATC GGC AGT CA-3' (forward) and 5'-GCC TGG ACT ATG CTT CAG AT-3'(reverse). For asymmetric PCR (aPCR), the second set of primers included a fluorescently labeled version of the forward primer and a biotin-labeled version of the reverse primer: (i) for MutS: 5'-Alexa Fluor488-CTC CTC TGA CTG TAA CCA CG-3'(forward) and 5'-Biotin-TEG-GGC TTC TGG ACT ACC TAT GC (reverse), and (ii) for thrombin: 5'-Alexa Fluor488-CTA CGG TAA ATC GGC AGT CA-3' (forward) and 5'-Biotin-TEG-GCC TGG ACT ATG CTT CAG AT-3'(reverse).

**3.2.2.3 CE Instrumentations.** All CE experiments were performed with a P/ACE MDQ apparatus (SCIEX, Concord, ON, Canada) equipped with a laser-induced fluorescence (LIF) detection system. Fluorescence was excited with a blue line (488 nm) of a solid-state laser and detected at 520 nm using a spectrally-optimized emission filter system.<sup>64</sup> The poly(vinyl alcohol) (PVA)-coated capillaries were prepared as described elsewhere.<sup>65</sup> The total length of the capillary was 80 cm for most of the experiments, except for the bulk affinity tests conducted for MutS selection, where the capillary length was 50 cm. In all cases, the detection window was positioned 10 cm away from the outlet of the capillary. Prior to every run, the PVA-coated capillary was rinsed with the running buffer at 20 psi (138 kPa) for 8 min. The coolant temperature was set at 15 °C.

**3.2.2.4 Specifics of CE-based fraction collection.** In Round 1, the equilibrium mixture contained the annealed starting library of 10  $\mu$ M and the protein target of chosen concentration; 330 nM binder-enriched library was used for Rounds 2 and 3 instead of 10  $\mu$ M. The target concentration in the equilibrium mixture was kept constant throughout the three rounds of selection. The equilibrium mixtures were incubated for 1 h to approach chemical equilibrium in the binding reaction. The equilibrium mixture was injected into the capillary by a pressure pulse of 1 psi (6.9 kPa)  $\times$  28 s, resulting in a sample plug of 3.7 cm in length. The sample plug was propagated by a pressure pulse of 0.9 psi (6.2 kPa)  $\times$  45 s (to yield

a 5.4 cm-long buffer plug) to pass the uncooled region of the capillary before applying the electric field. Partitioning was carried out using reversed polarity (anode at the outlet) at 25 kV for 26 and 20 min for MutS and thrombin selections, respectively. After CE-based partitioning, elution of the target–binder complex was facilitated by pressure at 5 psi (34.5 kPa) for 1 min into a fraction-collection vial containing 20  $\mu$ L of the running buffer.

**3.2.2.5 PCR procedures and generation of binder-enriched library.** The eluted binder-enriched library was amplified and quantitated by two rounds of qPCR using CFX Connect instrument (Bio-Rad, ON, Canada). The qPCR reagent mixture was prepared to obtain final concentrations of 1 $\times$ Q5 High-Fidelity 2 $\times$ Master Mix (New England BioLabs, Whitby, ON, Canada), 1 $\times$ SYBR Green (Fisher Scientific, Mississauga, ON, Canada), 500 nM unlabeled forward primer, and 500 nM unlabeled reverse primer. Before thermocycling, the qPCR reaction mixture was prepared by adding a 2  $\mu$ L aliquot of the eluted fraction to 18  $\mu$ L of the qPCR reagent mixture. The PCR thermocycling protocol was as follows: 98  $^{\circ}$ C for 30 s (initialization, performed once), 98  $^{\circ}$ C for 10 s (denaturation), 65  $^{\circ}$ C for 20 s (annealing), and 72  $^{\circ}$ C for 20 s (extension), followed by a plate read at 72  $^{\circ}$ C and a return to the denaturation step for a total of 40 cycles. All qPCR reactions were performed in duplicate. In the first round of qPCR, the eluted fraction was quantitated using an eight-point calibration curve. An S-shaped amplification curve was then plotted for the eluted fraction. In the second round of the qPCR, the qPCR product of the eluted fraction was removed when it was two cycles into the exponential phase of the previously plotted amplification curve. After qPCR, 100  $\mu$ L of the qPCR product was later purified using the MinElute<sup>®</sup> PCR purification kit (QIAGEN, Mississauga, ON, Canada) as per manufacturer’s instructions. Once product’s purity was verified by native PAGE, it was subjected to aPCR. Five  $\mu$ L of DNA was added to 45  $\mu$ L of aPCR reagent mixture from New England Biolabs Inc. (Whitby, ON, Canada). Final concentrations of PCR reagents in the reaction mixture were: 1 $\times$ Q5<sup>®</sup> Reaction Buffer, 1  $\mu$ M fluorescently labeled forward primer, 50 nM biotin-labeled reverse primer, 0.02 units/ $\mu$ L Q5<sup>®</sup> High-Fidelity DNA Polymerase, and 200  $\mu$ M dNTPs mix. The reaction was performed in duplicates with the following temperature protocol:

98 °C for 30 s (initial denaturation, performed once), 98 °C for 10 s (denaturation), 65 °C for 20 s (annealing), and 72 °C for 20 s (extension). Eighteen cycles of aPCR were run. Ten µL of MagnaBind™ streptavidin beads suspension (Fisher Scientific, Mississauga, ON, Canada) was washed three times and resuspended in bead washing/binding buffer (10 mM Tris-HCl, 50 mM NaCl, 1 mM EDTA pH 8.0). Once amplified, the duplicate PCR reactions were combined and incubated with streptavidin magnetic beads for 30 min at a room temperature ( $23 \pm 1$  °C). The beads were magnetized, discarded, and the PCR product was then purified using the MinElute® PCR purification kit as per manufacturer's instructions. To quantitate the DNA concentration in the binder-enriched library, serial dilutions of the fluorescently labelled forward primer (2 µM, 1 µM, 500 nM, 250 nM, 125 nM, 62.5 nM, and 31.25 nM) were prepared to build a standard curve by measuring fluorescence intensity at 519 nm with NanoDrop 3300 Fluorospectrometer (Fisher Scientific, Mississauga, ON, Canada). The purified binder-enriched library was then ready for the next round of selection.

**3.2.2.6 Specifics of bulk affinity test.** Equilibrium mixtures of either the starting library or the binder-enriched library and varying target concentrations were prepared and incubated at room temperature for 1 h prior to injection into the capillary. Throughout all the bulk affinity tests, the concentrations of the starting library or the binder-enriched library remained constant (i.e., 1 nM for MutS selection and 20 nM for thrombin selection). In the case of MutS bulk affinity tests, a 50-cm capillary was used to shorten the separation time while still ensuring the desired resolution between the unbound library and the target–binder complex. As such, the conditions for MutS bulk affinity tests were readjusted as follows: (i) sample injection at 0.5 psi (3.4 kPa) × 20 s to create a 2.1 cm-long sample plug, (ii) buffer propagation at 0.9 psi (6.2 kPa) × 30 s to yield a 5.8 cm-long buffer plug and pass the uncooled capillary region and (iii) separation at 25 kV with reversed polarity (anode at the capillary outlet) for a duration of 15 min. Due to the poor resolution in thrombin selections, the bulk affinity tests were continued to be conducted using an 80-cm capillary. The conditions for thrombin bulk affinity tests were the same as conditions used in the binder selection with the total separation time of 25 min.

### 3.2.3 Results and Discussion

To be successful and instructive, an experimental study of the influence of target concentration on aptamer selection by SELEX requires several right choices to be made. First, such a study requires a highly efficient partitioning method so that the chances of failure are minimized, and the timescale of the study is kept reasonable (months rather than years). We chose partitioning by CE which reliably supports partitioning efficiency of  $10^4$ – $10^9$  (orders of magnitude higher than for surface-based partitioning).<sup>74</sup> Partitioning by CE typically facilitates aptamer selection in less than five rounds of SELEX. Second, objective comparison of the SELEX results for different target concentrations requires a reliable bulk affinity assay. We chose a recently-published bulk-affinity workflow relying on optimized measurements of the fraction of unbound library ( $R$ ).<sup>77</sup> We chose four target concentrations covering two orders of magnitude to work with: 500, 100, 10, and 1 nM. Accordingly, we planned for conducting four selections with constant target concentrations (500, 100, 10, and 1 nM). Finally, such a study requires well understood and confirmed targets for aptamer selection by SELEX. We chose two proteins, His-tagged MutS (93 kDa) and non-tagged thrombin (35 kDa) for which successful aptamer selections were performed several times.<sup>78,79</sup>

Our first task was to determine suitable modes of CE partitioning for the two protein targets: His-tagged MutS and thrombin. We found that both, His-tagged MutS and thrombin excessively adhered to the inner fused silica capillary wall while coating the wall with polyvinyl alcohol (PVA) suppressed this adsorption along with suppressing the electroosmotic flow.<sup>73</sup> A side-effect of PVA coating is the suppressed electroosmotic flow, which forced us to use the “complex-last” mode of NECEEM-based partitioning in which the unbound DNA (nonbinders)

moves faster than the protein–DNA (target–binder) complexes. For each target concentration, we conducted 3 rounds of selection, as typical for a NECEEM-based selection routine.<sup>74</sup>

We then conducted the NECEEM-based selections of binders for MutS and thrombin from a DNA library with 40 random nucleotides. In Step 1, the target was mixed with the library, and the mixture was incubated for 1 h to allow the formation of target–binder complexes, serving as a positive control. As a negative control, we used a mixture of the library with target matrix void of the target. In Step 2, a small volume of the mixture was injected inside the capillary (the length of the resulting sample plug was approximately 5% of the capillary length), and target–binder complexes were separated from the unbound library. A fraction was collected in a pre-determined time window, where binders should elute (see **Note C1** for determination of binder-elution window). In Step 3, the collected fraction was subjected to a two-stage PCR amplification —qPCR followed by asymmetric PCR (aPCR) — to produce the enriched library the next round of SELEX. The bulk-affinity assay was performed for the starting library and for each of the enriched libraries, and its results were used to judge the progress of selection. qPCR was used to obtain two quantitative parameters (**Figure 16**): (i) a transmittance of partitioning for nonbinders ( $k_N$ ),<sup>74</sup> often referred to as the nonbinder background, and (ii) a relative yield of DNA ( $q$ ). The transmittance is defined as the ratio between the quantities of nonbinders at the output ( $N_{out}$ ) and input ( $N_{in}$ ) of partitioning, in the absence of the target (negative control):

$$k_N = N_{out} / N_{in}$$

15

In the presence of the target and formation of target–binder complexes, the output quantity of the library ( $L_T$ ) is the sum of the output quantity of binders ( $B_{out}$ ) and nonbinders

( $N_{out}$ ). We define the relative yield of DNA,  $q$  as the ratio between the output quantity of the library in the presence of the target ( $L_T$ ) and the output quantity of nonbinder ( $N_{out}$ ).

$$q = L_T / N_{out} = (B_{out} + N_{out}) / N_{out} = 1 + (B_{out} / N_{out}) \quad 16$$

For the selection to be meaningful,  $B_{out}$  must not only be larger than 0 but also exceed the limit of detection in PCR (typically ranging from 10 to 100 DNA molecules). Therefore,  $q$  must be statistically significantly greater than unity for the selection to proceed. To assess the experimental errors associated with calculation of  $q$ , multiple sets of positive control and negative control experiment for one constant target concentration were conducted to determine  $L_T$  and  $N_{out}$  respectively. The mean value of  $q$  and its relative standard deviation (RSD) were then estimated (Note C2).

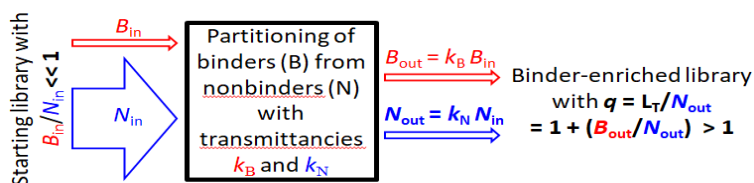


**Figure 16.** Schematic representation of efficient partitioning of binders (B) from nonbinders (N) in a mixture of oligonucleotide library and protein target. At the input of partitioning, the binder-to-nonbinder ratio ( $B_{in}/N_{in}$ ) is typically  $\ll 1$ . After the partitioning with transmittancies  $k_B$  and  $k_N$  for binder and nonbinder respectively, the binder-enriched library is expected to have output binder-to-nonbinder ratio ( $B_{out}/N_{out}$ )  $> B_{in}/N_{in}$ , with the relative yield of DNA,  $q > 1$ . In this study, we utilized two experimental parameters,  $k_N$  and  $q$  to draw the conclusion about the choice of target concentration for selection. See text for more details.

As per our plan, we completed three-round selections for His-tagged MutS and thrombin with four constant round-to-round target concentrations. We followed the established bulk affinity work flow, as previously published, to evaluate the affinity of the enriched libraries to the protein target after each round.<sup>77</sup> For consistency across selections, we used a constant concentration of 10  $\mu$ M of the 80-nt starting library in Round 1. Subsequently, we employed a 330 nM binder-enriched library for later rounds. To confirm the robustness and the reproducibility of the results of selections, we repeated two of four selections for thrombin.

After every round of selection,  $k_N$  and  $q$  values were determined via qPCR using the procedure outlined in the above section (see **Note C2** for a detailed summary of  $k_N$  and  $q$  values). Notably, the  $k_N$  values were found to be in the range of  $10^{-3}$  and  $10^{-5}$  for NECEEM-based selection for thrombin and MutS respectively. While the  $k_N$  value of MutS selection was typical of NECEEM-based partitioning,<sup>74</sup> the  $k_N$  of thrombin selection was higher than expected. This variance in  $k_N$  values was attributed to the differential resolution from the DNA nonbinders, upon complexation with thrombin, a smaller-sized protein target. In essence, thrombin selections suffered from a significantly higher nonbinder background, approximately 100 times higher than MutS selections. Considering that  $q$  is inversely proportional to the nonbinder background (eqs 15 & 16), it is expected that the theoretical range of  $q$  values in MutS selection would be approximately two orders of magnitude higher than that in thrombin selection, given the same target concentration and input quantity of library molecules. Indeed, the experimental values of  $q$  in MutS selection were consistently within 1 to 2 orders of magnitude higher than those in thrombin selection for the same target concentration scheme (**Figure 17A**). In addition to the nonbinder background, variations in experimental  $q$  values could arise from the following factors. First, the uncertainty associated with the qPCR-determined  $L_T$  and  $N_{out}$  values can lead to potential variations of up to 14% under the same experimental conditions (see calculation of RSD in **Note C2**). Second, the nature of the target, specifically its aptagenicity or affinity to oligonucleotide binders, played a pivotal role in dictating the binder abundance in the starting library and setting the upper theoretical limit of  $L_T$ . Intuitively, an ideal selection would have a high binder abundance in the starting library (high  $L_T$ ) and low nonbinder background (low  $k_N$  or  $N_{out}$ ), leading to a high  $q$  value significantly greater than 1.

A consistent trend observed in the  $q$ -value data for both targets was a decrease in  $q$  as target concentration decreased, ultimately reaching unity (**Figure 17A**). This trend was expected; at higher target concentration, more target molecules will be available to bind the DNA molecules, increasing  $L_T$  and  $q$ . On the other hand, when there is a depletion in the target concentration, only the most tightly bound binders remain bound to target and are collected at the output of partitioning, resulting in lower  $L_T$  and  $q$  values. For thrombin selection, the  $q$  value decreased to near unity when the target concentration reached (on the way down) 10 nM. Since MutS selection experienced a lower nonbinder background, the  $q$  value was close to unity at a lower target concentration of 1 nM. Another important observation from Figure 3a was that when  $q$  value in Round 1 was near unity (as seen in the 1-nM and 10-nM selection for Thrombin, as well as the 1-nM selection for MutS), there was no subsequent increase in the  $q$  value between rounds for a given target concentration scheme. However, when  $q$  value in Round 1 was significantly greater than 1, it consistently increased from round to round, peaking in Round 3 (e.g., 100-nM and 500-nM thrombin selections; and 10-nM, 100-nM and 500-nM MutS selections). This increase of  $q$  between rounds for such target concentration schemes means that the yield of DNA binders was enriched throughout the selection process, possibly indicating a positive selection outcome (which will be discussed in details in the following section).

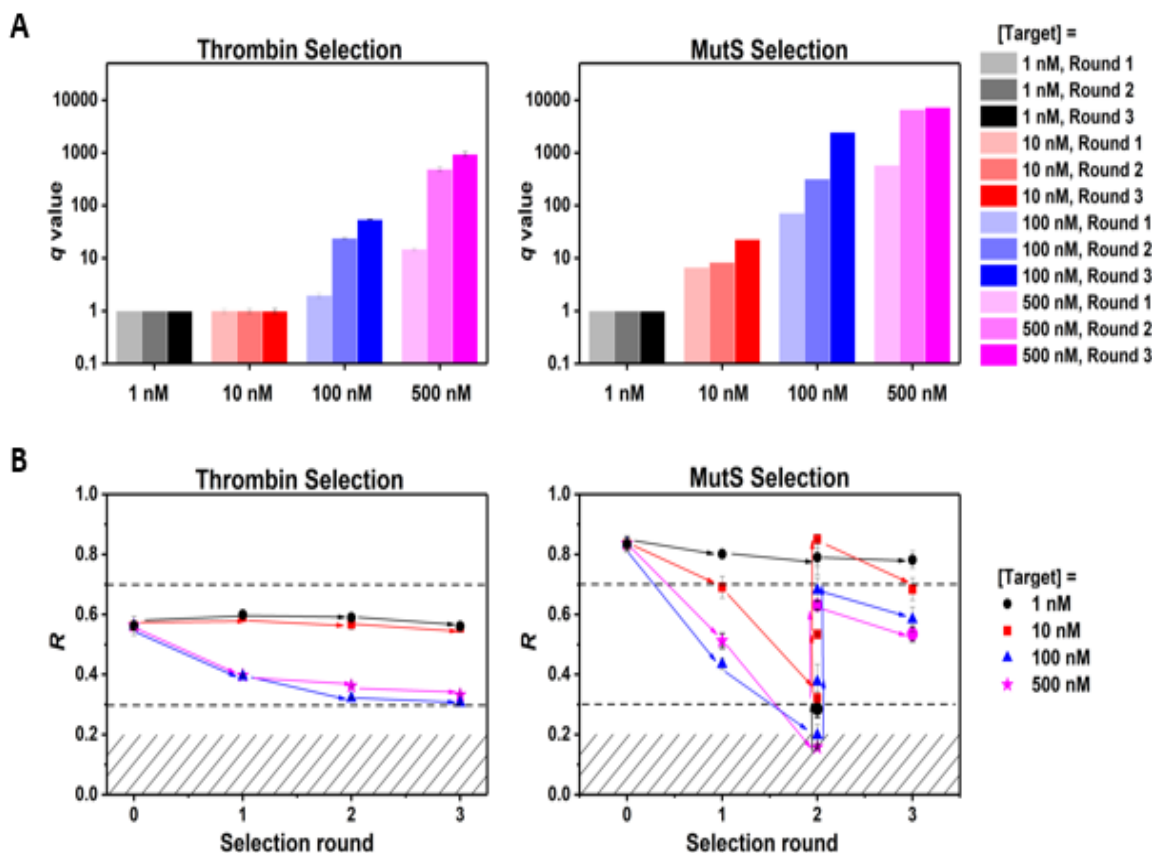


**Figure 17.** Comparison of  $q$  values (a) and bulk affinities represented by  $R$  values (b) to evaluate the selection outcomes for MutS and thrombin under four different schemes of constant target concentrations throughout the selection. In (b) the experimental thrombin and MutS protein bulk affinity assay conducted according to the proposed workflow. Within the shaded region, the  $R$  value signifies the critical threshold where it is imperative to reduce the target concentration until it falls within the boundaries defined by the dashed lines. The directional arrows, proceeding from left to right, indicate the progression of the bulk affinity assays. For thrombin selections at 500 nM, 100 nM, 10 nM, and 1 nM, the data points represent 1 nM DNA with (i) 100 nM protein in rounds 0, 1, 2, and 3. For MutS selections at 500 nM, 100 nM, and 10 nM, the data points correspond to 1 nM DNA under various conditions: (i) 1000 nM protein in rounds 0, 1, and 2; (ii) 100 nM protein in round 2; and (iii) 10 nM protein in rounds 2 and 3 while for MutS selections at 1 nM, the data points corresponds to 1 nM DNA under various conditions: (i) 1000 nM protein in rounds 0, 1, 2 and 3 See text for more details.

To accurately evaluate and compare the selection outcomes across different target concentration schemes, we conducted a previously published bulk affinity workflow for every binder-enriched library obtained in the selections for both targets.<sup>77</sup> The results of bulk affinity assays are summarized in **Figure 17B**, where  $R$  is plotted against the selection round for every

target concentration scheme, with Round 0 being the starting library prior to the selection (see **Note C3** for the detailed electropherograms and calculation of  $R$  values).  $R$ , representing the fraction of unbound library obtained in the bulk affinity test, serves as an indicator of enrichment progress: lower  $R$  values indicate improved affinity to the target. It is expected that  $R > 0$  is typically observed for Round 0 while enrichment progressively reduces  $R$  for subsequent rounds. To mitigate poor accuracy associated with  $R$  measurement close to its limits (0–1), we systematically adjusted the protein concentration in the bulk affinity test in a stepwise fashion to maintain  $R$  within the range of 0.3 to 0.7 (as indicated by the vertical arrow between the points in **Figure 17B**).<sup>77</sup>

In the case of thrombin selection, the improvement of  $R$  throughout the selection was observed for 100-nM and 500-nM target concentration schemes while  $R$  value remained unchanged when the target concentration decreased down to 10 nM — corresponding to the point where  $q$  reached near unity. A similar trend was seen in MutS selection: the progression of  $R$  eventually ceased at a target concentration of 1 nM, where  $q$  was close to unity. Overall, successful selections with increasing binder enrichment were achieved for the target concentration schemes where  $q$  value in the Round 1 exceeded unity.

The combined results from qPCR measurements of DNA quantity and bulk affinity assays allow us to draw the following key conclusions. First, election outcomes are contingent upon a critical “threshold” target concentration; selection fails below this threshold but proceeds when target concentration exceeds it. Second, as target concentration decreases,  $q$  value is getting smaller until it gets closer to unity (i.e.,  $q = 1 + n\sigma$  where  $\sigma$  is the standard deviation of  $q$  at  $q = 1$ , which was  $\sim 0.14$  in our assay, as detailed in **Note C2**) at the “threshold” target concentration. Therefore, we recommend using target concentrations resulting in  $q$  values that are statistically

significantly greater than unity (i.e.,  $q > 1 + n\sigma$ ) to achieve successful selection with enrichment of binders. Should experimentalists aim to increase the selection stringency by utilizing a lower target concentration to drive the selection towards selecting binders with lower affinity, caution must be taken to ensure that the resulting  $q$  value remains above unity. In certain cases, it may be necessary to expand the  $q$  range. Elevating the  $q$  value will lead to a lower “threshold” target concentration at which enrichment of binders can still be achieved. In essence, a more reliable selection with higher chance of success, even at low target concentrations, is characterized by high  $q$  values. While the range of  $q$  may be largely influenced by the nature of protein target, enhancing  $q$  can be achieved by decreasing the nonbinder background ( $k_N$ ) of the partitioning method or increasing  $L_T$  through the means of a more superior starting library, such as a chemically modified DNA library with greater affinity to the target.<sup>80</sup>

### **3.2.4 Conclusion**

To conclude, our data further underscores the critical role of target concentration in the performance of SELEX. We have established that SELEX succeeds when the target concentration surpasses a specific threshold value and halts when the concentration falls below this threshold. This threshold value varies depending on several factors, including the nature of the target, the nonbinder background and the quality of PCR; however, it can be readily identified on a case-to-case basis using a simple quantitative parameter —  $q$  or the relative yield of DNA after partitioning in the presence versus absence of the target. We encourage experimentalists to choose the target concentration that results in  $q$  values statistically greater than one. The use of this straightforward parameter will prove invaluable in rational determination of the target concentration, ultimately enhancing the prospect of success within the SELEX community.

## LIMITATIONS

Antibodies have been widely used in LFIA due to their high specificity and affinity for their target antigens. However, they do have some limitations, which have led researchers to explore alternatives, such as aptamers. Some limitations of antibodies in LFIA are batch-to-batch variability which can affect the consistency and reliability of LFIA, high production cost which can limit assay's affordability and accessibility, cross-reactivity which can lead to false-positive results or reduced assay specificity and large size which can hinder their penetration into certain sample types, limiting the assay's sensitivity. Additionally, antibodies can be sensitive to harsh environmental conditions, such as temperature and pH changes, leading to decreased stability and shelf life of lateral flow test strips. In contrast, aptamers are stable, have long shelf life and have high specificity.

There are several factors that can influence the success and efficiency of aptamer selection. Although the newly developed bulk affinity workflow and identifying optimum protein concentration are a positive step in the right direction, there are limitations that need to be addressed. The main challenge arises from the nature of protein targets. Aptamer selection for complex protein targets can be challenging due to several factors that arise from the structural and functional complexity of these proteins. Complex protein targets often have multiple conformations, making it challenging for aptamers to bind specifically to the active site or functional regions. Because of the conformational diversity, irreproducible bulk affinity assays might be observed thus selecting aptamers that recognize specific conformations can be difficult.

Moreover, some regions of complex proteins, particularly those involved in protein-protein interactions or buried within the protein structure, may be less accessible to aptamers, limiting the pool of potential binding sites thus it might be difficult to determine the maximum protein target

concentration one need to start with. Moreover, some complex protein targets may be present in low abundance in biological samples, making it hard to predict the highest target concentration to begin with. Another big limitation is that aptamer selection relies on thermodynamic interactions between the aptamers and the target. Complex protein targets may have weaker binding affinities or faster dissociation rates, making the selection process more difficult to monitor. Nevertheless, the bulk affinity workflow and the determination of optimum target concentration provides an instructive approach for conventional aptamer selection that doesn't require the development of specialized selection strategies.

Thus, antibodies can be replaced by aptamers to evade their limitations. Hence, addressing those limitations will further improve the electrophoresis driven LFIA and push forward its development as a commercial point of care.

## CONCLUSION AND FUTURE WORKS

We validated and optimized enhanced LFIA for RBD protein. However, as mentioned in the limitation section, antibodies have many disadvantages on the other hand aptamers have high specificity, affinity, small size, stability under harsh environmental conditions, lower production cost, rapid development, batch consistency and reduced cross-reactivity. In this work, we reported a single approach by proving bulk affinity assays as the only analytical tool to examine the progress of an aptamer selection and proposing a new bulk affinity assay workflow. Using this bulk affinity workflow, we also identified optimum target concentration in aptamer selection which plays a key role in the efficiency of an aptamer selection. Both optimum target concentration and bulk affinity workflow can be used to successfully select aptamers where then careful study is required in modifying aptamers for the purpose of LFIA such as immobilizing aptamers on NC and conjugating aptamers with GNP. In the future, aptamer-based LFIA have the potential to revolutionize point-of-care diagnostics and other applications where quick and reliable detection is essential.

## LIST OF PUBLICATION

1. **Teclmichael, E.**, Le, A. T. H., Krylova, S. M., Wang, T. Y., & Krylov, S. N. Bulk Affinity Assays in Aptamer Selection: Challenges, Theory, and Workflow. *Analytical Chemistry* **2022**, 94, 15183–15188.

## REFERENCES

- (1) Miryala, S. K.; Anbarasu, A.; Ramaiah, S. Discerning molecular interactions: A comprehensive review on biomolecular interaction databases and network analysis tools. *Gene* **2018**, *642*, 84-94. DOI: 10.1016/j.gene.2017.11.028
- (2) Ma, W.; Yang, L.; He, L. Overview of the detection methods for equilibrium dissociation constant K(D) of drug-receptor interaction. *J Pharm Anal* **2018**, *8* (3), 147-152. DOI: 10.1016/j.jpha.2018.05.001
- (3) Bansal, R.; Care, A.; Lord, M. S.; Walsh, T. R.; Sunna, A. Experimental and theoretical tools to elucidate the binding mechanisms of solid-binding peptides. *N Biotechnol* **2019**, *52*, 9-18. DOI: 10.1016/j.nbt.2019.04.001
- (4) Arora, S.; Saxena, V.; Ayyar, B. V. Affinity chromatography: A versatile technique for antibody purification. *Methods* **2017**, *116*, 84-94. DOI: 10.1016/j.ymeth.2016.12.010
- (5) Beloborodov, S. S.; Bao, J.; Krylova, S. M.; Shala-Lawrence, A.; Johnson, P. E.; Krylov, S. N. Aptamer facilitated purification of functional proteins. *J Chromatogr B Analyt Technol Biomed Life Sci* **2018**, *1073*, 201-206. DOI: 10.1016/j.jchromb.2017.12.024
- (6) Chan, H. C. S.; Shan, H.; Dahoun, T.; Vogel, H.; Yuan, S. Advancing Drug Discovery via Artificial Intelligence. *Trends Pharmacol Sci* **2019**, *40* (10), 801. DOI: 10.1016/j.tips.2019.07.013
- (7) Thevendran, R.; Citartan, M. Assays to Estimate the Binding Affinity of Aptamers. *Talanta* **2022**, *238* (Pt 1), 122971. DOI: 10.1016/j.talanta.2021.122971
- (8) Kairys, V.; Baranauskiene, L.; Kazlauskiene, M.; Matulis, D.; Kazlauskas, E. Binding affinity in drug design: experimental and computational techniques. *Expert Opin Drug Discov* **2019**, *14* (8), 755-768. DOI: 10.1080/17460441.2019.1623202
- (9) Trier, N.; Hansen, P.; Houen, G. Peptides, Antibodies, Peptide Antibodies and More. *Int J Mol Sci* **2019**, *20* (24). DOI: 10.3390/ijms20246289
- (10) Elshiaty, M.; Schindler, H.; Christopoulos, P. Principles and Current Clinical Landscape of Multispecific Antibodies against Cancer. *Int J Mol Sci* **2021**, *22* (11). DOI: 10.3390/ijms22115632
- (11) Chau, C. H.; Steeg, P. S.; Figg, W. D. Antibody-drug conjugates for cancer. *Lancet* **2019**, *394* (10200), 793-804. DOI: 10.1016/S0140-6736(19)31774-X
- (12) Kumar, M.; Thangavel, C.; Becker, R. C.; Sadayappan, S. Monoclonal Antibody-Based Immunotherapy and Its Role in the Development of Cardiac Toxicity. *Cancers (Basel)* **2020**, *13* (1). DOI: 10.3390/cancers13010086
- (13) Kandari, D.; Bhatnagar, R. Antibody engineering and its therapeutic applications. *Int Rev Immunol* **2023**, *42* (2), 156-183. DOI: 10.1080/08830185.2021.1960986
- (14) Gao, Y.; Huang, X.; Zhu, Y.; Lv, Z. A brief review of monoclonal antibody technology and its representative applications in immunoassays. *J Immunoassay Immunochem* **2018**, *39* (4), 351-364. DOI: 10.1080/15321819.2018.1515775
- (15) Xiao, X.; Hu, S.; Lai, X.; Peng, J.; Lai, W. Developmental trend of immunoassays for monitoring hazards in food samples: A review. *Trends in Food Science & Technology* **2021**, *111*, 68-88. DOI: <https://doi.org/10.1016/j.tifs.2021.02.045>
- (16) Di Nardo, F.; Chiarello, M.; Cavalera, S.; Baggiani, C.; Anfossi, L. Ten Years of Lateral Flow Immunoassay Technique Applications: Trends, Challenges and Future Perspectives. *Sensors (Basel)* **2021**, *21* (15). DOI: 10.3390/s21155185

- (17) Banerjee, R.; Jaiswal, A. Recent advances in nanoparticle-based lateral flow immunoassay as a point-of-care diagnostic tool for infectious agents and diseases. *Analyst* **2018**, *143* (9), 1970-1996. DOI: 10.1039/c8an00307f
- (18) Tsai, T. T.; Huang, T. H.; Chen, C. A.; Ho, N. Y.; Chou, Y. J.; Chen, C. F. Development a stacking pad design for enhancing the sensitivity of lateral flow immunoassay. *Sci Rep* **2018**, *8* (1), 17319. DOI: 10.1038/s41598-018-35694-9
- (19) Wang, C.; Peng, J.; Liu, D. F.; Xing, K. Y.; Zhang, G. G.; Huang, Z.; Cheng, S.; Zhu, F. F.; Duan, M. L.; Zhang, K. Y.; et al. Lateral flow immunoassay integrated with competitive and sandwich models for the detection of aflatoxin M(1) and Escherichia coli O157:H7 in milk. *J Dairy Sci* **2018**, *101* (10), 8767-8777. DOI: 10.3168/jds.2018-14655
- (20) Boehringer, H. R.; O'Farrell, B. J. Lateral Flow Assays in Infectious Disease Diagnosis. *Clin Chem* **2021**, *68* (1), 52-58. DOI: 10.1093/clinchem/hvab194
- (21) Park, J. Lateral Flow Immunoassay Reader Technologies for Quantitative Point-of-Care Testing. *Sensors (Basel)* **2022**, *22* (19). DOI: 10.3390/s22197398
- (22) Yen, C. W.; de Puig, H.; Tam, J. O.; Gomez-Marquez, J.; Bosch, I.; Hamad-Schifferli, K.; Gehrke, L. Multicolored silver nanoparticles for multiplexed disease diagnostics: distinguishing dengue, yellow fever, and Ebola viruses. *Lab Chip* **2015**, *15* (7), 1638-1641. DOI: 10.1039/c5lc00055f
- (23) Panferov, V. G.; Ivanov, N. A.; Mazzulli, T.; Brinc, D.; Kulasingam, V.; Krylov, S. N. Electrophoresis-Assisted Multilayer Assembly of Nanoparticles for Sensitive Lateral Flow Immunoassay. *Angew Chem Int Ed Engl* **2023**, *62* (2), e202215548. DOI: 10.1002/anie.202215548
- (24) Zhou, J.; Rossi, J. Aptamers as targeted therapeutics: current potential and challenges. *Nat Rev Drug Discov* **2017**, *16* (6), 440. DOI: 10.1038/nrd.2017.86
- (25) Murakami, K.; Izuo, N.; Bitan, G. Aptamers targeting amyloidogenic proteins and their emerging role in neurodegenerative diseases. *J Biol Chem* **2022**, *298* (1), 101478. DOI: 10.1016/j.jbc.2021.101478
- (26) Kumar Kulabhusan, P.; Hussain, B.; Yüce, M. Current Perspectives on Aptamers as Diagnostic Tools and Therapeutic Agents. *Pharmaceutics* **2020**, *12* (7). DOI: 10.3390/pharmaceutics12070646
- (27) Qian, S.; Chang, D.; He, S.; Li, Y. Aptamers from random sequence space: Accomplishments, gaps and future considerations. *Anal Chim Acta* **2022**, *1196*, 339511. DOI: 10.1016/j.aca.2022.339511
- (28) Komarova, N.; Kuznetsov, A. Inside the Black Box: What Makes SELEX Better? *Molecules* **2019**, *24* (19). DOI: 10.3390/molecules24193598
- (29) Krebs, F.; Zagst, H.; Stein, M.; Ratih, R.; Minkner, R.; Olabi, M.; Hartung, S.; Scheller, C.; Lapizco-Encinas, B. H.; Sanger-van de Griend, C.; et al. Strategies for capillary electrophoresis: Method development and validation for pharmaceutical and biological applications-Updated and completely revised edition. *Electrophoresis* **2023**, *44* (17-18), 1279-1341. DOI: 10.1002/elps.202300158
- (30) Petrov, A.; Okhonin, V.; Berezovski, M.; Krylov, S. N. Kinetic capillary electrophoresis (KCE): a conceptual platform for kinetic homogeneous affinity methods. *J Am Chem Soc* **2005**, *127* (48), 17104-17110. DOI: 10.1021/ja056232l
- (31) Berezovski, M. V.; Musheev, M. U.; Drabovich, A. P.; Jitkova, J. V.; Krylov, S. N. Non-SELEX: selection of aptamers without intermediate amplification of candidate oligonucleotides. *Nat Protoc* **2006**, *1* (3), 1359-1369. DOI: 10.1038/nprot.2006.200

- (32) Krylov, S. N. Nonequilibrium capillary electrophoresis of equilibrium mixtures (NECEEM): A novel method for biomolecular screening. *J Biomol Screen* **2006**, *11* (2), 115-122. DOI: 10.1177/1087057105284339
- (33) Hajizadeh, F.; Khanizadeh, S.; Khodadadi, H.; Mokhayeri, Y.; Ajorloo, M.; Malekshahi, A.; Heydari, E. SARS-COV-2 RBD (Receptor binding domain) mutations and variants (A sectional-analytical study). *Microb Pathog* **2022**, *168*, 105595. DOI: 10.1016/j.micpath.2022.105595
- (34) Gumanova, N. G.; Gorshkov, A. U.; Bogdanova, N. L.; Korolev, A. I.; Drapkina, O. M. Detection of Anti-SARS-CoV-2-S1 RBD-Specific Antibodies Prior to and during the Pandemic in 2011-2021 and COVID-19 Observational Study in 2019-2021. *Vaccines (Basel)* **2022**, *10* (4). DOI: 10.3390/vaccines10040581
- (35) Alhabbab, R. Y. Lateral Flow Immunoassays for Detecting Viral Infectious Antigens and Antibodies. *Micromachines (Basel)* **2022**, *13* (11). DOI: 10.3390/mi13111901
- (36) Prakashan, D.; Shrikrishna, N. S.; Byakodi, M.; Nagamani, K.; Gandhi, S. Gold nanoparticle conjugate-based lateral flow immunoassay (LFIA) for rapid detection of RBD antigen of SARS-CoV-2 in clinical samples using a smartphone-based application. *J Med Virol* **2023**, *95* (1), e28416. DOI: 10.1002/jmv.28416
- (37) Frens, G. Controlled Nucleation for the Regulation of the Particle Size in Monodisperse Gold Suspensions. *Nature Physical Science* **1973**, *241* (105), 20-22. DOI: 10.1038/physci241020a0.
- (38) Agostino, F. J.; Evenhuis, C. J.; Krylov, S. N. Milli-free flow electrophoresis: I. Fast prototyping of mFFE devices. *J Sep Sci* **2011**, *34* (5), 556-564. DOI: 10.1002/jssc.201000758
- (39) Razo, S. C.; Panferova, N. A.; Panferov, V. G.; Safenkova, I. V.; Drenova, N. V.; Varitsev, Y. A.; Zherdev, A. V.; Pakina, E. N.; Dzantiev, B. B. Enlargement of Gold Nanoparticles for Sensitive Immunochromatographic Diagnostics of Potato Brown Rot. *Sensors (Basel)* **2019**, *19* (1). DOI: 10.3390/s19010153
- (40) Hoshyar, N.; Gray, S.; Han, H.; Bao, G. The effect of nanoparticle size on in vivo pharmacokinetics and cellular interaction. *Nanomedicine (Lond)* **2016**, *11* (6), 673-692. DOI: 10.2217/nmm.16.5
- (41) Zhang, L.; Mazouzi, Y.; Salmain, M.; Liedberg, B.; Boujday, S. Antibody-Gold Nanoparticle Bioconjugates for Biosensors: Synthesis, Characterization and Selected Applications. *Biosens Bioelectron* **2020**, *165*, 112370. DOI: 10.1016/j.bios.2020.112370
- (42) Englebienne, P. Use of colloidal gold surface plasmon resonance peak shift to infer affinity constants from the interactions between protein antigens and antibodies specific for single or multiple epitopes. *Analyst* **1998**, *123* (7), 1599-1603. DOI: 10.1039/a804010i
- (43) Geoghegan, W. D. The effect of three variables on adsorption of rabbit IgG to colloidal gold. *J Histochem Cytochem* **1988**, *36* (4), 401-407. DOI: 10.1177/36.4.3346540
- (44) Sotnikov, D. V.; Safenkova, I. V.; Zherdev, A. V.; Avdienko, V. G.; Kozlova, I. V.; Babayan, S. S.; Gergert, V. Y.; Dzantiev, B. B. A Mechanism of Gold Nanoparticle Aggregation by Immunoglobulin G Preparation. *Applied Sciences* **2020**, *10* (2), 475.
- (45) Iarossi, M.; Schiattarella, C.; Rea, I.; De Stefano, L.; Fittipaldi, R.; Vecchione, A.; Velotta, R.; Ventura, B. D. Colorimetric Immunosensor by Aggregation of Photochemically Functionalized Gold Nanoparticles. *ACS Omega* **2018**, *3* (4), 3805-3812. DOI: 10.1021/acsomega.8b00265

- (46) Bahadır, E. B.; Sezgintürk, M. K. Lateral flow assays: Principles, designs and labels. *TrAC Trends in Analytical Chemistry* **2016**, *82*, 286-306. DOI: <https://doi.org/10.1016/j.trac.2016.06.006>.
- (47) Mirica, A. C.; Stan, D.; Chelcea, I. C.; Mihailescu, C. M.; Ofiteru, A.; Bocancia-Mateescu, L. A. Latest Trends in Lateral Flow Immunoassay (LFIA) Detection Labels and Conjugation Process. *Front Bioeng Biotechnol* **2022**, *10*, 922772. DOI: 10.3389/fbioe.2022.922772
- (48) Ellington, A. D.; Szostak, J. W. In vitro selection of RNA molecules that bind specific ligands. *Nature* **1990**, *346* (6287), 818-822. DOI: 10.1038/346818a0
- (49) Gold, L.; Ayers, D.; Bertino, J.; Bock, C.; Bock, A.; Brody, E. N.; Carter, J.; Dalby, A. B.; Eaton, B. E.; Fitzwater, T.; et al. Aptamer-based multiplexed proteomic technology for biomarker discovery. *PLoS One* **2010**, *5* (12), e15004. DOI: 10.1371/journal.pone.0015004
- (50) Quang, N. N.; Miodek, A.; Cibiel, A.; Ducongé, F. Selection of Aptamers Against Whole Living Cells: From Cell-SELEX to Identification of Biomarkers. *Methods Mol Biol* **2017**, *1575*, 253-272. DOI: 10.1007/978-1-4939-6857-2\_16
- (51) Navani, N. K.; Mok, W. K.; Yingfu, L. In vitro selection of protein-binding DNA aptamers as ligands for biosensing applications. *Methods Mol Biol* **2009**, *504*, 399-415. DOI: 10.1007/978-1-60327-569-9\_22
- (52) Keefe, A. D.; Pai, S.; Ellington, A. Aptamers as therapeutics. *Nature Reviews Drug Discovery* **2010**, *9* (7), 537-550. DOI: 10.1038/nrd3141.
- (53) German, I.; Buchanan, D. D.; Kennedy, R. T. Aptamers as ligands in affinity probe capillary electrophoresis. *Anal Chem* **1998**, *70* (21), 4540-4545. DOI: 10.1021/ac980638h
- (54) Zhang, H.; Wang, Z.; Li, X. F.; Le, X. C. Ultrasensitive detection of proteins by amplification of affinity aptamers. *Angew Chem Int Ed Engl* **2006**, *45* (10), 1576-1580. DOI: 10.1002/anie.200503345
- (55) Yi, M.; Yang, S.; Peng, Z.; Liu, C.; Li, J.; Zhong, W.; Yang, R.; Tan, W. Two-photon graphene oxide/aptamer nanosensing conjugate for in vitro or in vivo molecular probing. *Anal Chem* **2014**, *86* (7), 3548-3554. DOI: 10.1021/ac5000015
- (56) Zhu, C.; Li, L.; Wang, Z.; Irfan, M.; Qu, F. Recent advances of aptasensors for exosomes detection. *Biosensors and Bioelectronics* **2020**, *160*, 112213. DOI: <https://doi.org/10.1016/j.bios.2020.112213>
- (57) Gerasimova, Y. V.; Nedorezova, D. D.; Kolpashchikov, D. M. Split light up aptamers as a probing tool for nucleic acids. *Methods* **2022**, *197*, 82-88. DOI: 10.1016/j.ymeth.2021.05.008
- (58) Berezovski, M.; Musheev, M.; Drabovich, A.; Krylov, S. N. Non-SELEX selection of aptamers. *J Am Chem Soc* **2006**, *128* (5), 1410-1411. DOI: 10.1021/ja056943j
- (59) McKeague, M.; Bradley, C. R.; De Girolamo, A.; Visconti, A.; Miller, J. D.; Derosa, M. C. Screening and initial binding assessment of fumonisin b(1) aptamers. *Int J Mol Sci* **2010**, *11* (12), 4864-4881. DOI: 10.3390/ijms11124864
- (60) Valenzano, S.; De Girolamo, A.; DeRosa, M. C.; McKeague, M.; Schena, R.; Catucci, L.; Pascale, M. Screening and Identification of DNA Aptamers to Tyramine Using in Vitro Selection and High-Throughput Sequencing. *ACS Comb Sci* **2016**, *18* (6), 302-313. DOI: 10.1021/acscombsci.5b00163
- (61) Mohammadinezhad, R.; Jalali, S. A. H.; Farahmand, H. Evaluation of different direct and indirect SELEX monitoring methods and implementation of melt-curve analysis for rapid

- discrimination of variant aptamer sequences. *Anal Methods* **2020**, *12* (30), 3823-3835. DOI: 10.1039/d0ay00491j
- (62) Luo, Z.; He, L.; Wang, J.; Fang, X.; Zhang, L. Developing a combined strategy for monitoring the progress of aptamer selection. *Analyst* **2017**, *142* (17), 3136-3139. DOI: 10.1039/c7an01131h
- (63) Mencin, N.; Šmuc, T.; Vraničar, M.; Mavri, J.; Hren, M.; Galeša, K.; Krkoč, P.; Ulrich, H.; Šolar, B. Optimization of SELEX: comparison of different methods for monitoring the progress of in vitro selection of aptamers. *J Pharm Biomed Anal* **2014**, *91*, 151-159. DOI: 10.1016/j.jpba.2013.12.031
- (64) Galievsky, V. A.; Stasheuski, A. S.; Krylov, S. N. Improvement of LOD in Fluorescence Detection with Spectrally Nonuniform Background by Optimization of Emission Filtering. *Anal Chem* **2017**, *89* (20), 11122-11128. DOI: 10.1021/acs.analchem.7b03400
- (65) de Jong, S.; Krylov, S. N. Pressure-based approach for the analysis of protein adsorption in capillary electrophoresis. *Anal Chem* **2012**, *84* (1), 453-458. DOI: 10.1021/ac2030333
- (66) Musheev, M. U.; Filiptsev, Y.; Krylov, S. N. Temperature difference between the cooled and the noncooled parts of an electrolyte in capillary electrophoresis. *Anal Chem* **2010**, *82* (20), 8692-8695. DOI: 10.1021/ac101980k
- (67) Sisavath, N.; Rukundo, J. L.; Le Blanc, J. C. Y.; Galievsky, V. A.; Bao, J.; Kochmann, S.; Stasheuski, A. S.; Krylov, S. N. Transient Incomplete Separation Facilitates Finding Accurate Equilibrium Dissociation Constant of Protein-Small Molecule Complex. *Angew Chem Int Ed Engl* **2019**, *58* (20), 6635-6639. DOI: 10.1002/anie.201901345
- (68) Rukundo, J. L.; Le Blanc, J. C. Y.; Kochmann, S.; Krylov, S. N. Assessing Accuracy of an Analytical Method In Silico: Application to "Accurate Constant via Transient Incomplete Separation" (ACTIS). *Anal Chem* **2020**, *92* (17), 11973-11980. DOI: 10.1021/acs.analchem.0c02405
- (69) Rukundo, J. L.; Kochmann, S.; Wang, T. Y.; Ivanov, N. A.; Le Blanc, J. C. Y.; Gorin, B. I.; Krylov, S. N. Template Instrumentation for "Accurate Constant via Transient Incomplete Separation". *Anal Chem* **2021**, *93* (34), 11654-11659. DOI: 10.1021/acs.analchem.1c02007
- (70) Kanoatov, M.; Mehrabanfar, S.; Krylov, S. N. Systematic Approach to Optimization of Experimental Conditions in Nonequilibrium Capillary Electrophoresis of Equilibrium Mixtures. *Anal Chem* **2016**, *88* (18), 9300-9308. DOI: 10.1021/acs.analchem.6b02882
- (71) Spill, F.; Weinstein, Z. B.; Irani Shemirani, A.; Ho, N.; Desai, D.; Zaman, M. H. Controlling uncertainty in aptamer selection. *Proc Natl Acad Sci U S A* **2016**, *113* (43), 12076-12081. DOI: 10.1073/pnas.1605086113
- (72) Kanoatov, M.; Galievsky, V. A.; Krylova, S. M.; Cherney, L. T.; Jankowski, H. K.; Krylov, S. N. Using nonequilibrium capillary electrophoresis of equilibrium mixtures (NECEEM) for simultaneous determination of concentration and equilibrium constant. *Anal Chem* **2015**, *87* (5), 3099-3106. DOI: 10.1021/acs.analchem.5b00171
- (73) Liyanage, R.; Krylova, S. M.; Krylov, S. N. Minimizing adsorption of histidine-tagged proteins for the study of protein-deoxyribonucleic acid interactions by kinetic capillary electrophoresis. *J Chromatogr A* **2013**, *1322*, 90-96. DOI: 10.1016/j.chroma.2013.11.001
- (74) Le, A. T. H.; Wang, T. Y.; Krylova, S. M.; Beloborodov, S. S.; Krylov, S. N. Quantitative Characterization of Partitioning in Selection of DNA Aptamers for Protein Targets by Capillary Electrophoresis. *Analytical Chemistry* **2022**, *94* (5), 2578-2588. DOI: 10.1021/acs.analchem.1c04560.

- (75) Tuerk, C.; Gold, L. Systematic evolution of ligands by exponential enrichment: RNA ligands to bacteriophage T4 DNA polymerase. *Science* **1990**, *249* (4968), 505-510. DOI: 10.1126/science.2200121
- (76) Darmostuk, M.; Rimpelova, S.; Gbelcova, H.; Ruml, T. Current approaches in SELEX: An update to aptamer selection technology. *Biotechnol Adv* **2015**, *33* (6 Pt 2), 1141-1161. DOI: 10.1016/j.biotechadv.2015.02.008
- (77) Teclemichael, E.; Le, A. T. H.; Krylova, S. M.; Wang, T. Y.; Krylov, S. N. Bulk Affinity Assays in Aptamer Selection: Challenges, Theory, and Workflow. *Anal Chem* **2022**, *94* (44), 15183-15188. DOI: 10.1021/acs.analchem.2c03173
- (78) Drabovich, A. P.; Berezovski, M.; Okhonin, V.; Krylov, S. N. Selection of smart aptamers by methods of kinetic capillary electrophoresis. *Anal Chem* **2006**, *78* (9), 3171-3178. DOI: 10.1021/ac060144h
- (79) Bock, L. C.; Griffin, L. C.; Latham, J. A.; Vermaas, E. H.; Toole, J. J. Selection of single-stranded DNA molecules that bind and inhibit human thrombin. *Nature* **1992**, *355* (6360), 564-566. DOI: 10.1038/355564a0
- (80) Vaught, J. D.; Bock, C.; Carter, J.; Fitzwater, T.; Otis, M.; Schneider, D.; Rolando, J.; Waugh, S.; Wilcox, S. K.; Eaton, B. E. Expanding the chemistry of DNA for in vitro selection. *J Am Chem Soc* **2010**, *132* (12), 4141-4151. DOI: 10.1021/ja908035g

# APPENDICES

## Appendix A

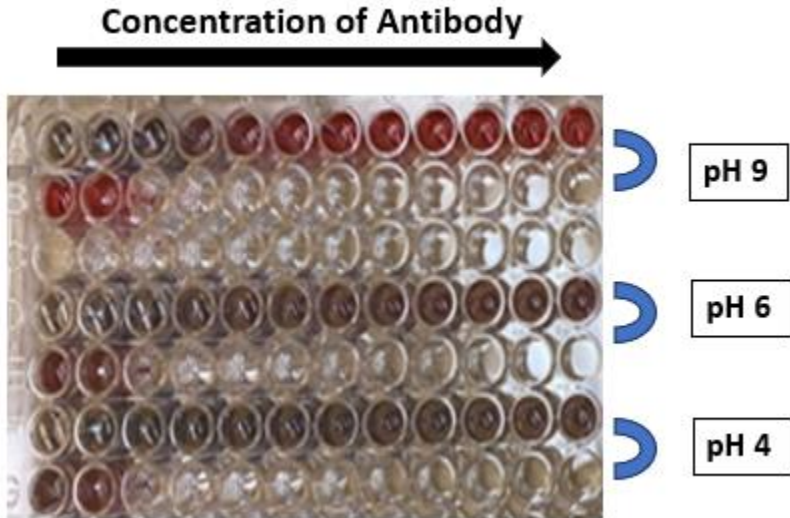


**Figure A1.** Determination of optimum pH for antibody conjugation. Three different GNP pH (4,6 and 9) in the addition of various antibody concentration (0, 1, 2, 3, 4, 5, 6, 8, 10, 12, 14, 16, 18 and 20 ug/ml) for conjugation were explored to determine the stability of antibody under the NaCl effect. The change in color indicates the degree of aggregation i.e purple or blue color indicate aggregated gold nanoparticles while red color is well-dispersed gold nanoparticle colloid dispersion.

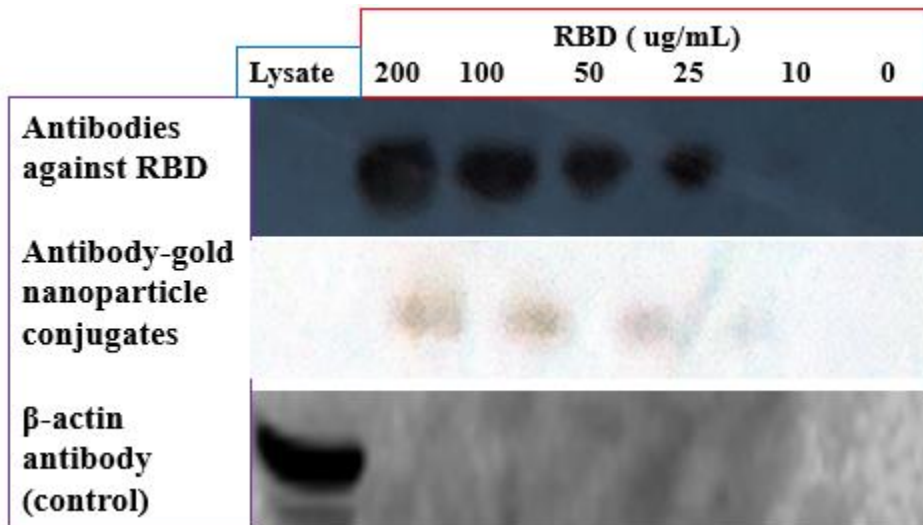


**Figure A2.** Western blot analysis for RBD antigen-antibody binding. The relative binding of RBD antibodies and conjugates to the different concentration of RBD antigen were evaluated. The image

presented in each row was generated by probing the membrane with the listed antibody (Polyclonal RBD antibody, polyclonal RBD antibody conjugates,  $\beta$ -actin antibody), which resulted in the band present on each blot.

## Appendix B

### Note B1: MinElute PCR purification procedure

DNA PCR products were purified using MinElute PCR purification kit from Qiagen as noted in Qiagen website with some modifications.

First 1: 250 volume pH indicator I was added to the buffer PB. Then, 500  $\mu$ L of buffer PB mixed with 100  $\mu$ L of the PCR reaction and mix. The color of the mixture was orange hence, 10  $\mu$ L 3M sodium acetate, pH 5.0 was added and mixed. After the color of the mixture turned to yellow, the sample was applied to the MinElute column placed in a provided 2 mL collection tube and centrifuged for 1 min at  $17,900 \times g$  (13,000 rpm). The flow-through was discarded and the MinElute column was placed back into the same collection tube. In the following step, 750  $\mu$ L buffer PE (initially prepared by adding 24  $\mu$ L of 96-100% ethanol to 6  $\mu$ L of PE) was added to the MinElute column and centrifuged for 1 min at  $17,900 \times g$  (13,000 rpm). The flow-through was discarded and the MinElute column was placed back in the same collection tube. The centrifuging step was repeated to remove residual ethanol and the flow-through was discarded. At the end, DNA was eluted in a clean 1.5 mL centrifuge tube using 20  $\mu$ L 50 mM Tris-HCl pH 8.0 buffer. After the elution buffer added, the column remained still for 2 min and centrifuged for 1 min at  $17,900 \times g$  (13,000 rpm).

### Note B2: Theoretical validation of superposition principle for $R$ and $\bar{K}_d$

#### Proof of $R$ satisfying the superposition principle:

According to the definition of  $R$  (fraction of unbound ligand), for each ligand,

$$R_1 = \frac{[L_1]}{[L_1]_0}, R_2 = \frac{[L_2]}{[L_2]_0}, \dots, R_N = \frac{[L_N]}{[L_N]_0} \quad (\text{B1})$$

where  $[L_1], [L_2], \dots, [L_N]$  represent the concentrations of ligand  $L_1, L_2, \dots, L_N$  at equilibrium;  $[L_1]_0, [L_2]_0, \dots, [L_N]_0$  represent the total concentrations of ligand  $L_1, L_2, \dots, L_N$ , respectively.

For the  $R$  value of the library,

$$R = \frac{[L]}{[L]_0} = \frac{[L_1] + [L_2] + \dots + [L_N]}{[L]_0} = \frac{[L_1]}{[L]_0} + \frac{[L_2]}{[L]_0} + \dots + \frac{[L_N]}{[L]_0} \quad (\text{B2})$$

where  $[L]$  represents the concentration of unbound ligand at equilibrium,  $[L]_0$  represents the total concentration of the  $N$  ligands.

Eq (S2) can be rearranged to be:

$$R = \frac{[L_1]}{[L_1]_0} \times \frac{[L_1]_0}{[L]_0} + \frac{[L_2]}{[L_2]_0} \times \frac{[L_2]_0}{[L]_0} + \dots + \frac{[L_N]}{[L_N]_0} \times \frac{[L_N]_0}{[L]_0} \quad (\text{B3})$$

Based on eq (S1) and (S3), we can get:

$$R = R_1 \frac{[L_1]_0}{[L]_0} + R_2 \frac{[L_2]_0}{[L]_0} + \dots + R_N \frac{[L_N]_0}{[L]_0} \quad (\text{B4})$$

Hence, parameter  $R$  satisfies the superposition principle that is defined by eq (9) in the main text.

### **Proof of $\bar{K}_d$ not satisfying the superposition principle:**

Based on the definition of equilibrium dissociation constant  $K_d$ , for each complex,

$$K_{d1} = \frac{[T][L_1]}{[TL_1]}, K_{d2} = \frac{[T][L_2]}{[TL_2]}, \dots, K_{dN} = \frac{[T][L_N]}{[TL_N]} \quad (\text{B5})$$

where  $[T]$  is the concentration of target at equilibrium;  $[TL_1]$ ,  $[TL_2]$ , ...,  $[TL_N]$  represent the concentrations of  $N$  different target-ligand complexes.

By referring to the definition of  $K_d$ , we can similarly define the equilibrium pseudo-constant  $\bar{K}_d$  as:

$$\bar{K}_d = \frac{[T][L]}{[TL]} = \frac{[T]([L_1] + [L_2] + \dots + [L_N])}{[TL]} \quad (\text{B6})$$

Here,  $[TL]$  represents the concentration of all target-ligand complexes at equilibrium (*i.e.*,  $[TL] = [TL_1] + [TL_2] + \dots + [TL_N]$ ).

Now, we can do the following rearrangements for eq (S6):

$$\bar{K}_d = \frac{[T][L_1]}{[TL]} + \frac{[T][L_2]}{[TL]} + \dots + \frac{[T][L_N]}{[TL]} \quad (\text{B7})$$

$$\bar{K}_d = \frac{[T][L_1]}{[TL]} \times \frac{[TL_1]}{[TL_1]} + \frac{[T][L_2]}{[TL]} \times \frac{[TL_2]}{[TL_2]} + \dots + \frac{[T][L_N]}{[TL]} \times \frac{[TL_N]}{[TL_N]} \quad (\text{B8})$$

According to eqs (S5) and (S8), we get:

$$\bar{K}_d = K_{d1} \frac{[TL_1]}{[TL]} + K_{d2} \frac{[TL_2]}{[TL]} + \dots + K_{dN} \frac{[TL_N]}{[TL]} \quad (\text{B9})$$

In general,

$$\frac{[TL_i]}{[TL]} \neq \frac{[L_i]_0}{[L]_0} \quad i = 1, 2, 3, \dots, N \quad (\text{B10})$$

Therefore,

$$\bar{K}_d \neq K_{d1} \frac{[L_1]_0}{[L]_0} + K_{d2} \frac{[L_2]_0}{[L]_0} + \dots + K_{dN} \frac{[L_N]_0}{[L]_0} \quad (\text{B11})$$

which indicates that parameter  $\bar{K}_d$  does not satisfy the superposition principle.

### **Note B3: Theoretical bulk affinity model**

The excel file “Theoretical bulk affinity model.xlsx” contains a modeled distribution of  $K_d$  values and construction of bulk affinity workflow using  $R$ . First, a starting library of 24 unique oligonucleotides was constructed with the semi-log distribution of  $K_d$  values for multiple progressive library enrichments. A bulk  $R$  value for the libraries was calculated using the superposition principle for different target concentrations.  $R$  of various target concentration versus selection round was plotted for all rounds of selection and a suitable theoretical bulk affinity workflow was proposed.

### **Note B4: Data analysis for the bulk affinity assays**

#### **Electropherograms:**

The electropherograms are represented in accordance with the theoretical workflow. The concentration of DNA was kept as a constant of 1 nM while varying target concentration. For the first two rounds, 1000 nM target concentration was used until the  $R$  value fell below 0.2. Then, the concentration of target was decreased gradually from 1000 nM to 100 nM and 10 nM until the  $R$  value fell between 0.3 and 0.7. After that, 10 nM of target concentration was used for the remaining rounds of selection. The peak of the unbound DNA corresponds to  $R$  value.  $R$  value decreases as the unbound DNA peak decreases and vice-versa. All experiments were performed in triplicate. The representative CE electropherograms presented in Figure S1.

### Calculation of $R$ values:

Based on the electropherograms,  $R$  values were determined by using NAAP program. <sup>Error! Reference s</sup>  
 ource not found. The detailed results are shown in Table S1.

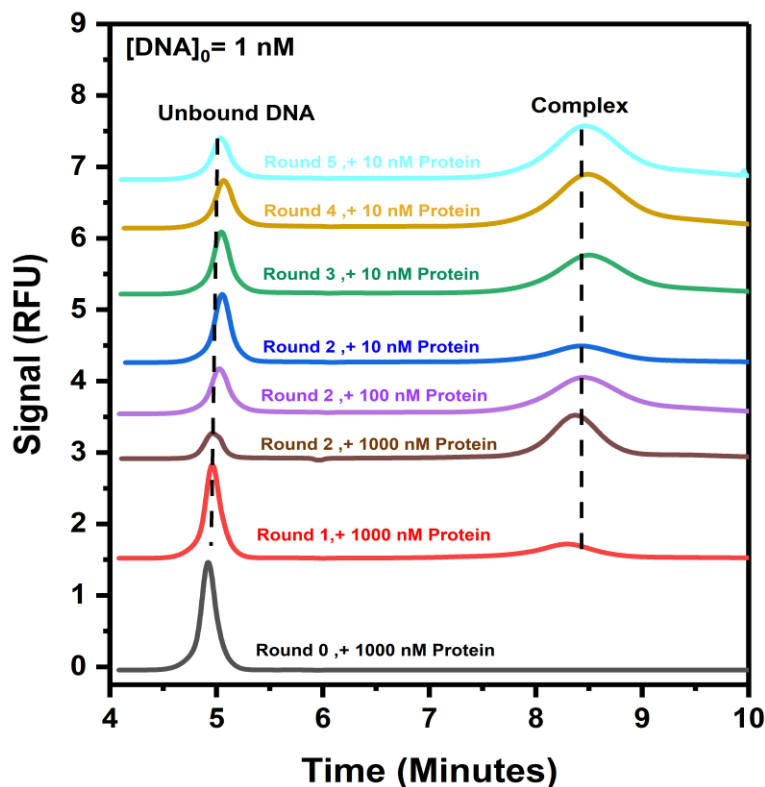


**Figure B1.** Experimental electropherograms of His-tagged MutS protein bulk affinity assay based on the proposed bulk affinity assay workflow. From bottom to top, the points represent 1 nM DNA with: (i) 1,000 nM protein in rounds 0, 1, and 2 (black, red, and maroon trace, respectively), (ii) 100 nM protein in round 2 (purple trace), and (iii) 10 nM protein in rounds 2, 3, 4, and 5 (blue, green, brown, and aqua trace, respectively)

**Table B1.** Determined *R* values at different selection round with adding different concentrations of target. The target was His-tagged MutS protein. The ligand (DNA) concentration was kept as a constant of 1 nM. The bulk affinity assays were conducted based on the proposed bulk affinity assay workflow.

Selection Round	Target Concentration (nM)	<i>R</i> value for triplicate experiments	Average <i>R</i>	Standard deviation
0	1000	0.82329	0.787	0.031
		0.76696		
		0.77095		
1	1000	0.41350	0.434	0.018
		0.44296		
		0.44717		
2	1000	0.21389	0.198	0.035
		0.22236		
		0.15755		
2	100	0.30876	0.376	0.058
		0.41004		
		0.40852		
2	10	0.63428	0.680	0.040
		0.69888		
		0.70740		
3	10	0.63428	0.584	0.056
		0.59257		
		0.52393		
4	10	0.29562	0.365	0.073
		0.44017		
		0.35795		
5	10	0.37501	0.326	0.051
		0.32829		
		0.27371		

## Appendix C

### Note C1: Determination of the binder-elution window

To determine the binder-elution window, NECEEM-based partitioning was conducted using a mixture of the starting DNA library (100 nM) and a relatively high concentration of the target (1  $\mu$ M). Peaks of protein–DNA complexes were detected for both protein targets at such high concentrations, allowing us to identify binder-elution windows to be used in aptamer selection. It is noted that in the case of thrombin, the resolution between target–binder complexes and DNA nonbinders was poorer than in the MutS case, primarily due to the smaller size of thrombin. As such, the partitioning in thrombin selections experienced

a much higher nonbinder background ( $10^{-4}$ – $10^{-3}$  for thrombin *versus*  $10^{-6}$ – $10^{-5}$  for MutS).

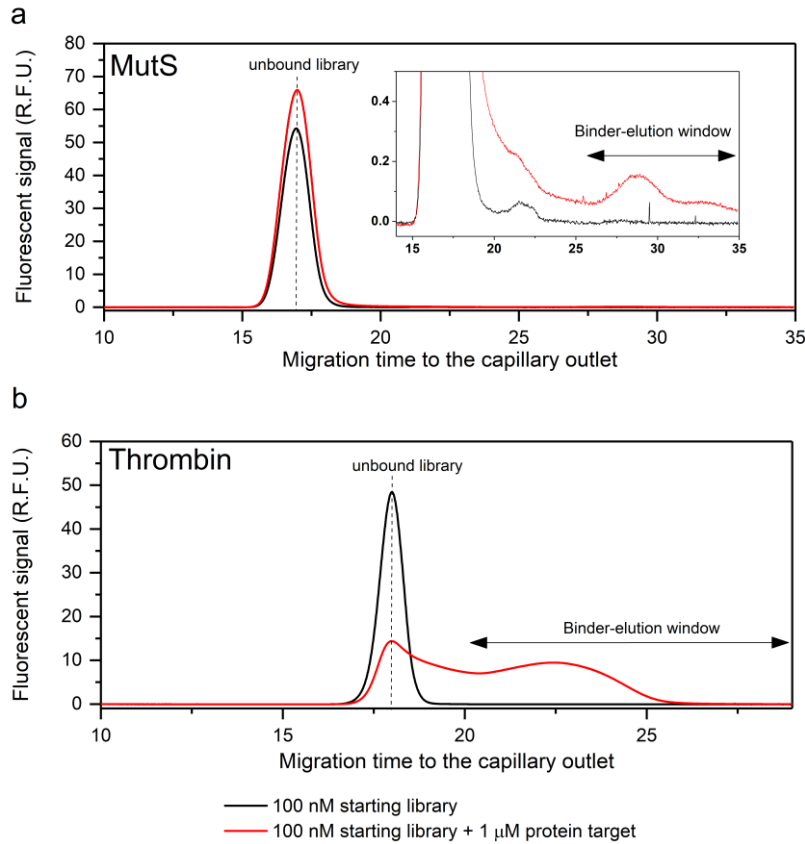


**Figure C1.** Determination of binder-elution window for NECEEM-based selection for MutS (a) and thrombin (b). Based on the migration profile of DNA nonbinders and target–binder complexes, elution of target–binder complexes was conducted using pressure after NECEEM-based partitioning for 26 min and 20 min for MutS and thrombin selections, respectively. In this complex-last NECEEM mode, the first peak (from the left) corresponds to the unbound library while the second peak corresponds to the target–binder complex.

## Note C2: Summary of nonbinder background ( $k_N$ ) and relative yield of DNA ( $q$ ) values obtained in MutS and thrombin selections

### Estimation of relative standard deviation of $q$

We conducted 5 sets of positive control (presence of target) and negative control (absence of target) using 10 μM DNA library and 500 nM thrombin; 5 sets of  $L_T$  and  $N_{out}$  values were obtained respectively.

The mean value of  $q$  ( $\bar{q}$ ) was calculated from mean values of  $L_T$  ( $\bar{L}_T$ ) and  $N_{out}$  ( $\bar{N}_{out}$ ) ( $n = 5$ ):

$$\bar{q} = \bar{L}_T / \bar{N}_{out} \quad (\text{C1})$$

Subsequently, the standard deviation ( $\sigma$ ) of  $q$  was estimated by applying the error-propagation rule for noncorrelated standard deviations of  $L_T$  and  $N_{out}$ :

$$\frac{\sigma_q}{\bar{q}} = \sqrt{\left(\frac{\sigma_{L_T}}{L_T}\right)^2 + \left(\frac{\sigma_{N_{out}}}{N_{out}}\right)^2} \quad (\text{C2})$$

The relative standard deviation (RSD) of  $q$  could then be calculated:

$$\text{RSD}_q = \frac{\sigma_q}{\bar{q}} \quad (\text{C3})$$

The results of calculations re shown in **Table C1** below.

**Table C1.** Relative standard deviation of  $q$ . Five sets of positive and negative controls were conducted using 10  $\mu\text{M}$  DNA library and 500 nM thrombin to find  $L_T$  and  $N_{out}$ , respectively.

Parameters	Quantity (number of DNA molecules)					Mean	$\sigma$	$\bar{q}$	$\text{RSD}_q$
$L_T$	$7.1 \times 10^9$	$5.9 \times 10^9$	$7.5 \times 10^9$	$6.9 \times 10^9$	$6.9 \times 10^9$	$6.9 \times 10^9$	$5.9 \times 10^8$	15	0.14 or 14%
$N_{out}$	$4.3 \times 10^8$	$4.0 \times 10^8$	$5.4 \times 10^8$	$4.6 \times 10^8$	$4.7 \times 10^8$	$4.6 \times 10^8$	$5.3 \times 10^7$		

## Summary of $k_N$ and $q$ values obtained in MutS selections

We conducted three-round SELEX for His-tagged MutS with four constant round-to-round target concentrations: 1, 10, 100 and 500 nM. Each round involved a set of positive controls (in the presence of target) and negative controls (in the absence of target) to determine  $L_T$  and  $N_{out}$ , respectively. After every round, DNA was quantitated with qPCR and  $k_N$  and  $q$  values were estimated. The results are shown in **Table C2** below.

**Table C2.** Summary of  $k_N$  and  $q$  values obtained in MutS selections. The values in the Table were presented as (Round 1, Round 2, Round 3).

Target concentration	$N_{in}$	$N_{out}$	$L_T$	$k_N$ ( $=N_{out}/N_{in}$ )	$q$ ( $=L_T/N_{out}$ )
<b>1 nM</b>	( $9.94 \times 10^{11}$ , $3.28 \times 10^{10}$ , $3.28 \times 10^{10}$ )	( $6.90 \times 10^7$ , $2.67 \times 10^6$ , $1.29 \times 10^6$ )	( $5.73 \times 10^7$ , $2.80 \times 10^6$ , $1.42 \times 10^6$ )	( $6.94 \times 10^{-5}$ , $8.14 \times 10^{-5}$ , $3.94 \times 10^{-5}$ )	<b>(0.83, 1.05, 1.1)</b>
<b>10 nM</b>	( $9.94 \times 10^{11}$ , $3.28 \times 10^{10}$ , $3.28 \times 10^{10}$ )	( $5.61 \times 10^7$ , $7.04 \times 10^5$ , $2.77 \times 10^6$ )	( $3.76 \times 10^8$ , $5.91 \times 10^6$ , $6.37 \times 10^7$ )	( $5.65 \times 10^{-5}$ , $2.15 \times 10^{-5}$ , $8.44 \times 10^{-5}$ )	<b>(6.7, 8.4, 23)</b>
<b>100 nM</b>	( $9.94 \times 10^{11}$ , $3.28 \times 10^{10}$ , $3.28 \times 10^{10}$ )	( $6.90 \times 10^6$ , $8.68 \times 10^5$ , $1.43 \times 10^5$ )	( $4.94 \times 10^8$ , $2.77 \times 10^8$ , $3.55 \times 10^8$ )	( $6.94 \times 10^{-6}$ , $2.65 \times 10^{-5}$ , $4.36 \times 10^{-6}$ )	<b>(71.6, 319, 2480)</b>
<b>500 nM</b>	( $9.94 \times 10^{11}$ , $3.28 \times 10^{10}$ , $3.28 \times 10^{10}$ )	( $5.23 \times 10^6$ , $7.69 \times 10^5$ , $1.86 \times 10^6$ )	( $3.05 \times 10^9$ , $5.08 \times 10^9$ , $1.36 \times 10^{10}$ )	( $5.26 \times 10^{-6}$ , $2.35 \times 10^{-5}$ , $5.67 \times 10^{-5}$ )	<b>(583, 6610, 7300)</b>

## Summary of $k_N$ and $q$ values obtained in thrombin selections

Similar to MutS selection procedures, we completed three-round SELEX for thrombin with four constant round-to-round target concentrations and estimated  $k_N$  and  $q$  values for every round after DNA quantitation with qPCR. We repeated two of four selections for thrombin to ensure the reproducibility of the results (10 nM and 500 nM selections). The data are shown in **Table C3** below.

**Table C3.** Summary of  $k_N$  and  $q$  values obtained in thrombin selections. The values are presented as (Round 1, Round 2, Round 3).

Target concentration	$N_{in}$	$N_{out}$	$L_T$	$k_N$ ( $=N_{out}/N_{in}$ )	$q$ ( $=L_T/N_{out}$ )
<b>1 nM</b>	( $9.94 \times 10^{11}$ , $3.28 \times 10^{10}$ , $3.28 \times 10^{10}$ )	( $5.17 \times 10^8$ , $2.12 \times 10^7$ , $2.24$ $\times 10^7$ )	( $4.48 \times 10^8$ , $2.00 \times 10^7$ , $2.36 \times 10^7$ )	( $5.20 \times 10^{-4}$ , $6.45 \times 10^{-4}$ , $6.83$ $\times 10^{-4}$ )	<b>(0.87, 0.94, 1.1)</b>
<b>10 nM</b>	( $9.94 \times 10^{11}$ , $3.28 \times 10^{10}$ , $3.28 \times 10^{10}$ )	( $4.86 \times 10^8$ , $9.61 \times 10^6$ , $1.36$ $\times 10^7$ )	( $4.69 \times 10^8$ , $1.01 \times 10^7$ , $1.27 \times 10^7$ )	( $4.89 \times 10^{-4}$ , $2.93 \times 10^{-4}$ , $4.14$ $\times 10^{-4}$ )	<b>(0.97, 1.1, 0.93)</b>
<b>10 nM (repetition)</b>	( $9.94 \times 10^{11}$ , $3.28 \times 10^{10}$ , $3.28 \times 10^{10}$ )	( $4.61 \times 10^8$ , $1.22 \times 10^7$ , $2.11$ $\times 10^7$ )	( $4.23 \times 10^8$ , $1.35 \times 10^7$ , $1.89 \times 10^7$ )	( $4.64 \times 10^{-4}$ , $3.73 \times 10^{-4}$ , $6.44$ $\times 10^{-4}$ )	<b>(0.92, 1.1, 0.90)</b>
<b>100 nM</b>	( $9.94 \times 10^{11}$ , $3.28 \times 10^{10}$ , $3.28 \times 10^{10}$ )	( $5.02 \times 10^8$ , $1.69 \times 10^7$ , $1.13$ $\times 10^7$ )	( $1.00 \times 10^9$ , $4.21 \times 10^8$ , $7.39 \times 10^9$ )	( $5.05 \times 10^{-4}$ , $5.15 \times 10^{-4}$ , $3.44$ $\times 10^{-4}$ )	<b>(2, 25, 66)</b>
<b>500 nM</b>	( $9.94 \times 10^{11}$ , $3.28 \times 10^{10}$ , $3.28 \times 10^{10}$ )	( $4.25 \times 10^8$ , $1.57 \times 10^7$ , $2.17$ $\times 10^7$ )	( $7.11 \times 10^9$ , $7.99 \times 10^9$ , $1.56 \times 10^{10}$ )	( $4.27 \times 10^{-4}$ , $4.78 \times 10^{-4}$ , $6.61$ $\times 10^{-4}$ )	<b>(17, 510, 720)</b>
<b>500 nM (repetition)</b>	( $9.94 \times 10^{11}$ , $3.28 \times 10^{10}$ , $3.28 \times 10^{10}$ )	( $3.96 \times 10^8$ , $1.60 \times 10^7$ , $1.85$ $\times 10^7$ )	( $5.90 \times 10^9$ , $6.88 \times 10^9$ , $1.48 \times 10^{10}$ )	( $3.98 \times 10^{-4}$ , $4.87 \times 10^{-4}$ , $5.63$ $\times 10^{-4}$ )	<b>(15, 430, 800)</b>

## Note C3: Data analysis for bulk affinity assays

### Electropherograms and calculation of $R$ for MutS selection

We used a previously published bulk affinity workflow to evaluate the progress of selection for MutS selection at four different target concentrations. The bulk affinity assay was conducted using a constant DNA concentration of 1 nM and a starting target concentration of 1  $\mu$ M (**Figure C2**).<sup>77</sup> The target concentration in the bulk affinity assay was subsequently decreased in a stepwise fashion (i.e., 1  $\mu$ M  $\rightarrow$  100 nM  $\rightarrow$  10 nM) to ensure that  $R$  value (fraction of unbound library) stays within its desired range of 0.3–0.7.

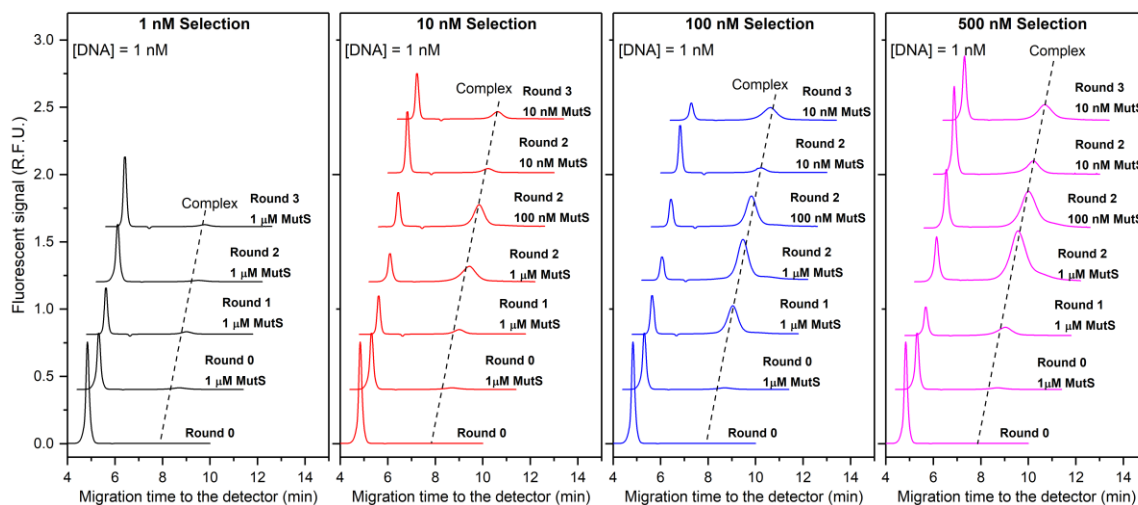


**Figure C2.** Bulk affinity tests of the starting library and the binder-enriched libraries obtained in MutS selections at four different target concentrations using the published bulk affinity workflow. Black, red, blue, and magenta traces represent selections using 1, 10, 100, and 500 nM MutS, respectively. The experiments were conducted in triplicates and only the representative electropherograms are shown here. The dashed line indicates the position of the target–binder complex in each electropherogram while the leftmost peak corresponds to the unbound DNA library.

The *R* value in the bulk affinity test was then estimated from the ratio of the peak area of unbound DNA library to the total peak area of unbound library and target–binder complex in the corresponding electropherograms using the NAAP program (Kanoatov, M.; Galievsky, V. A.; Krylova, S. M.; Cherney, L. T.; Jankowski, H. K.; Krylov, S. N. Using Nonequilibrium Capillary Electrophoresis of Equilibrium Mixtures (NECEEM) for Simultaneous Determination of Concentration and Equilibrium Constant. *Anal. Chem.* 2015, 87, 3099-3106). The results are shown in **Table C4** below.

**Table C4.** Summary of *R* values for the starting library (Round 0) and binder-enriched libraries (Round 1–3) obtained in MutS selections at 4 different target concentration schemes: 1, 10, 100 and 500 nM MutS. Note that *R* values for Round 0 were the same for all selections.

<b>Selection</b>	<b>Round</b>	<b>Target concentration used in the affinity test</b>	<b><i>R</i> values for triplicate runs</b>	<b>Mean <i>R</i> ± standard deviation</b>
	<b>0</b>	1 μM	0.802, 0.845, 0.857	<b>0.835 ± 0.024</b>
<b>1 nM MutS</b>	<b>1</b>	1 μM	0.822, 0.791, 0.791	<b>0.801 ± 0.015</b>
	<b>2</b>	1 μM	0.790, 0.865, 0.721	<b>0.792 ± 0.059</b>
	<b>3</b>	1 μM	0.763, 0.759, 0.823	<b>0.782 ± 0.029</b>
	<b>1</b>	1 μM	0.643, 0.700, 0.731	<b>0.691 ± 0.036</b>
<b>10 nM MutS</b>	<b>2</b>	1 μM	0.324, 0.296, 0.346	<b>0.322 ± 0.021</b>
	<b>2</b>	100 nM	0.531, 0.537, 0.535	<b>0.534 ± 0.003</b>
	<b>2</b>	10 nM	0.850, 0.871, 0.833	<b>0.851 ± 0.016</b>
	<b>3</b>	10 nM	0.634, 0.700, 0.719	<b>0.684 ± 0.037</b>
	<b>1</b>	1 μM	0.411, 0.443, 0.451	<b>0.435 ± 0.018</b>
<b>100 nM MutS</b>	<b>2</b>	1 μM	0.214, 0.231, 0.151	<b>0.198 ± 0.035</b>
	<b>2</b>	100 nM	0.376, 0.445, 0.304	<b>0.375 ± 0.058</b>
	<b>2</b>	10 nM	0.625, 0.709, 0.707	<b>0.680 ± 0.039</b>
	<b>3</b>	10 nM	0.637, 0.570, 0.542	<b>0.583 ± 0.400</b>
	<b>1</b>	1 μM	0.511, 0.482, 0.544	<b>0.512 ± 0.025</b>
<b>500 nM MutS</b>	<b>2</b>	1 μM	0.164, 0.159, 0.151	<b>0.158 ± 0.006</b>
	<b>2</b>	100 nM	0.325, 0.260, 0.274	<b>0.286 ± 0.028</b>
	<b>2</b>	10 nM	0.646, 0.633, 0.613	<b>0.631 ± 0.014</b>
	<b>3</b>	10 nM	0.508, 0.569, 0.528	<b>0.535 ± 0.025</b>

## Electropherograms and calculation of $R$ for thrombin selections

Similar to our treatment of MutS selection results, we applied the bulk affinity workflow to assess the progress of selection for thrombin across four different target concentrations. The workflow maintained a constant DNA concentration of 20 nM and began with a target concentration of 1  $\mu$ M (**Figure C3**). At 1  $\mu$ M target concentration, significant binding of the starting library to thrombin was observed as the corresponding  $R$  value was below 0.3. Consequently, the target concentration was reduced by 10 folds from 1  $\mu$ M to 100 nM. This adjustment was made to elevate the  $R$  value of the starting library (Round 0) to a level within the desired range (0.3–0.7); this target concentration (100 nM) remained fixed for later rounds.

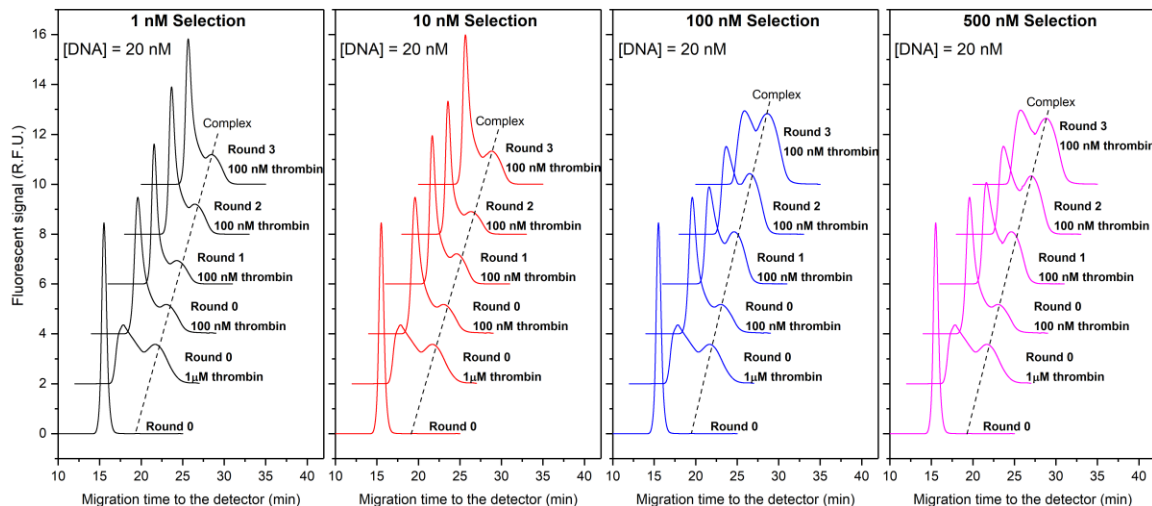


**Figure C3.** Bulk affinity tests of the starting library and binder-enriched libraries obtained from thrombin selections at four different target concentrations using the published bulk affinity workflow. Black, red, blue, and magenta traces represent selections using 1, 10, 100, and 500 nM thrombin, respectively. The affinity test for every round was conducted in triplicates and only the representative electropherograms are shown here. The dashed lines indicate positions of the target–binder complexes while the leftmost peak corresponds to the unbound DNA library.

In thrombin selections, the resolution between the unbound library and the target–binder complex was relatively poor (**Figure C3**), leading to challenges in calculating *R* based on distinct peak areas of the unbound library and target–binder complex. Therefore, for the thrombin case, we determined *R* value by utilizing the peak height ratio of unbound library in the presence of target to that in its absence. The peak heights and migration times were obtained with 32 Karat Software. The results can be found in **Table C5** below.

**Table C5.** Summary of *R* values for the starting library (Round 0) and binder-enriched libraries (Round 1–3) obtained in thrombin selections at four different target concentrations: 1, 10, 100 and 500 nM MutS. Note, *R* values for Round 0 were the same for all selections.

<b>Selection</b>	<b>Round</b>	<b>Target concentration used in the affinity test</b>	<b><i>R</i> values for triplicate runs</b>	<b>Mean <i>R</i> ± standard deviation</b>
–	<b>0</b>	1 μM	0.261, 0.266, 0.268	<b>0.265 ± 0.004</b>
	<b>0</b>	100 nM	0.640, 0.636, 0.644	<b>0.640 ± 0.004</b>
<b>1 nM thrombin</b>	<b>1</b>	100 nM	0.660, 0.663, 0.682	<b>0.669 ± 0.012</b>
	<b>2</b>	100 nM	0.644, 0.656, 0.665	<b>0.655 ± 0.011</b>
	<b>3</b>	100 nM	0.635, 0.627, 0.630	<b>0.631 ± 0.004</b>
<b>10 nM thrombin</b>	<b>1</b>	100 nM	0.649, 0.654, 0.662	<b>0.655 ± 0.007</b>
	<b>2</b>	100 nM	0.627, 0.635, 0.640	<b>0.634 ± 0.007</b>
	<b>3</b>	100 nM	0.653, 0.660, 0.651	<b>0.655 ± 0.005</b>
<b>10 nM thrombin (repetition)</b>	<b>1</b>	100 nM	0.683, 0.685, 0.682	<b>0.684 ± 0.002</b>
	<b>2</b>	100 nM	0.671, 0.671, 0.674	<b>0.672 ± 0.002</b>
	<b>3</b>	100 nM	0.640, 0.651, 0.653	<b>0.648 ± 0.007</b>
<b>100 nM thrombin</b>	<b>1</b>	100 nM	0.453, 0.429, 0.427	<b>0.436 ± 0.015</b>
	<b>2</b>	100 nM	0.403, 0.411, 0.435	<b>0.416 ± 0.016</b>
	<b>3</b>	100 nM	0.322, 0.320, 0.296	<b>0.313 ± 0.015</b>
<b>500 nM thrombin</b>	<b>1</b>	100 nM	0.474, 0.490, 0.515	<b>0.493 ± 0.021</b>
	<b>2</b>	100 nM	0.403, 0.470, 0.420	<b>0.431 ± 0.035</b>
	<b>3</b>	100 nM	0.341, 0.350, 0.313	<b>0.335 ± 0.020</b>
<b>500 nM thrombin (repetition)</b>	<b>1</b>	100 nM	0.489, 0.502, 0.501	<b>0.497 ± 0.008</b>
	<b>2</b>	100 nM	0.402, 0.427, 0.443	<b>0.424 ± 0.020</b>
	<b>3</b>	100 nM	0.349, 0.337, 0.338	<b>0.341 ± 0.007</b>